DALHOUSIE UNIVERSITY

GEOCHRONOLOGY OF THE CHICOUTIMI GNEISS BELT, ST. FULGENCE, QUEBEC

BEN ELLIS

SUBMITTED IN PARTIAL FULFILLMENT OF THE REQUIREMENTS FOR THE
DEGREE OF BACHELOR OF SCIENCES, HONOURS
DEPARTMENT OF EARTH SCIENCES
DALHOUSIE UNIVERSITY, HALIFAX, NOVA SCOTIA

APRIL 2018

Distribution License

DalSpace requires agreement to this non-exclusive distribution license before your item can appear on DalSpace.

NON-EXCLUSIVE DISTRIBUTION LICENSE

You (the author(s) or copyright owner) grant to Dalhousie University the non-exclusive right to reproduce and distribute your submission worldwide in any medium.

You agree that Dalhousie University may, without changing the content, reformat the submission for the purpose of preservation.

You also agree that Dalhousie University may keep more than one copy of this submission for purposes of security, back-up and preservation.

You agree that the submission is your original work, and that you have the right to grant the rights contained in this license. You also agree that your submission does not, to the best of your knowledge, infringe upon anyone's copyright.

If the submission contains material for which you do not hold copyright, you agree that you have obtained the unrestricted permission of the copyright owner to grant Dalhousie University the rights required by this license, and that such third-party owned material is clearly identified and acknowledged within the text or content of the submission.

If the submission is based upon work that has been sponsored or supported by an agency or organization other than Dalhousie University, you assert that you have fulfilled any right of review or other obligations required by such contract or agreement.

Dalhousie University will clearly identify your name(s) as the author(s) or owner(s) of the submission, and will not make any alteration to the content of the files that you have submitted.

If you have questions regarding this license please contact the repository manager at dalspace@dal.ca.

Grant the distribution license by signing and dating below.

_____ _____

Name of signatory Date

DALHOUSIE UNIVERSITY

Department of Earth Sciences
Halifax, Nova Scotia
Canada B3H 4R2
(902) 494-2358

DATE: 03/30/2018

AUTHOR: Ben Ellis

TITLE: Geochronology of the Chicoutimi Gneiss Belt, St. Fulgence, Quebec

DEGREE: Bachelor of Science CONVOCATION: June 1 YEAR: 2018

Abstract

The Grenvillian Orogeny was a drawn-out mountain building event occurring in the Mesoproterozoic Era induced by the formation of the supercontinent Rodinia. This event produced several distinguishable waves of metamorphism preserved throughout the Grenville Province. Although a significant portion of the Grenville province located in North America has been precisely dated, the Chicoutimi Gneiss Belt within the St. Fulgence region of Quebec is one region in which precise metamorphic dates have not been obtained. The aim of this project is to use the well-known Monazite dating method, in order to discover the metamorphic age(s) that are preserved in this particular suite of rocks. In the study, the monazite grains selected are analysed in situ, to allow for easier interpretation of their relationship to the metamorphic fabric seen throughout the terranes. Samples from the Cap a l'Est Gneiss Complex are also examined in this study. Metamorphic age peaks at 1060 ± 7.3 Ma and ~1145Ma ± 16 Ma were found in the Chicoutimi Gneiss samples, and age peaks of 969 ± 13 Ma and 1029.1 ± 8 Ma were found for the Cap a l'Est Gneiss samples. These metamorphic ages obtained are consistent with the ages of the orogenic events occurring in the area, as well as the plutonism, and show that there are several pulses of metamorphism preserved in these rocks, along with relict ages of the basement rock and xenocrysts.

Keywords: Grenville, Gneiss, Monazite, U-Th-Pb Dating, Electron Microprobe

Table of Contents

List of Figures

Acknowledgements

I would like to start off by giving an overwhelming thanks to my supervisor Richard Cox for providing me with this fascinating project, and incredible opportunity to see what researching in the field of geochronology would be like. He was always available and willing to explain concepts that I did not fully understand from the literature and doing the experiment itself, and always gave positive, encouraging feedback which was ever so much appreciated.

Another big thanks has to go out to the departments Electron Microprobe Technician Dan MacDonald, who without which I would not have been able to collect my data in such an efficient manor. He was always more than happy to answer absolutely any questions I had, and would explain a lot of the nitty gritty of how the microprobe and software does its thing, in a way that could be easily understood. He also ended up coming in on the weekend in order to help me acquire data when the probe was not working correctly, which I appreciate a lot.

Chapter 1: Introduction

1.1 Objective

Although much of the Grenville has been precisely dated, the Chicoutimi Gneiss Belt, outcropping in the St. Fulgence region of Quebec, has not. The aim of this study is to provide a precise estimation of the age for this particular suite of paragneisses. To obtain these ages, we will use the well-established U, Th, Pb dating method of monazite. From previous works completed in the surrounding areas, there are some constraints in the metamorphic ages of these rocks. The ages of metamorphism are limited by the Cap de la Mer amphibolite (1506 ± 13 Ma), the basement rock, and the Simoncouche gabbro, which is the youngest intrusion that cross-cuts the Chicoutimi Gneiss Belt (1045 ± 5 Ma) (Hébert and van Breemen, 2004). It is however possible for younger ages to occur as the Simoncouche gabbro is known to have experienced later metamorphism in the low to mid amphibolite facies. Therefore, with these constraints we expect to obtain ages younger than 1506 Ma and (potentially) older than 1045 Ma. Obtaining precise dates for this suite of rocks will help lead to a more complete metamorphic/ tectonic history of the Grenville province.

1.2 Monazite

Monazite is a rare earth element (REE) bearing phosphate, with the chemical formula (Ce, La, Nd, Th)PO_4. As seen from its principal formula its composition can vary, and upon analysis it is seen that it contains many other rare earth elements as well. This variability in its composition produces many different domains that are characteristic of specific metamorphic events experienced by the suite of rocks (Williams et al., 2007). Monazite also has some other very

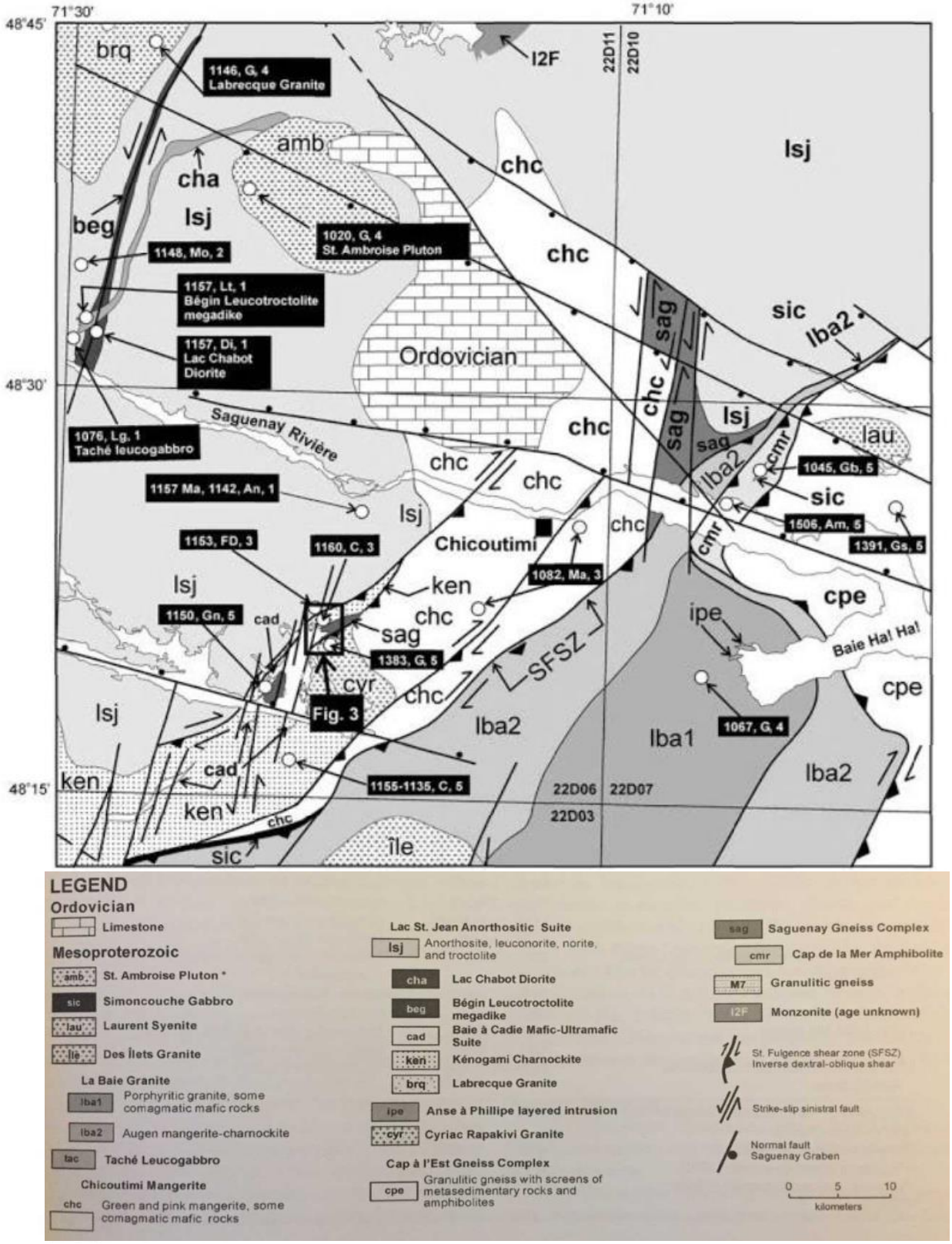

Figure 1.1: Geologic Map of the Chicoutimi region of the Grenville Province. The Chicoutimi Gneiss Belt is labelled cmr. After Hébert and van Breemen 2004.

useful properties that makes it a good candidate for age dating in this project. One being its slow rate of diffusion for many elements, which is important as it necessary for the different compositional domains to remain relatively constant through geologic time to obtain an accurate date on the metamorphic event that produced them (Williams et al., 2007). Another characteristic of monazite is that it contains relatively high concentrations of Thorium and Uranium, and a very small amount of common Lead (Williams et al., 2006). This is important in the fact that U-Th-Pb dating requires a measurable amount of U and Th, but a negligible amount of common Pb, as we only want to measure the amount of radiogenic lead produce by the U-Th-Pb decay series. It should be mentioned as well that radiogenic lead can accumulate relatively quickly in monazite grains, reaching hundreds to thousands of ppm in just 100 Ma. As this study is dealing with rocks above 1000 Ma, this is most certainly way above the detectable limits (Williams et al. 2007). All of these properties combined make it an extremely good device for finding an accurate metamorphic age for this suite of rocks.

1.3 Microprobe Analysis

This project uses the EMPA method for the analysis of monazites to date this suite of rocks. One of the biggest advantages to using the electron microprobe is its spatial resolution. With its ability to do analysis at a one-micron beam size, it is ideal for producing ages of small grains and compositional domains. Compared to other methods of dating such as LA-ICPMS analysis, it is also a fairly non-destructive technique (Williams et al., 2006). However, there are disadvantages as well, the most prominent being its precision compared to that of LA-ICPMS, which does isotopic dating of the monazites and zircons. There are ways of increasing its precision, such as increasing count times on specific trace elements, however due to time

constraints this may not always be possible, and this may end up causing more damage to the samples.

Chapter 2: Geologic Background

2.1 Overview of the Grenvillian Orogeny

The Grenvillian Orogeny generally refers to the late Mesoproterozoic mountain building event caused by the formation of the supercontinent Rodinia. The suites of rock analysed in this paper are between ~1-1.5 Ga (Hebert and van Breeman, 2004). This period is when the bulk of tectonic activity (convergence) was occurring in the region, which at the time was the Southeastern margin of Laurentia (Tollo et al., 2004). Rivers et al. (2008) separated the orogeny into two phases, the older Ottawan orogenic phase and younger Rigolet orogenic phase (Figure 2.1), which induced prolonged amphibolite facies metamorphism on the Grenville terrane. The Ottawan orogenic phase is thought to be a result of the collision of Amazonia and Laurentia, while the Rigolet orogenic phase is interpreted to be renewed contraction in the area (McLelland et al., 2010). The two different phases of metamorphism are proclaimed to be caused by the large extent of the area involved in the orogenesis. The orogenic core experienced the effects of the orogenesis during the Ottawan orogenic phase, while the northwestern margin experienced the effects during the Rigolet orogenic phase. These two regions are separated by a large crustal scale thrust (Rivers et al., 2008).

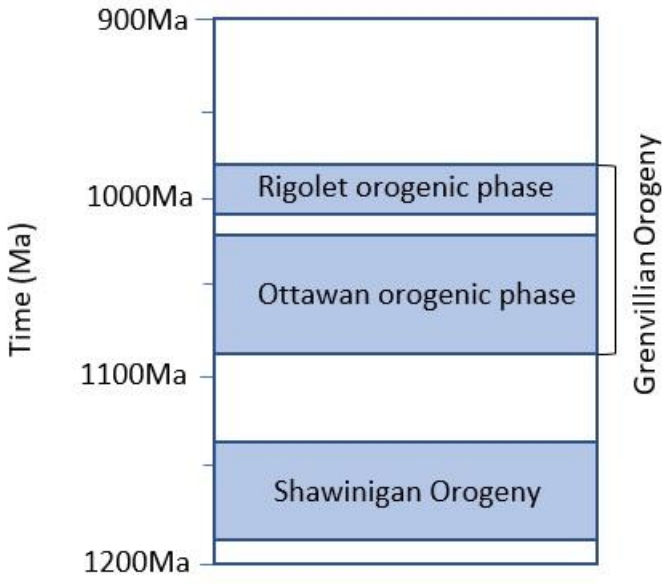

Figure 2.1: Timeline of different orogenic events in the St. Fulgence region. After Rivers et al. (2008)

One other orogenic event that predates the Grenvillian orogeny is the Shawinigan Orogeny occurring ~1140-1190 Ma (Rivers et al., 2008). However, Rivers et al., 2008 states that the effects of this orogeny are contained within the terranes in the southwestern Grenville Province. An explanation as to why this is important to mention is in Section 5.2.1.

2.2 Geologic Units

The basement rock in the area of study is the Cap de la Mer Amphibolite, which Hebert and van Breemen (2004) described as medium- to fine- grained, foliated amphibolite. The rock consists mainly of plagioclase and amphiboles, with little secondary quartz. Using zircons found within the samples analysed, Hebert and van Breemen (2004) determine upper and lower intercept ages of 1506 ± 13 Ma and 1077 ± 12 Ma, respectively. They interpreted the upper age intercept as the formation of the original gabbro, while the lower age intercept was interpreted to be the growth of new zircon during the Grenvillian Orogeny.

The Cap a l'Est Gneiss Complex is a course grained gneiss containing predominantly quartz and microcline, with small amounts of plagioclase and biotite as well (See Section 4.1.1 for brief textural description). Hebert and van Breemen (2004) mention the presence of pyroxenes in their samples, but none were seen in the sections analysed here. Once again, a Concordia diagram was created by Hebert and van Breemen (2004) to give an upper and lower age intercept of 1391 +8/-7 Ma and 1027 ± 18 Ma, respectively. The upper age is interpreted as the original age of crystallization, while the lower is thought to be lead loss during the Grenvillian Orogeny.

The Lac-Saint-Jean Anorthosite Complex (labelled lsj in Figure 1.1) is a large ensemble of plutons within the Grenville province that began forming at ~1160 Ma and continued through to the end of the Grenvillian orogeny, although those yielding younger ages are found in Southern regions (Higgins et al., 2002). The range in composition of the plutons vary from anorthosite to leucogabbro (Higgins and van Breemen, 1992), however each pluton is rich in plagioclase and has variable amounts of olivine and pyroxene throughout (Higgins et al., 2002). There are many shear zones and faults present throughout this complex, and it is thought that the deformation that caused this was somewhat synchronous with the emplacement of the plutons due to the deformation within and around the individual plutons (Higgins et al., 2002).

The Chicoutimi Gneiss Belt itself is composed mainly of paragneisses, which show various degrees of partial melting, from local development of garnet-bearing leucosomes to small (<10m wide) granitic dikes. A textural description of the samples examined will be provided in Section 4.1.2. The relation between the Chicoutimi Gneiss Belt and the Cap de la Mer Amphibolite would presumably be deformational, with the former being deposited on the latter. However, no contact between the two could be seen in the field, so this an assumption

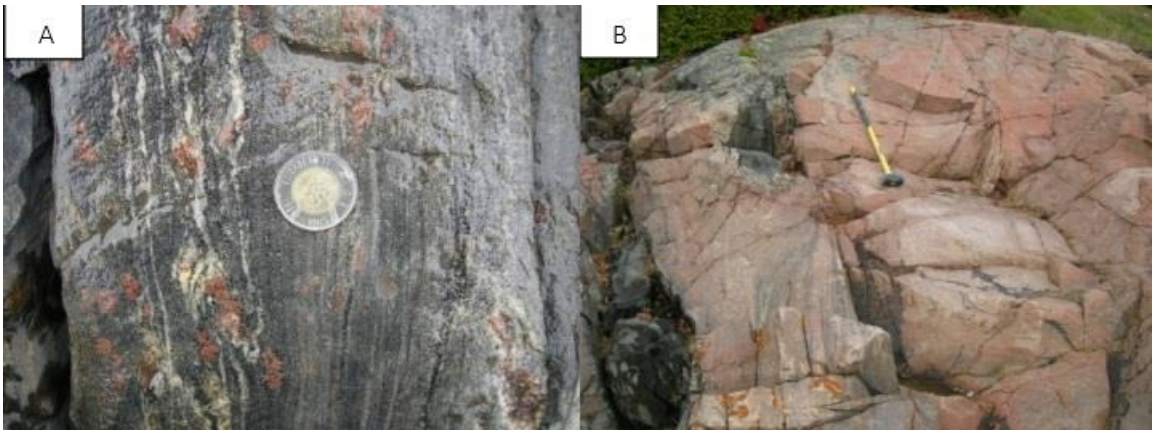

Figure 2.2: Pictures from field showing the various degrees of partial melting in the Chcicoutimi Gneiss terrane. A shows small scale plagioclase-quartz rich leucosomes, with garnet porphyroblasts. B shows a larger scale granitic dike.

based on the fact that the Cap de la Mar Amphibolite is defined as the basement rock. The metamorphic grade of this suite would be upper amphibolite into granulite facies. This was determined from the fact that Hebert and van Breeman (2004) stated that the Cap de la Mer amphibolite, which is the proposed basement rock, as well as the Cap a l'Est Gneiss (neighbouring terrane) experienced granulite facies metamorphism. This is supported by the presence of cordierite, sillimanite, and orthopyroxene seen within the outcrops. The fact that leucosomes are present is further evidence for granulite facies metamorphism, as high temperatures would be required for partial melting of the rock.

Chapter 3: Methods

3.1 Textural Analysis

The first step in this project is to complete a textural analysis of the thin sections that house the analysed grains. The purpose of this is not only to understand the metamorphic textures displayed by the two terranes, but also to be able to later observe the relationships between the ages found and the textures within the rocks.

3.2 Electron Microprobe

The process used for this project is based on Williams et al. (2006) procedure for analyzing monazite, but follows closely to Gagne et al. (2004) procedure designed specifically for the microprobe in the Robert MacKay Electron Microprobe Laboratory at Dalhousie.

3.2.1 Compositional Mapping

Before the analysis of the grains, composition maps were produced to distinguish compositional zoning throughout the grains. Four maps were produced using the JEOL JXA-8200 Superprobe software for each grain, displaying the distribution of Uranium, Thorium, Lead, and Yttrium throughout the grains (Figure 3.1). In these particular samples, the BSE imaging of the grains displayed the same zoning seen in the composition maps. It is however recommended that composition maps always be produced, as if the variation in the average atomic number between zones is not significant, the zones will not be distinguishable in the image (Williams et al., 2007). It should be as to why Uranium, Thorium, and Lead were chosen to be mapped, as they are the three elements that this dating method is concerned with. It may however not be as obvious as to why yttrium was also chosen. One reason is that the Y lγ peak

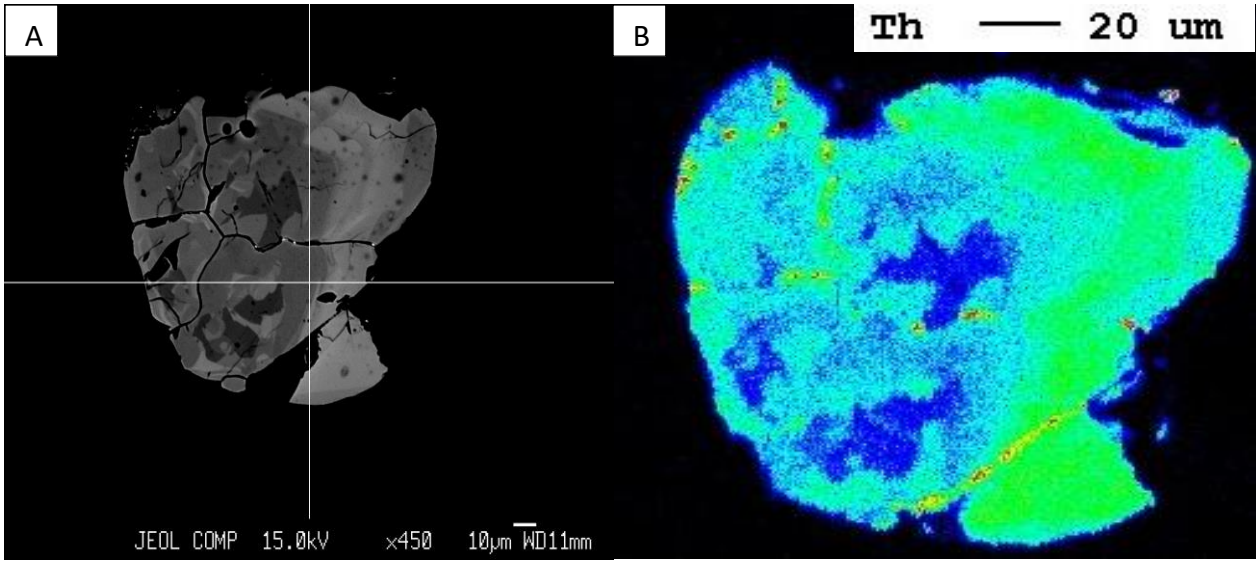

Figure 3.1: Comparison between BSE image (A) and composition map (B) of the same monazite grain (3NO* MNT5), showing that the zonation shown in the BSE image is the same as that shown in the composition map.

produces a peak overlap with the Pb lα peak, which was being measured originally, which meant that improper correction of this overlap could (and did) lead to false lead counts (Hetherington et al., 2008). This would not necessarily be an issue in domains where the yttrium concentration was relatively constant throughout. However, it could cause issues in smaller grains or domains where only one or two analyses are being done, because if one of the points of analysis has a high yttrium count then it is more likely that that point will also be not corrected properly, therefore leading to an inaccurate age. This particular reason however did not end up being an issue in this experiment as the Pb mβ line was measured instead of mα in the end.

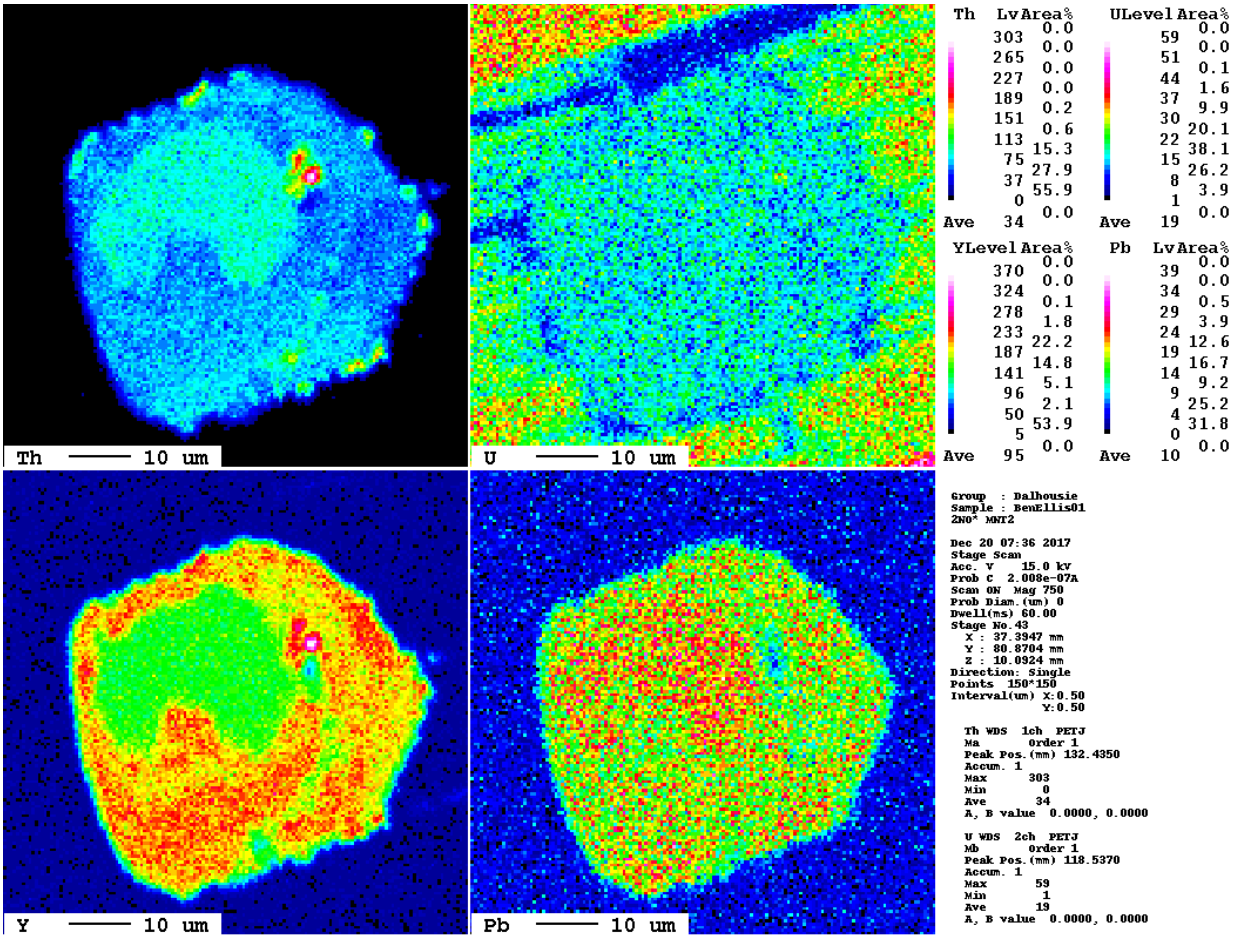

Figure 3.2: Example of four composition maps showing Th, U, Y, Pb. Th and Y show the most distinct zonation within the monazite grain (2NO* MNT2). Complex zonation seen suggests growth during deformation.

Another reason as to why yttrium is a good element to map is that it could also show the grains/ zones age relative to the growth of garnet in the samples, as garnet tends to take up yttrium before monazite and many other minerals including xenotime (Hetherington et al., 2008). Therefore, zones of higher yttrium could potentially indicate that they formed before the growth of the garnet. Thorium and yttrium showed the most distinct compositional zonation, this is probably because compared to uranium and lead, these two had relatively high abundances (Figure 3.2). Appendix 4 and 5 display all the BSE and composition maps, respectively.

3.2.2 Major Element Analysis

From the composition maps produced, the zonation of the crystals can be determined and analysis of each domain can begin. The first step is to complete major element analysis. The precision of the analysis was periodically checked by analysing Monazite53, a major element standard used in the lab. The major elements analysed on Probe for EPMA Xtreme Edition were: P, Ca, Si, S, Th, Y, Ce, Gd, Nd, Dy, U, Pr, Sm, La. U, Th, Y will be analysed once again in the minor analysis, however they are in somewhat greater concentrations (specifically thorium) and it is important when analysing to get a sum as close to 100 as possible. One analysis per compositional domain was completed, as it was assumed that the majors for a domain remained relatively constant throughout. The on-peak count time for all elements, except for P and La (which were 20s), was 40s with a beam current of 20nA and spot size of one micron. See Appendix 1 for element/ cation properties used in the major element analysis.

3.2.3 Minor Element Analysis

With the major element analysis completed, the next step is analysis of the minor elements. We once again analysed Y, Th, U, but this time Pb was added to the analysis, the other major elements measured above were entered as fixed values for each domain. JEOL JXA-8200 Superprobe was used to analyse the minors, as there were issues in the yttrium correction (mentioned in Section 3.3) using Probe for EPMA. A count time of 360s was used for each of the four elements, with a background count time of 180s. A beam current of 200nA was used. The beam size was a micron, and the amount of analyses per zone/ grain was based on its size, anywhere between one and seven, obviously as the number of analyses per zone is increased,

the statistics on the answer will become better. Table 1 gives an overview of the general conditions used to measure the four minor elements.

However, it should be mentioned that before accurate analysis of these 4 minor elements can be obtained, background wavescans for each of the four elements in each compositional domain must be completed using the Probe for EPMA software. An appropriate place must be chosen to measure the backgrounds for that particular element within a particular domain. A spot is chosen on either side of the peak, and the average is taken (Figure 3.3). The purpose of this portion of the procedure is to chose where an appropriate place to measure background signal for each of the four elements is, so that the computer can accurately subtract them. Without this subtraction, false counts would be added to the measurements. Once a spot is

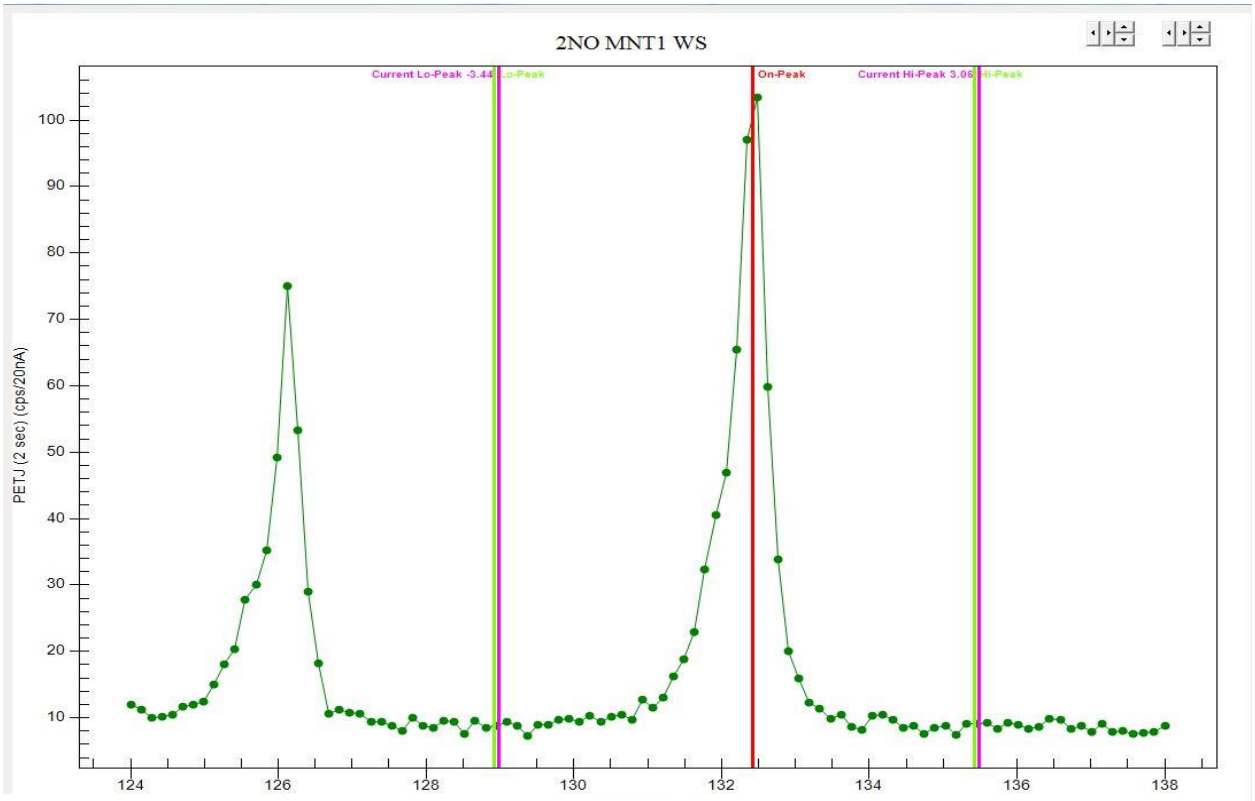

Figure 3.3: Example of background scan from Probe for EPMA software, the green lines represent the chosen positions to measure the background, the red line in the center represents the on-peak position. The horizontal axis is the position of the measured x-ray in millimeters, while the vertical axis represents the counts per second (normalized to 20Na) of the element in question (Thorium here)

chosen, the high and low background values are entered into the element conditions window of the minor's and that is where the background is measured.

Element	Th	U	Y	Pb
X-ray Measured	mα	Mβ	lα	mβ
Channel	1	2	4	5
Crystal	PETJ	PETJ	TAP	PETH
PHA Gain	16	64	16	64
High V. (V)	1682	1716	1724	1716
Base L. (V)	1.00	2.50	1.00	0.70
Window (V)	5.00	3.00	6.00	9.30
Diff/ Int	Diff	Diff	Diff	Diff

Table 1: Acquisition parameters for minor element analysis. Data collection done at 15keV, 200nA

To acquire the age using the minor element data found from the process given above, a spreadsheet designed (by John Foster, Dalhousie University) specifically for this monazite dating procedure (using JEOL) was used. This spreadsheet not only calculated the ages of each individual point, by use of the Montel Equation (Equation 1) (Montel et al., 1996), but also their errors based on ZAF corrections, k-raw%. From the ages found, a probability distribution plot was created using Isoplot 4.15 in order to define different groups of ages seen throughout the suite. A GSC standard (8153) of monazite was analysed several times throughout the data acquisition to check that the procedure was being followed correctly and that the technology was working properly.

$$Pb = \left[\frac{Th}{232}(e^{\lambda^{232}t} - 1)\right]208 + \left[\frac{U}{238}0.9928(e^{\lambda^{238}t} - 1)\right]206 + \left[\frac{U}{235}0.0072(e^{\lambda^{235}t} - 1)\right]207 \quad (1)$$

3.3 Sources of Error

When the major element analysis was being performed, the largest potential source of error was peak drift, specifically on the phosphorous peak. From the time peak searches were performed, to the time points had been set, the phosphorous peak had shifted, which was noticed by inconsistencies in the standard's output. This was hard to control as the room's temperature fluctuated, especially into the night.

During the minor element analysis, the greatest source of error would most likely have come from the background estimations as there is no specific formula to choose these, and it is different for each element and each domain. It is quite possible that in some domains, a background was chosen too high, therefore removing counts of the minor elements, or vice versa. There are options on the Probe for EPMA Xtreme Edition software to model the background, however it has never been tested before here, so for the sake of saving time, the well established (yet more manual) way was chosen.

Another issue that occurred during the minor element analysis was improper counts on the lead peaks which lead to calculated ages on the GSC monazite standard to come out to 440-470 Ma, when it should actually be 495-505 Ma (490-510 Ma acceptable). The hypothesized reason for this is the use of yttrium aluminum garnet (YAG) to standardize Y as opposed to an yttrium phosphate (xenotime). YAG is a garnet, and is therefore isometric, while xenotime is tetragonal, this difference in crystal structure leads to differences in the fluorescence of the two standards.

Because YAG is isometric, it has a higher fluorescence and therefore produces an overcorrection of lead, as (mentioned before) there is a peak overlap of Y lγ on Pb mα (Jercinovic and Williams, 2005). To fix the over correction of yttrium on the mα peak, it was decided that the Pb mβ peak would be measured instead as it does not have a significant yttrium overlap, however its count intensity is less than that of the Pb mα peak which could cause issues with domains of low lead content. It should be mentioned that there is a second order overlap of Ce lα on the Pb mβ line, however the interference affects on the Pb mβ in general are much lower than those on the Pb mα line (Pyle et al., 2002).

Chapter 4: Results

4.1 Textural Description

An attempt to locate monazite grains was made while looking at the textures of the sections examined. Essentially any small grain that had high relief and very high birefringence was targeted, although these criteria could potentially lead to finding zircon as well, however, EDS was used on the microprobe to confirm that the chosen grains were in fact monazite.

4.1.1 Cap a l'Est Terrane

The minerology of the samples analysed here is: Microcline (~50%), Quartz (~40%), Plagioclase (~5%), Biotite (<5%), muscovite (<1%). In general, the samples are coarse-grained, inequigranular interbolate, with quartz and microcline grains growing to 11+ mm. Most grains of plagioclase show extensive sericitization, and several areas display small scale myrmekite.

4.1.2 Chicoutimi Gneiss Belt

The dominant mineralogy exhibited by the samples examined here is: Quartz (50%), Biotite (30%), Plagioclase (20%). This list of minerals is what makes up the fine-grained (average 0.25mm), granoblastic matrix. Larger veins (leucosomes) composed of coarse grained (11+ mm) quartz and plagioclase (70% and 30% respectively) are present, as well as what appear to be some mylonitic bands (composed of quartz). There is schistosity defined by the biotite within the matrix, and also large garnet porphyroblasts exhibiting abundant inclusions (predominantly quartz), which upon close inspection shows evidence of the garnet growing syntectonic. Strain shadows defined by the biotite support this syntectonic growth as well.

The zonation seen in all of the monazite grains (see Appendix 5) analysed is quite complex, suggesting that their growth was during the deformation experienced by the two terranes.

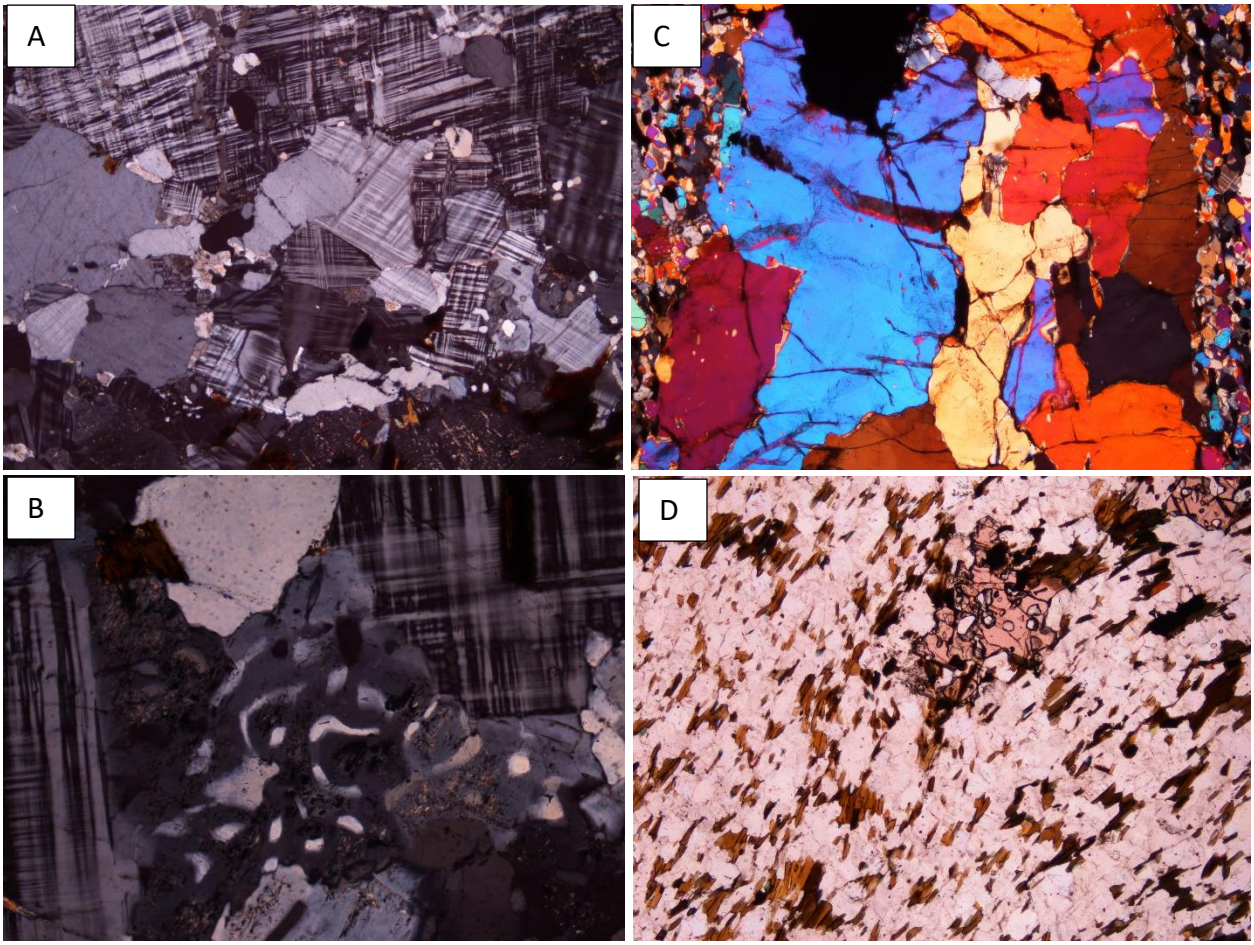

Figure 4.1: Textures seen in samples 2NO (A &B), 4NO* (C), and 5NO* (D). Field of view for A, C, and D is 6mm, B is 1.1mm. **A** shows the course grained inequigranular interbolate texture seen in the Cap a l'Est Gneiss samples, microcline and quartz dominating. **B** displays small scale myrmekite seen in the Cap a l'Est terrane. **C** shows large vein composed predominately of quartz surrounded by the finer grained matrix. Birefringence appears unusually high here due to a thicker thin section. **D** shows aligned biotites in the Chicoutimi Gneiss terrane, forming a strain shadow around the small garnet porphyroblast seen, which contain even smaller inclusions of quartz.

4.2 Monazite Geochemistry

A complete table of the major element geochemistry for each compositional domain can be found in Appendix 2. Figure 4.2 shows that the major element weight oxide percents were relatively constant throughout all of the domains being measured, other than the xenotime core that was discovered in one of the grains which showed anonymously low concentrations for all elements, apart from phosphorous and yttrium (not shown in figure). As expected, phosphorus showed the highest weight percent, followed by Cerium, Lanthanum, and Neodymium which of course are all present in the principal formula for monazite. The other 4 REE measured along with Calcium were in low concentrations (<5 wt%) and varied much less than the elements mentioned above. Sulphur was also analysed as a major, however in many domains the counts were negative, and the overall average across the grains was ~0.03 wt%,

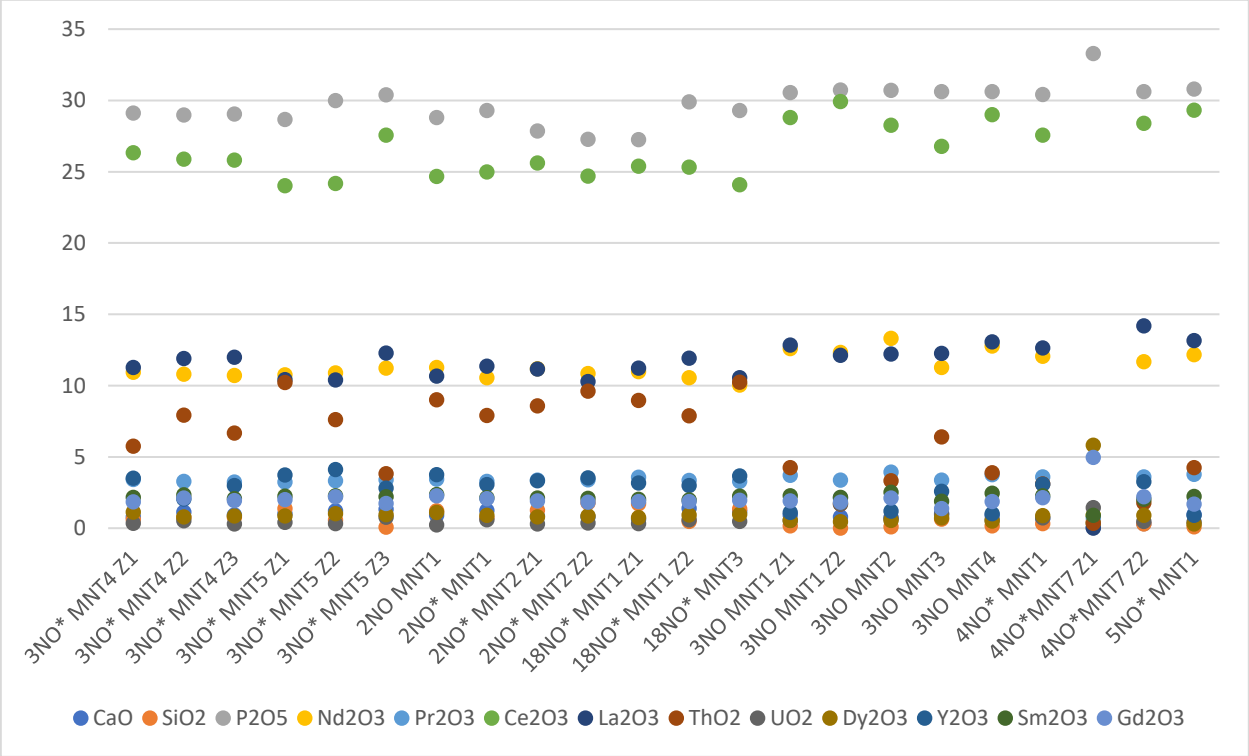

Figure 4.2: Plot of the major elements for each of the compositional domains showing little variations throughout the suite.

which is negligible. It was however a good choice to analyse sulphur as there was a crystal containing only Copper, Iron, and Sulphur (potentially chalcopyrite), meaning that there had to have been a significant amount of sulphur in the area to form this mineral.

The minors showed much more variability in their concentrations, although they were of course in much smaller concentrations (ppm). Figure 4.3 illustrates the consistency of the REE trend seen throughout all the measured domain (aside from the yttrium core). Figure 4.4 shows the variability in minor element concentrations for the Cap a l'Est terrane. However, this variability is not seen in yttrium. It makes sense that these elements would not be at consistent values throughout the Cap a l'Est terrane, as each analysis and/ or domain hypothetically yields a different age, and therefore has different concentrations of U, Th, Pb, based on how much decay has occurred.

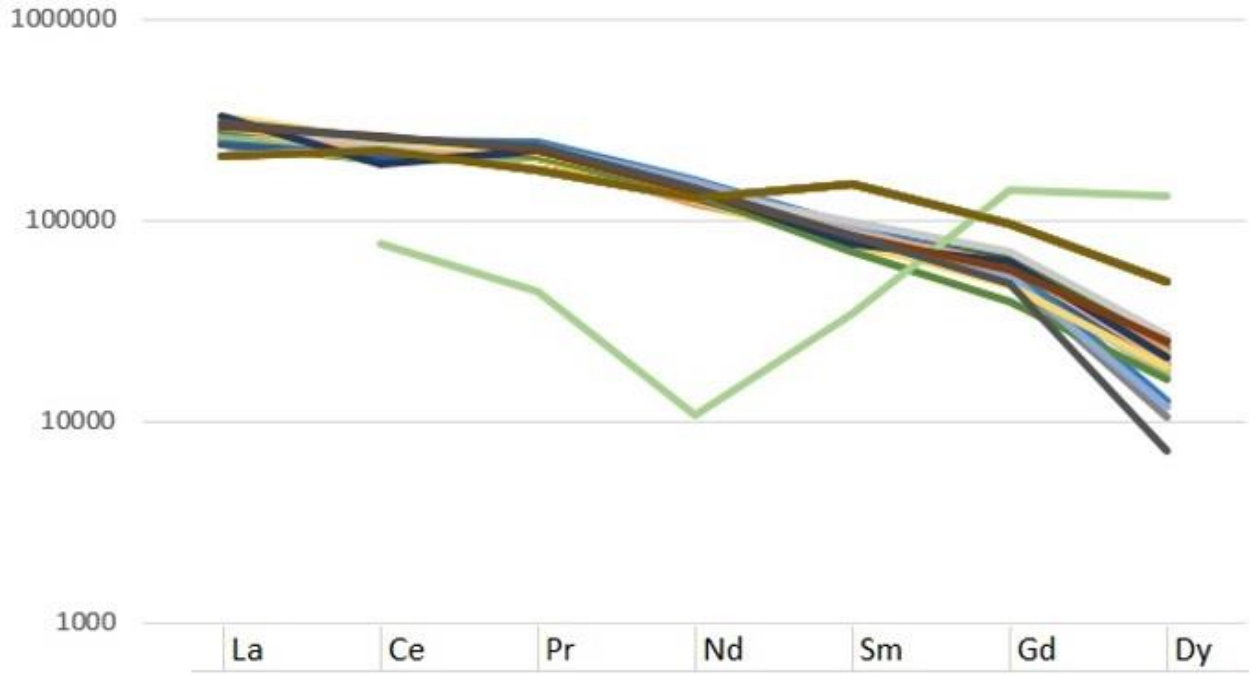

Figure 4.3: REE plot of the LREE, normalized to chondrite (ppm). All samples analysed show similar trend, apart from the obvious anomaly (green line), which represents the xenotime core discovered in one of the grains. This shows that the concentrations of the REE's is relatively constant throughout all the different age domains and terranes that were studied.

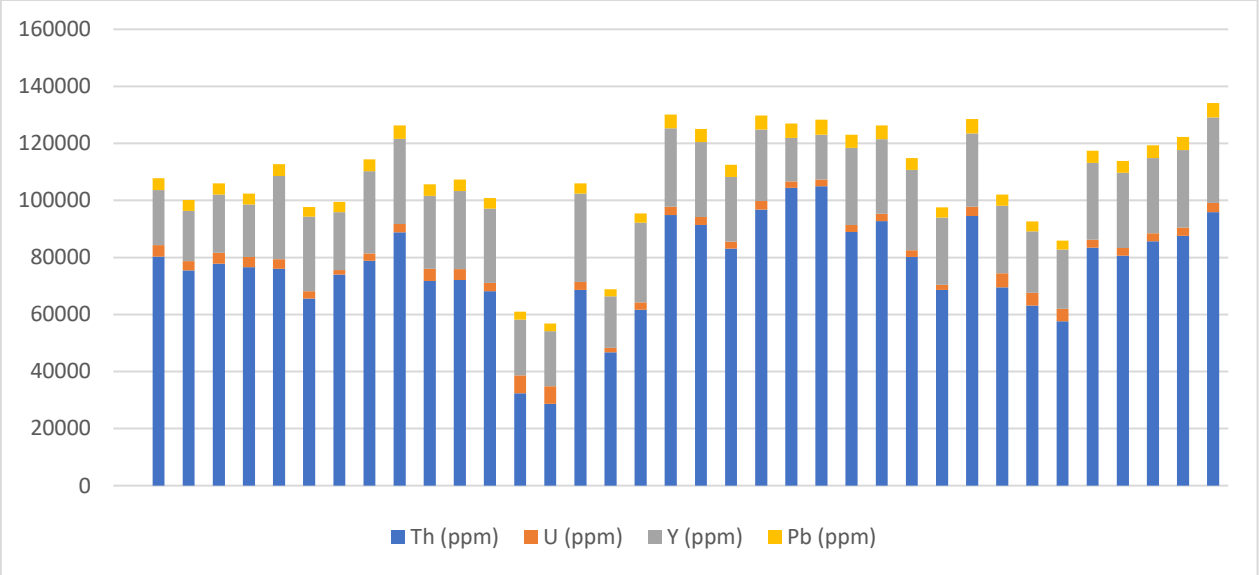

Figure 4.4: Graph of the analysed minor elements (in ppm) from the Cap a l'Est terrane. This shows that there is a fair amount of variability of thorium alone throughout the terrane, and on a much smaller scale, the uranium and lead also tend to vary.

4.3 Monazite Ages

In the end, a total of 97 analysis across 24 grains were completed, 34 of which were completed in an earlier analysis from Cox (unpublished data). It should be noted that there were several monazite grains that had been mapped and analysed for majors, but due to their small size, re-analysis was not able to be completed. All but three of the grains in this analysis were found within the matrix. Two were inclusions in biotite grains, while the other was an inclusion in a large grain of potassium feldspar, however this did not have any apparent affect on their age.

Figure 4.5 shows the probability distribution (made with Isoplot) of all the ages obtained from this and the previously done analysis (Cox, unpublish data). Table 2 gives the average (weighted) ages of the domains measured in this analysis. It should be noted that three ages (1545, 1535, and 2164 Ma) were left out when making this diagram so that the distribution among the bulk of the data could be could be seen clearly. There are three distinguishable peaks: one around 970 Ma, ~1040 Ma, and ~1150 Ma.

Domain	Age (Ma)	2σ	MSWD	Prob.
3NO* MNT4 Zone1	1031	25	0.47	0.49
3NO* MNT4 Zone 2	964	16	0.074	0.97
3NO* MNT4 Zone 3	1021	26	1.5	0.23
2NO MNT1	1038	29	0.59	0.44
2NO* MNT1	1039	21	0.2	0.82
3NO* MNT5 Zone 1	1130	27	2.9	0.089
3NO* MNT5 Zone 2	1032	28	0.56	0.57
3NO* MNT5 Zone 3	1013	19	0.15	0.93
2NO* MNT2 Zone 1	1005	31	1.8	0.18
2NO* MNT2 Zone 2	1031	25	0.12	0.88
18NO* MNT1 Zone 1	1049	31	0.14	0.70
18NO* MNT1 Zone 2	975	19	1.03	0.36
18NO* MNT 3	1035	18	0.22	0.93
3NO MNT1 Zone 1	1063	31	-	-
3NO MNT Zone 2	1036	18	0.99	0.4
3NO MNT2	1065	41	-	-
3NO MNT3	1084	20	0.106	0.9
3NO MNT4	1049	28	0.48	0.49
4NO* MNT1	1078	21	1.6	0.2
4NO* MNT5	1127	36	3.2	0.074
4NO* MNT7 Zone 1	1075	49	0.043	0.84
4NO* MNT7 Zone 2	1090	38	0.027	0.87
5NO* MNT1	1057	14	0.48	0.83

Table 2: Weighted average of ages, with the 2σ errors, found for each composition domain. See Appendix 5 for legend of domains within grains. The MSWD represents the Mean Square Weighted Deviation, which is a goodness of fit test, this is preferably as close to one. Chicoutimi Gneiss Terrane includes: 3NO, 4NO*, 5NO*. Cap a l'Est Gneiss Terrane includes: 3NO*, 2NO, 2NO*, 18NO*

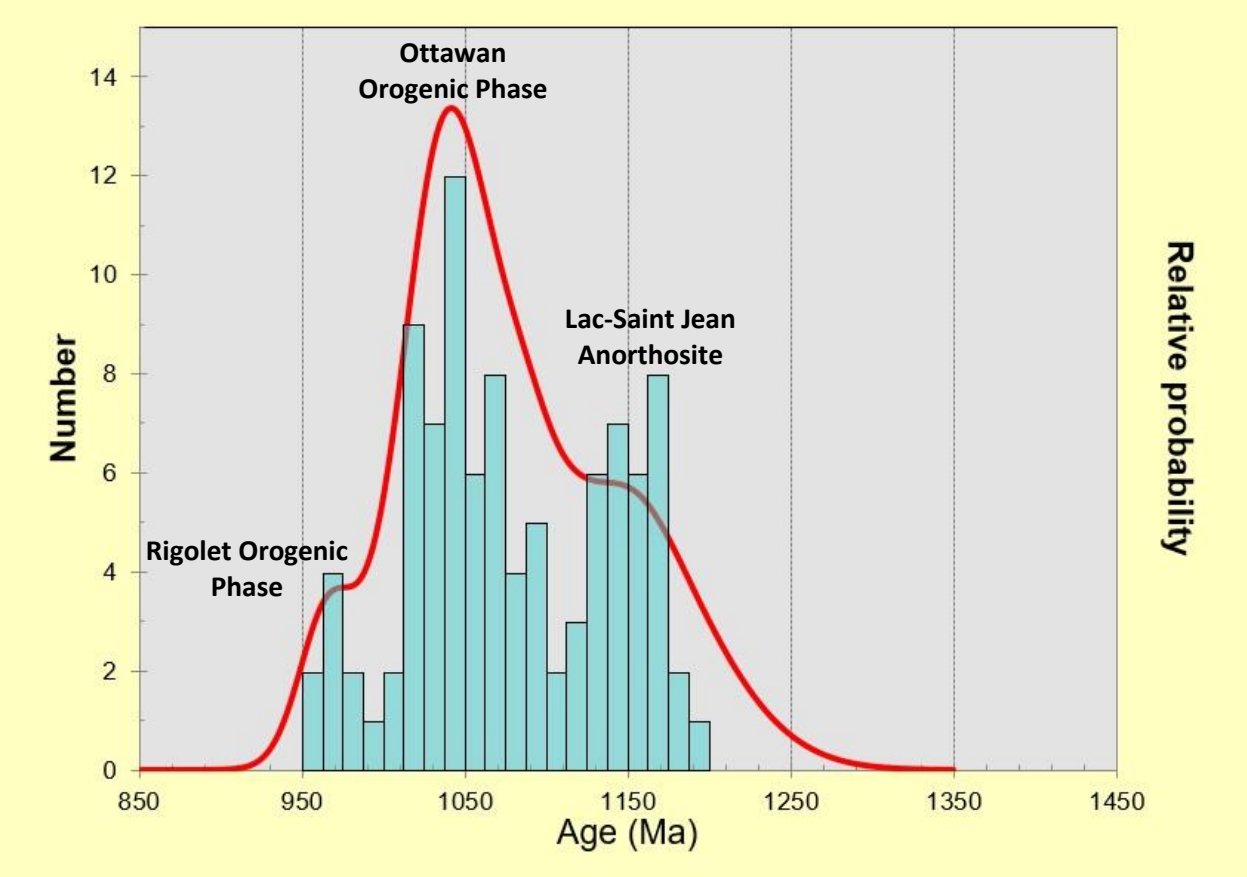

Figure 4.5: Probability distribution diagram of the obtained ages from both terranes showing a trimodal distribution with peaks at 970, 1040, and 1150 Ma.

Figure 4.6 shows the probability distribution of the Cap a l'Est terrane, which appears to have two peaks at 969 ± 13 Ma and 1029.1 ± 8 Ma. The data for the Cap a l'Est terrane was inspected and it was determined that two of the domains measured within two different grains were the cause of the younger peak, while the rest of the data produced the peak at the greater age. These two different age groups were plotted as separate normal distributions shown in Figure 4.7. The lower age group is more tightly constrained as seen by its tight probability density curve, compared to the higher age group which had a few outliers on either end, although it should be noted that the "outliers" on the upper end of the spectrum were from small domains within the core of one of the grains.

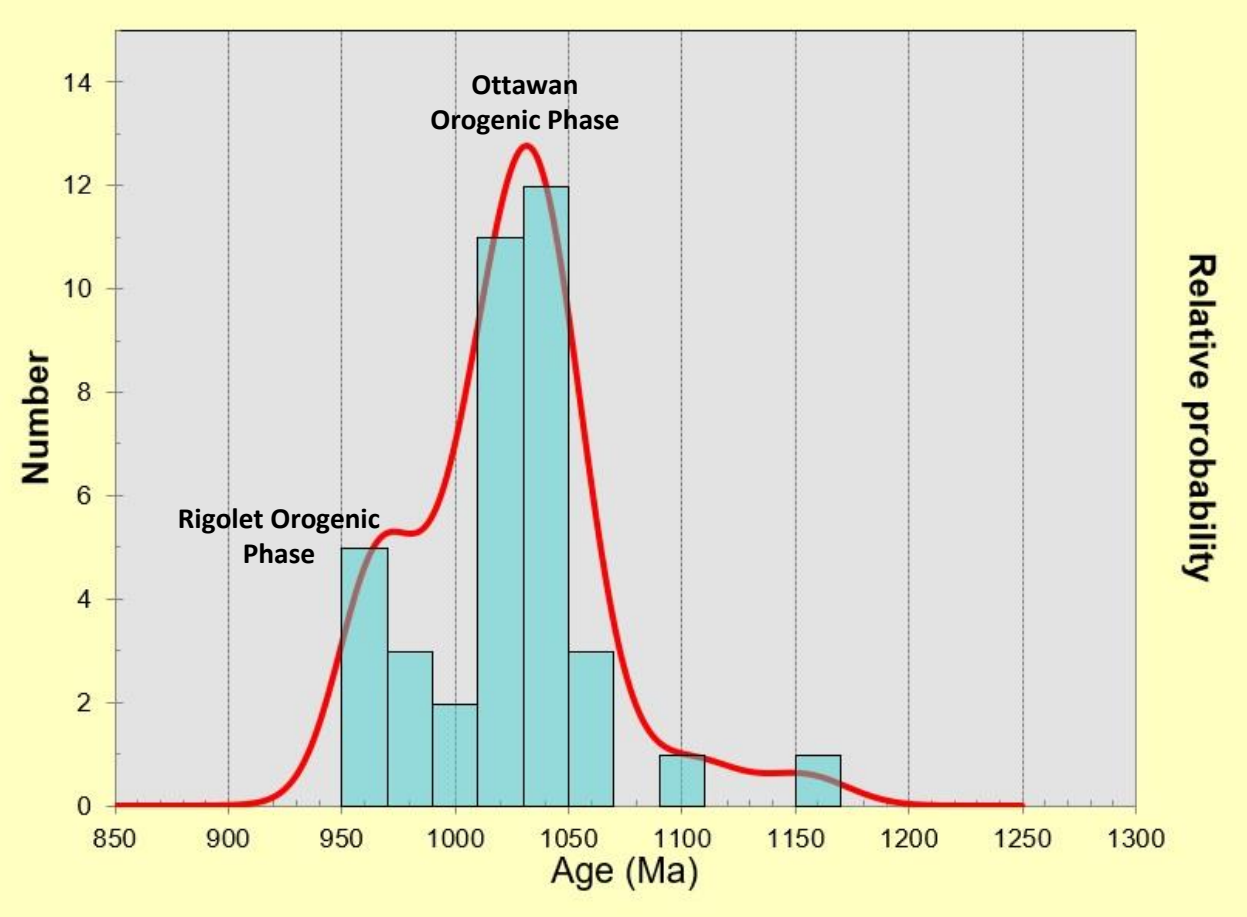

Figure 4.6: Probability distribution diagram of the obtained ages in the Cap a l'Est terrane. Two peaks at 969 ± 13 Ma and 1029.1 ± 8 Ma are present with two outliers greater than 1100 Ma.

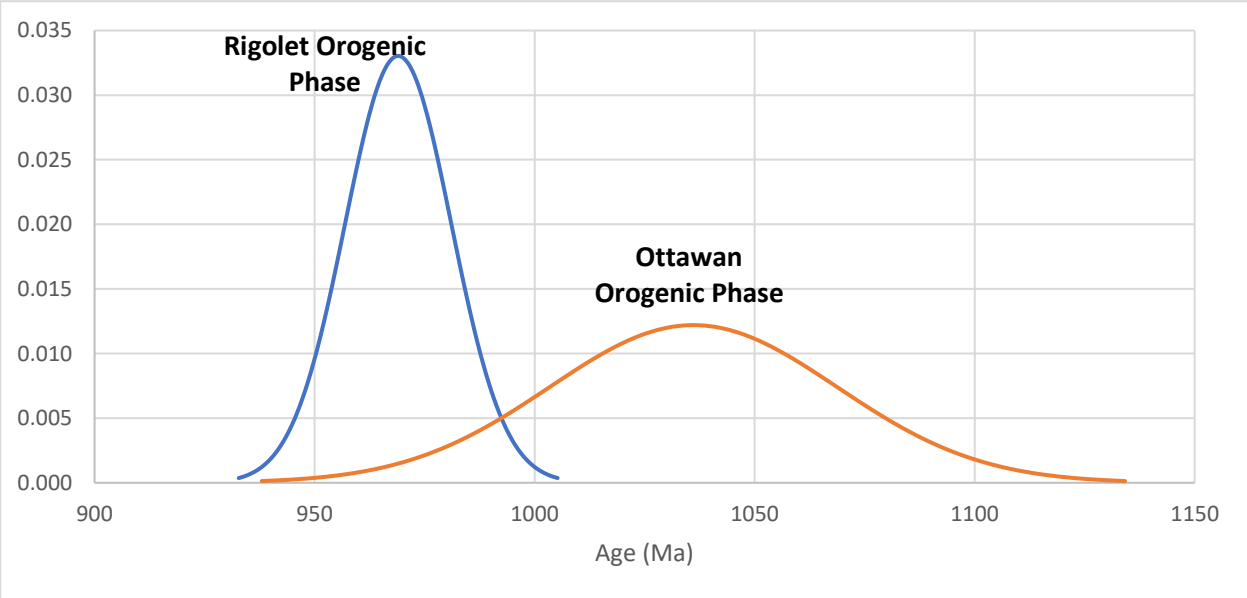

Figure 4.7: Normalized probability distribution of the Cap a l'Est terrane separated into two distinct age groups at 969 ± 13 Ma and 1029.1 ± 8 Ma

Moving onto the Chicoutimi Gneiss Suite, it is seen that there are also two distinct peaks, one at around 1060.1 ± 7.3, while the other is at 1145 ± 16 Ma (Figure 4.8). The peak at ~1060 Ma contains the data that was analysed in this experiment, while the peak at ~1145 Ma contains the majority of the data from the previous analysis (Cox, unpublished data). A probability distribution plot of the two peaks is shown in Figure 4.9. It should be noted that these plots are plotting normalized data and are using the arithmetic mean, as opposed to a weighted average, and are not taking the individual point's errors into effect.

Although there are several distinguishable peaks overall, when looking at a plot of all of the ages (Figure 4.10), it is seen that there is still a wide swath of ages that were observed in both terranes. This makes sense as the periods of metamorphism are caused by orogenic events which last millions to tens of millions of years. The errors of the unpublished data from Cox are

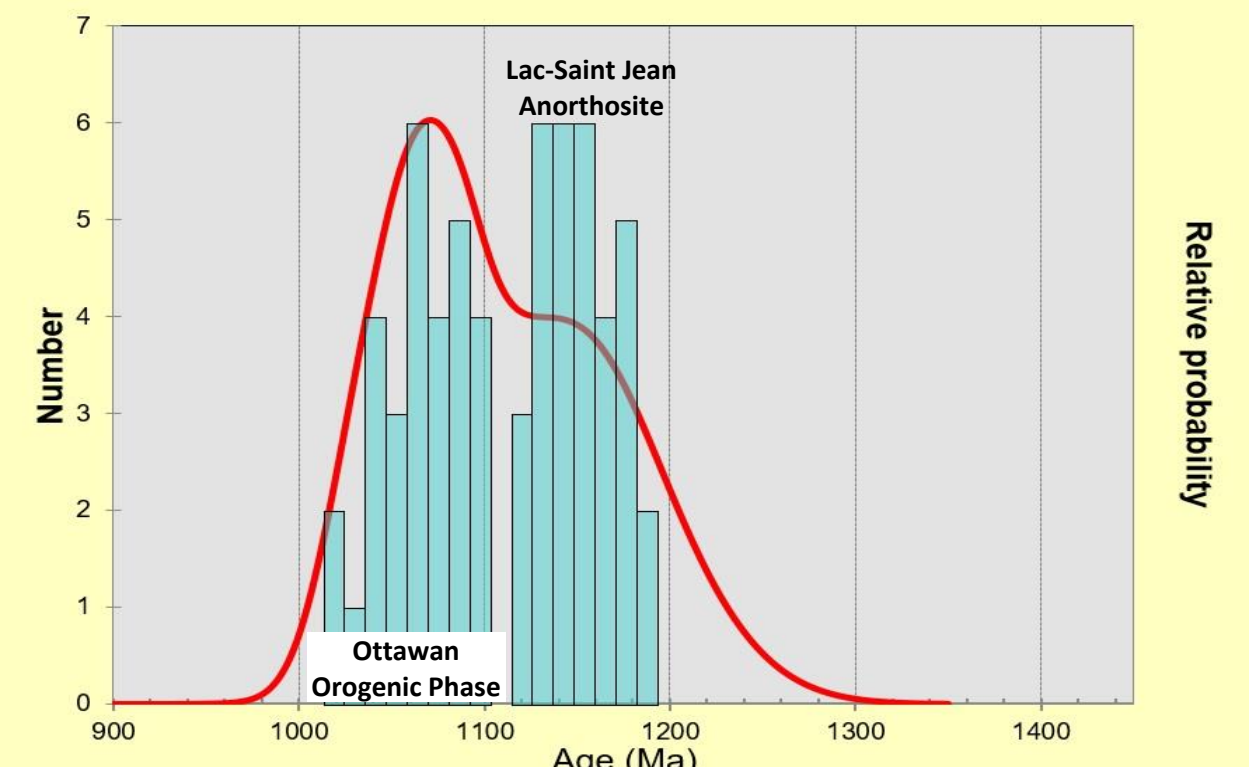

Figure 4.8: Probability distribution diagram of the obtained ages in the Chicoutimi Gneiss Belt. Two peaks at 1060.1 ± 7.3 Ma and ~1145 ± 16 Ma

much bigger than those collected in this study because of the fact that the errors in the unpublished data represent the absolute minimum and maximum ages, whereas here, the 1σ values are used in the plot.

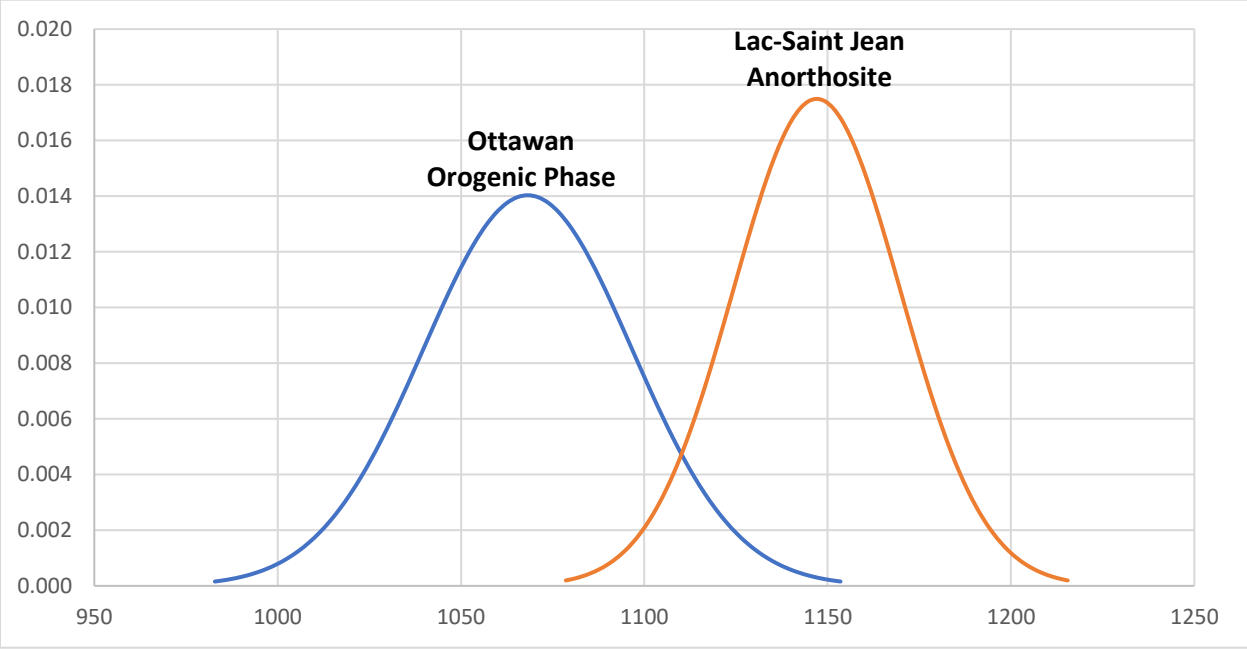

Figure 4.9: Normalized probability distribution of the Chicoutimi Gneiss Belt separated into two distinct age groups at 1060.1 ± 7.3 Ma and ~1145 ± 16 Ma.

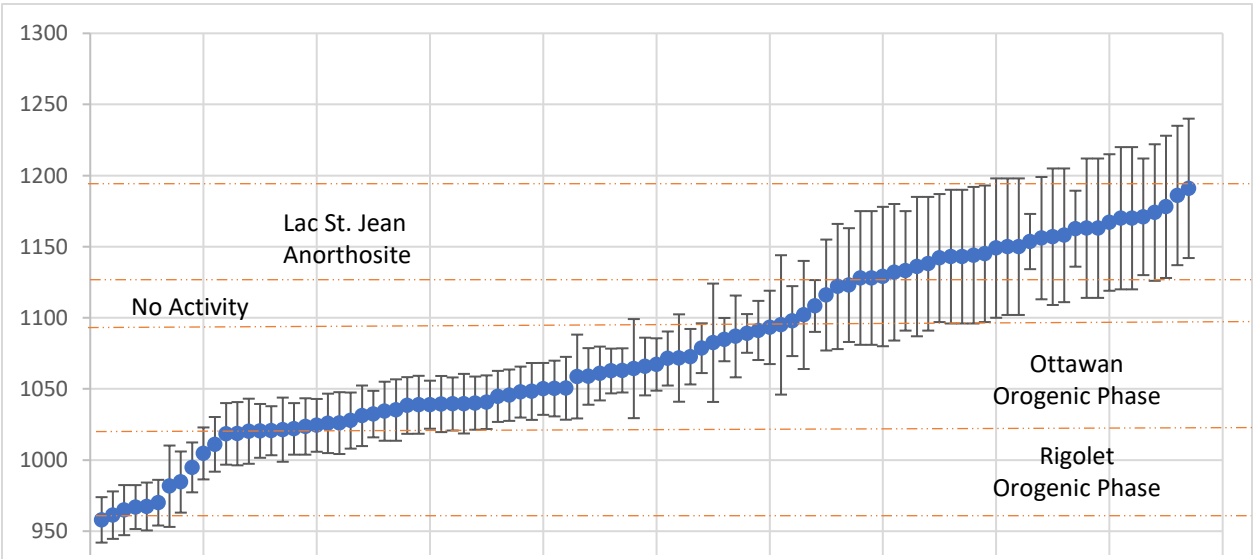

Figure 4.10: Plot of ages obtained ordered from least to greatest. Areas that contain steeper slopes indicate little deformation, or little effect of deformation on the monazite growth.

Chapter 5: Discussion

5.1 Entire Suite

As discussed in Section 4.2, and seen in Figure 4.4, there are three distinct peaks seen throughout the two terranes observed. These three peaks are actually quite consistent with the timing of the different orogenies defined in this region. The data that gave the highest age peak, is presented as a weighted average in Figure 5.1. The average is 1145 ± 16 Ma, which is time at which is around the time at which a) the Shawinigan Orogeny occurred in the Southern region of the Grenville province, and b) the emplacement of the Lac-Saint-Jean-Anorthosite Suite occurred. As for the intermediate aged peak, its data corresponds to the Ottawan orogenic phase of the Grenvillian Orogeny, as defined by Rivers et al. (2008). The lower end of this peak, along with the upper end of the lowest aged peak is thought to correspond to the

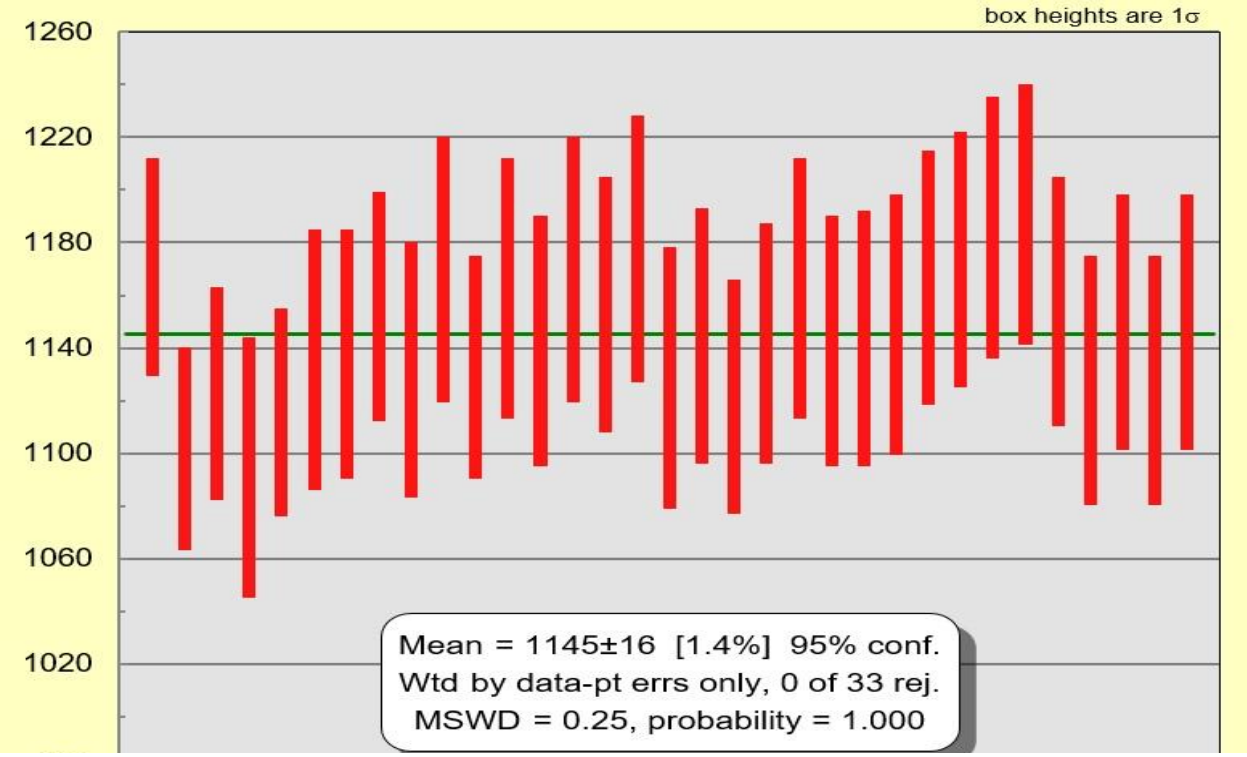

Figure 5.1: Weighted average of the ages that formed the oldest aged peak in the probability distribution plot shown in Figure 4.5

Rigolet orogenic phase of the Grenvillian Orogeny which occurred from ~980 Ma-1010 Ma (Rivers et al., 2008). Most of the points analysed that gave ages younger than 980 Ma, seen in the youngest age peak of Figure 4.5, are thought to be due to lead loss that may have occurred following the end of the Grenvillian Orogeny (specifically the Rigolet orgonic phase). An explanation for lead loss after the orogeny would be that the age preserved in these domains represent growth along the retrograde path (i.e. when temperature is decreasing), as the closure temperature for monazite is ~800˚c (Williams et al., 2007). So, the terrane would have experienced the upper amphibolite into granulite facies metamorphism (>800˚c), then when the rocks began retrogression (cooling) lead loss could have kept occurring until they reached 800˚c.

Three analysed points were omitted from Figure 4.5 as they were several hundred million years older than the rest. Two of these omitted ages are 1545 ± 47 Ma and 1535 ± 47 Ma, these two "outliers" are interpreted to represent monazite growth (potentially xenocrysts inherited) from the basement rock of the complex, which is the Cap de la Mer Amphibolite. This basement rock was dated at 1506 ± 13 Ma by Hébert and van Breemen (2004), which is equal within error to the ages listed here. These grains/ domains from the basement rock may be found in the Chicoutimi Gneiss sample because of melting that occurred due to the prolonged high temperatures and pressures experienced during the Ottawan orogenic phase. The other point that was omitted in Figure 4.4 was 2164 ± 44 Ma, according to the literature there are no suites of rock exposed in this region that are older than the Cap de la Mer amphibolite. So, this age is interpreted as the age of an undissolved xenocryst that was in place before the formation of the gabbro which formed the protolith of the Cap de la Mer Amphibolite.

Figure 4.10 shows that there was a wide range of ages observed from the analysis. There are two small areas which show steeper slopes which correspond to the ages of ~980-1020 Ma and ~1100-1130 Ma. The first of the two suggests that we have very little ages from the Rigolet orogenic phase, which perhaps means that its affect was not as significant on this suite compared to that from the Ottawan orogenic phase. This could also suggest that these lower ages are just due to lead loss (also mentioned later). The second of the two (~1100-1130 Ma) is consistent with the fact that there is no orogenic/ metamorphic activity occurring at that time in the area (other than localized emplacement of plutons), meaning that there in fact should be a minimal of ages in that range. The sections with a shallower slope suggest that there is more age data from that range, the two predominate ranges with a shallow slope are ~1020-1100 Ma and ~1130-1190 Ma. These two ranges correspond to the Ottawan orogenic phase and the emplacement of the Lac-Saint-Jean Anorthosite Complex, respectively.

5.2 Terrane Ages

5.2.1 Chicoutimi Gneiss Belt

When looking at Figure 4.8 it is seen that the Chicoutimi Gneiss suite shows a broad range of ages, and (as mentioned before) two distinct peaks of ages. The lower aged peak is at 1060 ± 7.3 Ma, with its spread ranging from ~1020-1100 Ma which corresponds to the Ottawan orogenic phase that occurred from 1090-1020 Ma, defined by Rivers et al. (2008). The higher aged peak has an average age of 1145 ± 16 Ma as mention in Section 5.1 and corresponds to the age of the emplacement of the Lac-Saint-Jean Anorthosite Complex as mentioned previously and the associated deformation that occurred with it, as the Chicoutimi Gneiss Belt is

in very close proximity to it (<1 km in some places, see Figure 1.1). This close proximity would have caused partial melting and therefore an opportunity for these monazite crystals to form. These ages also correspond to the age of the Shawinigan Orogeny, and may mean that most previous studies in the area were only able to find the metamorphic overprint from the Ottawan orogenic phase. However, it is the former that is most likely in this case, as the thrusting and deformation associated with the Shawinigan Orogeny is only known to have been present in the Southeastern portions of the Grenville Province (as mention in Section 2.1).

All of the analysed points that yielded an age of ~1145 Ma were found within the garnet which were placed within leucosomes, Pyle et al. (2001) mentions that unless extremely high-grade metamorphism is reached, monazite inclusions in garnet will not re-equilibrate with the surrounding garnet over a geologically relevant time frame. This would be the reason these ages are not found in monazite grains of the matrix, with the exception of small domains found within larger grains as mentioned in Section 5.2.2. The yttrium content in these analyses were also lower (on average), suggesting that the growth of these monazites must have occurred at the same time the garnets were forming. The process that would have formed this garnet, and the leucosomes is shown in Equation 2. All the analysed points in the Chicoutimi Gneiss Belt gave ages above 1020 Ma, suggesting that it was not significantly affected by the metamorphism associated with the Rigolet orogenic phase.

$$\text{Biotite} + \text{sillimanite} + \text{plagioclase} + \text{quartz} = \text{garnet} + \text{k-feldspar} + \text{melt} \qquad (2)$$

5.2.2 Cap a l'Est Terrane

Figure 4.6 in Section 4.2 shows that the Cap a l'Est terrane also displays two age peaks, with a trail of higher ages. The higher peak is at 1029.1 ± 8 Ma which agrees with the ages obtained by Hébert and van Breemen (2004), who interpreted this age to be a result of lead loss during the Ottawan orogenic phase. This lead loss would be due to re-equilibration or new monazite growth. The low peak yields ages younger than the Rigolet orogeny (969 ± 13 Ma), there are however no defined metamorphic events that occurred at this period of time, so a possible explanation would be lead loss, once again due to re-equilibration of the monazite, as the two domains that displayed these ages were overgrowths on older cores.

There were two outliers in the data at 1108 ± 18 Ma and 1153 ± 19 Ma, the first of the two could potentially belong to the Ottawan orogenic, although it was measured within the same compositional domain (Thorium depleted, dark blue, domains seen in Figure 3.1) as the latter point which has an age consistent with that of the emplacement of the Lac-Saint-Jean Anorthosite Complex. The compositional domain that hosted these ages were small and separated throughout the monazite grain hosting them. As none of the grains analysed here were in garnet, all of them were susceptible to overprinting during the Ottawan orogenic phase, this lasted ~50 Ma and involved high temperatures and pressures meaning that little relict monazite (in the matrix) from ~1145 Ma would have remained in equilibrium.

Chapter 6: Conclusion and Recommendations

6.1 Conclusion

After thorough analysis of monazite grains found throughout samples collected from the Chicoutimi Gneiss Belt, two distinct metamorphic ages were found through the use of U-Th-Pb dating. An older age of ~1145 Ma (~1120-1190 Ma range) was found from monazite grains present as inclusions in large garnet porphyroblasts. The garnet protected these monazites, presumably formed by the emplacement of the Lac-Saint-Jean Anorthosite Complex, to be preserved and not overprinted by the amphibolite facies metamorphism experienced during the Ottawan orogenic phase. The lower age was ~1050 Ma (~1020-1100 Ma range), which is most definitely explained by the Ottawan orogenic phase of the Grenvillian Orogeny. Therefore, this belt experienced two separate metamorphic events, the second of which overprinted much evidence of the first (aside from the grains within the garnet).

Samples from the Cap a l'Est terrane in the same area were also analysed, and were also found to have two distinct age groups. The older of the two (average of ~1030 Ma) agrees with previous ages obtained via dating of zircons in other studies, and are thought to represent lead loss (or monazite growth/ re-equilibration) during the Ottawan orogenic phase. The younger of the two could possibly represent the effects of the Rigolet orogenic phase, or post-Grenvillian lead loss.

6.2 Recommendations

One recommendation for future projects involving the dating of this suite of rocks would be to analyse more samples to look for more monazites within the garnet. This could potentially show even older monazites preserved within the rocks (potentially detrital grains). An analysis of more grains in general would be highly recommended, with an emphasis on larger grains, as the more analyses completed per domain, the more certainty there is in the answer.

Attempting to use LA-ICPMS technique to analyse not only monazite, but also zircon would be recommended as it produces more accurate ages from isotopic analyses. This along with the dates from the EPMA method would provide more confidence in the obtained ages. It is cautioned however that this method is very destructive and the section you wish to analyse should be one in which you do not plan to go back to in the future.

References

Gagne, S. 2004. Textural, Chemical and Age variation in Monazites of the Paleoproterozoic Lonstaff Bluff Formation, Central Baffin Island, Nunavut. M.Sc Thesis, Dalhousie University, Halifax, Nova Scotia.

Hébert, C., van Breemen, O. (2004). Mesoproterozoic basement of the Lac St. Jean Anorthosite Suite and younger Grenvillian intrusions in the Saguenay region, Quebec: Structural relationships and U-Pb geochronology. *Geological Society of America* **197**, 65-79.

Hetherington, C.J., Jercinovic, M.J., Williams, M.L., Mahan, K. (2008). Understanding geologic processes with xenotime: Composition, chronology, and a protocol for electron probe microanalysis. *Chemical Geology* **254**, 133-147.

Higgins, M.D., van Breemen, O. (1992). The age of the Lac-Saint-Jean Anorthosite Complex and associated mafic rocks, Grenville Province, Canada. *Canadian Journal of Earth Sciences* **29**, 1412-1423.

Higgins, D.H., Ider, M., van Breemen, O. (2002). U-Pb ages of plutonism, wollastonite formation, and deformation in the central part of the Lac-Saint-Jean anorthosite suite. *Canadian Journal of Earth Sciences* **39**, 1093-1105.

Jercinovic MJ, Williams ML. (2005). Analytical perils (and progress) in electron microprobe trace element analysis applied to geochronology: background acquisition interferences, and beam irradiation effects*. American Mineralogist* **90**, 526–46

McLelland, J.M., Selleck, B.W., Bickford, M.E. (2010). Review of the Proterozoic evolution of the Grenville Province, its Adirondack outlier, and the Mesoproterozoic inliers of the Appalachians. *Geological Society of America* **206**, 1-29.

Montel J, Foret S, Veschambre M, Nicollet C, Provost A. (1996). Electron microprobe dating of monazite. *Chem. Geol.* **131**, 37–53

Pyle, J.M., Spear, F.S., Wark, D.A. (2002). Electron microprobe analysis of REE in apatite, monazite, and xenotime: Protocols and pitfalls. *Reviews in Mineralogy and Geochemistry* **48**, 337-362.

Pyle, J.M., Spear, F.S., Rudnick, R.L., McDonough, W.F. (2001). Monazite-xenotime-garnet equilibrium in metapelites and a new monazite-garnet thermometer. *Journal of Petrology* **42**, 2083-2107.

Rivers, T. (2008). Assembly and preservation of lower, mid, and upper orogenic crust in the Grenville Province—Implications for the evolution of large hot long-duration orogens. *Precambrian Research* **167**, 237-259.

Tollo, R.P., Corriveau, L., McLelland, J., Bartholomew, M.J. (2004). Proterozoic tectonic evolution of the Grenville orogen in North America: An introduction. *Geological Society of America* **197**, 1-18.

Williams, M.L., Goncalves, P., Jercinovic, M.J., Maham, K. (2006). Format and philosophy for collecting, compiling, and reporting microprobe monazite ages. *Chemical Geology* **225**, 1-15.

Williams, M.L., Jercinovic, M.J., Hetherington, C.J. (2007). Microprobe monazite geochronology: Understanding geologic processes by integrating composition and chronology. *Annual Review of Earth and Planetary Sciences* **35**, 137-175.

Appendices

Appendix 1: Analytical Conditions for Major Element

Element	Ca	Si	P	S	Nd	Pr	Ce	La	Th	U	Dy	Y	Sm	Gd
X-ray Measured	kα	kα	kα	kα	lβ	lβ	lα	lα	mα	mβ	lα	lα	lβ	lβ
Channel	1	4	1	1	5	5	2	2	1	1	2	4	5	5
Crystal	PETJ	TAP	PETJ	PETJ	LiFH	LiFH	LiF	LiF	PETJ	PETJ	LiF	TAP	LiFH	LiFH
PHA Gain	16	32	16	16	32	32	32	32	16	16	32	16	32	32
High V (V)	1718	1700	1730	1708	1730	1750	1780	1750	1682	1690	1730	1756	1730	1610
Base Line (V)	0.7	1	0.7	1	1	0.7	0.7	0.7	1	2	0.7	1	1	1
Window (V)	9.3	9.3	5	9.3	8	9.3	9.3	9.3	5	5	9.3	6	8	9
Diff/ Int	Int	Diff	Diff	Diff	Diff	Diff	Diff	Diff	Diff	Diff	Diff	Diff	Diff	Diff

Appendix 2: Major Element Data

3NO* MNT4 ZONE1													
"CaO"	"SiO2"	"P2O5"	"SO3"	"Nd2O3"	"Pr2O3"	"Ce2O3"	"La2O3"	"ThO2"	"UO2"	"Dy2O3"	"Y2O3"	"Sm2O3"	"Gd2O3"
0.803	0.607	29.116	0.027	10.946	3.417	26.338	11.270	5.747	0.353	1.128	3.522	2.175	1.856
3NO* MNT4 ZONE2													
"CaO"	"SiO2"	"P2O5"	"SO3"	"Nd2O3"	"Pr2O3"	"Ce2O3"	"La2O3"	"ThO2"	"UO2"	"Dy2O3"	"Y2O3"	"Sm2O3"	"Gd2O3"
1.135	0.744	28.979	-0.009	10.798	3.292	25.892	11.916	7.926	0.517	0.802	2.052	2.336	2.112
3NO* MNT4 ZONE3													
"CaO"	"SiO2"	"P2O5"	"SO3"	"Nd2O3"	"Pr2O3"	"Ce2O3"	"La2O3"	"ThO2"	"UO2"	"Dy2O3"	"Y2O3"	"Sm2O3"	"Gd2O3"
0.934	0.773	29.059	0.050	10.720	3.239	25.829	11.997	6.670	0.306	0.864	3.004	2.070	1.949
3NO* MNT5 ZONE1													
"CaO"	"SiO2"	"P2O5"	"SO3"	"Nd2O3"	"Pr2O3"	"Ce2O3"	"La2O3"	"ThO2"	"UO2"	"Dy2O3"	"Y2O3"	"Sm2O3"	"Gd2O3"
1.019	1.382	28.664	-0.015	10.753	3.252	24.031	10.429	10.232	0.404	0.858	3.732	2.247	2.008
3NO* MNT5 ZONE2													
"CaO"	"SiO2"	"P2O5"	"SO3"	"Nd2O3"	"Pr2O3"	"Ce2O3"	"La2O3"	"ThO2"	"UO2"	"Dy2O3"	"Y2O3"	"Sm2O3"	"Gd2O3"
1.216	0.577	29.994	0.004	10.905	3.329	24.182	10.413	7.613	0.319	1.019	4.115	2.274	2.207
3NO* MNT5 ZONE3													
"CaO"	"SiO2"	"P2O5"	"SO3"	"Nd2O3"	"Pr2O3"	"Ce2O3"	"La2O3"	"ThO2"	"UO2"	"Dy2O3"	"Y2O3"	"Sm2O3"	"Gd2O3"
1.344	0.070	30.408	0.568	11.239	3.409	27.566	12.292	3.826	0.768	0.962	2.819	2.213	1.731
2NO MNT1													
"CaO"	"SiO2"	"P2O5"	"SO3"	"Nd2O3"	"Pr2O3"	"Ce2O3"	"La2O3"	"ThO2"	"UO2"	"Dy2O3"	"Y2O3"	"Sm2O3"	"Gd2O3"
0.899	1.220	28.803	-0.025	11.279	3.439	24.670	10.674	9.013	0.233	1.108	3.751	2.361	2.281
2NO* MNT1													
"CaO"	"SiO2"	"P2O5"	"SO3"	"Nd2O3"	"Pr2O3"	"Ce2O3"	"La2O3"	"ThO2"	"UO2"	"Dy2O3"	"Y2O3"	"Sm2O3"	"Gd2O3"
1.254	0.737	29.289	-0.066	10.553	3.293	24.988	11.370	7.921	0.595	0.913	3.066	2.132	2.067
2NO* MNT2 ZONE1													
"CaO"	"SiO2"	"P2O5"	"SO3"	"Nd2O3"	"Pr2O3"	"Ce2O3"	"La2O3"	"ThO2"	"UO2"	"Dy2O3"	"Y2O3"	"Sm2O3"	"Gd2O3"
0.835	1.262	27.872	0.034	11.180	3.383	25.624	11.171	8.574	0.298	0.803	3.334	2.111	1.918

2NO* MNT2 ZONE2													
"CaO"	"SiO2"	"P2O5"	"SO3"	"Nd2O3"	"Pr2O3"	"Ce2O3"	"La2O3"	"ThO2"	"UO2"	"Dy2O3"	"Y2O3"	"Sm2O3"	"Gd2O3"
0.790	1.773	27.280	-0.002	10.859	3.399	24.691	10.285	9.625	0.369	0.865	3.523	2.099	1.840
18NO* MNT1 ZONE1													
"CaO"	"SiO2"	"P2O5"	"SO3"	"Nd2O3"	"Pr2O3"	"Ce2O3"	"La2O3"	"ThO2"	"UO2"	"Dy2O3"	"Y2O3"	"Sm2O3"	"Gd2O3"
0.638	1.708	27.260	0.012	10.981	3.578	25.404	11.221	8.970	0.331	0.748	3.186	2.041	1.881
18NO* MNT1 ZONE2													
"CaO"	"SiO2"	"P2O5"	"SO3"	"Nd2O3"	"Pr2O3"	"Ce2O3"	"La2O3"	"ThO2"	"UO2"	"Dy2O3"	"Y2O3"	"Sm2O3"	"Gd2O3"
1.396	0.486	29.894	0.065	10.552	3.361	25.322	11.922	7.882	0.587	0.927	3.003	1.985	1.876
18NO* MNT3													
"CaO"	"SiO2"	"P2O5"	"SO3"	"Nd2O3"	"Pr2O3"	"Ce2O3"	"La2O3"	"ThO2"	"UO2"	"Dy2O3"	"Y2O3"	"Sm2O3"	"Gd2O3"
1.169	1.351	29.301	0.017	10.036	3.282	24.100	10.565	10.243	0.487	0.981	3.663	2.251	1.954
3NO MNT1 ZONE1													
"CaO"	"SiO2"	"P2O5"	"SO3"	"Nd2O3"	"Pr2O3"	"Ce2O3"	"La2O3"	"ThO2"	"UO2"	"Dy2O3"	"Y2O3"	"Sm2O3"	"Gd2O3"
0.932	0.157	30.560	0.034	12.610	3.713	28.808	12.846	4.254	0.554	0.557	1.100	2.272	1.913
3NO MNT1 ZONE2													
"CaO"	"SiO2"	"P2O5"	"SO3"	"Nd2O3"	"Pr2O3"	"Ce2O3"	"La2O3"	"ThO2"	"UO2"	"Dy2O3"	"Y2O3"	"Sm2O3"	"Gd2O3"
0.785	0.002	30.738	-0.016	12.331	3.377	29.921	12.139	1.701	1.714	0.461	2.134	2.161	1.834
3NO MNT2													
"CaO"	"SiO2"	"P2O5"	"SO3"	"Nd2O3"	"Pr2O3"	"Ce2O3"	"La2O3"	"ThO2"	"UO2"	"Dy2O3"	"Y2O3"	"Sm2O3"	"Gd2O3"
0.768	0.105	30.720	0.007	13.318	3.933	28.264	12.230	3.334	0.660	0.555	1.199	2.521	2.110
3NO MNT3													
"CaO"	"SiO2"	"P2O5"	"SO3"	"Nd2O3"	"Pr2O3"	"Ce2O3"	"La2O3"	"ThO2"	"UO2"	"Dy2O3"	"Y2O3"	"Sm2O3"	"Gd2O3"
1.050	0.640	30.624	0.027	11.273	3.374	26.794	12.262	6.404	0.954	0.718	2.596	1.889	1.391
3NO MNT4													
"CaO"	"SiO2"	"P2O5"	"SO3"	"Nd2O3"	"Pr2O3"	"Ce2O3"	"La2O3"	"ThO2"	"UO2"	"Dy2O3"	"Y2O3"	"Sm2O3"	"Gd2O3"
0.911	0.163	30.620	0.013	12.782	3.761	29.008	13.067	3.890	0.590	0.514	1.031	2.464	1.877

4NO* MNT1													
"CaO"	"SiO2"	"P2O5"	"SO3"	"Nd2O3"	"Pr2O3"	"Ce2O3"	"La2O3"	"ThO2"	"UO2"	"Dy2O3"	"Y2O3"	"Sm2O3"	"Gd2O3"
0.681	0.324	30.420	-0.022	12.051	3.605	27.581	12.643	3.112	0.736	0.880	3.086	2.280	2.151
4NO* MNT5 ZONE2													
"CaO"	"SiO2"	"P2O5"	"SO3"	"Nd2O3"	"Pr2O3"	"Ce2O3"	"La2O3"	"ThO2"	"UO2"	"Dy2O3"	"Y2O3"	"Sm2O3"	"Gd2O3"
0.384	0.478	30.343	0.015	11.959	3.497	28.506	14.129	2.621	0.592	0.807	2.855	2.123	1.681
4NO*MNT7 ZONE1													
"CaO"	"SiO2"	"P2O5"	"SO3"	"Nd2O3"	"Pr2O3"	"Ce2O3"	"La2O3"	"ThO2"	"UO2"	"Dy2O3"	"Y2O3"	"Sm2O3"	"Gd2O3"
0.061	0.462	33.289	0.016	0.903	0.719	0.346	-0.034	0.355	1.448	5.831	41.426	0.919	4.962
4NO*MNT7 ZONE2													
"CaO"	"SiO2"	"P2O5"	"SO3"	"Nd2O3"	"Pr2O3"	"Ce2O3"	"La2O3"	"ThO2"	"UO2"	"Dy2O3"	"Y2O3"	"Sm2O3"	"Gd2O3"
0.332	0.298	30.624	0.012	11.686	3.598	28.409	14.193	1.793	0.481	0.907	3.266	2.033	2.203
5NO* MNT1													
"CaO"	"SiO2"	"P2O5"	"SO3"	"Nd2O3"	"Pr2O3"	"Ce2O3"	"La2O3"	"ThO2"	"UO2"	"Dy2O3"	"Y2O3"	"Sm2O3"	"Gd2O3"
0.970	0.107	30.810	0.003	12.166	3.770	29.325	13.159	4.254	0.437	0.311	0.911	2.231	1.696

Appendix 3: Minor Element and Age Data

Grain/Zone	Age (Ma)	ERROR 1σ (Ma)	ERROR 2σ (Ma)	Th (ppm)	Th error (%)	U (ppm)	U error (%)	Y (ppm)	Y error (%)	Pb (ppm)	Pb error (%)
3NO*MNT4Z2P1	966.93	15.44	30.88	80260	0.18	4050	1.30	19310	0.18	4130	0.89
3NO*MNT4Z2P2	964.78	17.61	35.22	75460	0.19	3310	1.53	17590	0.20	3800	0.95
3NO*MNT4Z2P3	957.92	15.97	31.94	77820	0.18	3820	1.36	20450	0.18	3950	0.93
3NO*MNT4Z2P4	967.33	16.83	33.66	76650	0.18	3560	1.44	18340	0.19	3900	0.93
3NO*MNT4Z3P1	1039.99	18.69	37.39	76010	0.19	3350	1.54	29250	0.13	4140	0.89
3NO*MNT4Z3P2	1018.52	22.24	44.47	65590	0.20	2600	1.90	26090	0.14	3450	1.04
3NO*MNT4Z3P3	981.58	28.59	57.19	74010	0.19	1570	2.71	20320	0.17	3540	1.03
2NOMNT1P1	1050.44	22.09	44.18	78820	0.18	2570	1.89	28830	0.14	4190	0.89
2NOMNT1P2	1027.73	19.72	39.45	88850	0.17	2850	1.72	29940	0.13	4610	0.82
2NO*MNT1P1	1032.30	16.36	32.72	71740	0.19	4300	1.27	25530	0.15	4060	0.90
2NO*MNT1P2	1047.77	17.91	35.82	72150	0.19	3730	1.42	27450	0.14	4050	0.91
2NO*MNT1P3	1039.61	20.95	41.90	68180	0.20	2930	1.74	25970	0.14	3700	0.98
3NO*MNT5Z3P1	1108.30	18.21	36.42	32400	0.31	6290	0.97	19540	0.18	2730	1.27
3NO*MNT5Z3P2	1153.60	19.42	38.84	28680	0.34	6160	0.99	19350	0.18	2630	1.30
3NO*MNT5Z2P1	1031.10	21.29	42.57	68620	0.20	2810	1.79	30950	0.13	3670	0.99
3NO*MNT5Z2P2	1064.27	34.84	69.68	46750	0.25	1590	2.96	18000	0.19	2530	1.36
3NO*MNT5Z2P3	1020.24	22.88	45.76	61650	0.21	2580	1.94	27960	0.14	3270	1.09
3NO*MNT5Z1P1	1020.49	18.92	37.84	94900	0.16	2930	1.66	27420	0.14	4870	0.78
3NO*MNT5Z1P2	1011.03	19.21	38.42	91370	0.17	2860	1.70	26230	0.14	4650	0.81
3NO*MNT5Z1P3	1018.38	21.66	43.31	83130	0.18	2460	1.92	22690	0.16	4240	0.87
3NO*MNT5Z1P4	1004.65	18.27	36.55	96810	0.16	3000	1.63	25090	0.15	4890	0.78
2NO*MNT2Z1P1	984.51	21.50	43.00	104440	0.15	2210	2.03	15270	0.21	5010	0.77
2NO*MNT2Z1P2	1025.96	21.74	43.48	105040	0.15	2300	1.97	15660	0.21	5270	0.73
2NO*MNT2Z2P1	1035.14	21.60	43.20	88890	0.22	2500	1.90	27040	0.14	4590	0.81
2NO*MNT2Z2P2	1034.31	20.75	41.51	92700	0.17	2590	1.83	26190	0.14	4780	0.79
2NO*MNT2Z2P3	1021.34	22.55	45.11	80150	0.18	2370	2.00	28210	0.14	4100	0.90
18NO*MNT1Z1P1	1058.71	29.47	58.94	68680	0.20	1750	2.58	23530	0.16	3600	1.00
18NO*MNT1Z1P2	1045.58	18.05	36.10	94530	0.16	3260	1.53	25680	0.15	5030	0.76
18NO*MNT1Z2P1	994.81	17.54	35.08	69550	0.16	4900	1.57	23730	0.15	3900	0.77

18NO*MNT1Z2P2	970.00	16.07	32.13	63120	0.21	4530	1.25	21530	0.17	3460	1.05
18NO*MNT1Z2P3	961.25	16.68	33.37	57630	0.22	4410	1.28	20690	0.17	3170	1.13
18NO*MNT3P1	1023.60	19.83	39.65	83430	0.18	2860	1.72	26860	0.14	4340	0.85
18NO*MNT3P2	1025.77	20.90	41.80	80660	0.18	2670	1.82	26330	0.14	4190	0.88
18NO*MNT3P3	1038.84	20.37	40.74	85740	0.17	2760	1.76	26350	0.14	4500	0.83
18NO*MNT3P4	1038.34	19.93	39.86	87630	0.17	2840	1.72	27160	0.14	4600	0.81
18NO*MNT3P5	1044.74	17.95	35.90	95880	0.16	3260	1.53	29940	0.13	5090	0.75
3NOMNT2	1065.73	20.28	40.57	37020	0.29	4530	1.26	11020	0.28	2550	1.39
3NOMNT3P1	1078.64	17.50	35.00	36260	0.29	6220	1.00	24290	0.15	2830	1.23
3NOMNT3P2	1091.11	20.80	41.59	44720	0.26	4020	1.44	21540	0.17	2910	1.21
3NOMNT3P3	1084.67	15.21	30.43	43510	0.26	7310	0.87	22040	0.16	3390	1.05
3NOMNT1Z1	1063.01	15.54	31.08	33240	0.31	8330	0.79	19510	0.18	2990	1.18
3NOMNT1Z2P1	1024.38	18.56	37.12	40420	0.27	4880	1.19	12900	0.25	2660	1.32
3NOMNT1Z2P2	1040.65	18.86	37.72	41220	0.27	4680	1.22	8200	0.36	2710	1.29
3NOMNT1Z2P3	1060.82	18.92	37.84	42490	0.26	4700	1.23	8380	0.35	2830	1.25
3NOMNT1Z2P4	1020.60	17.24	34.49	35460	0.29	6210	0.97	10140	0.30	2630	1.33
3NOMNT4P1	1058.77	19.90	39.80	39420	0.28	4420	1.29	8740	0.34	2630	1.32
3NOMNT4P2	1039.36	19.73	39.47	39960	0.27	4390	1.30	8310	0.36	2600	1.34
4NO*MNT1P1	1089.01	13.61	27.22	30290	0.33	11430	0.58	27590	0.14	3450	1.04
4NO*MNT1P2	1062.60	15.74	31.48	41980	0.26	6690	0.90	26860	0.14	3140	1.13
5NO*MNT1P1	1071.37	19.00	38.00	41610	0.27	4660	1.22	9170	0.33	2810	1.24
5NO*MNT1P2	1048.21	20.00	39.99	42140	0.26	4100	1.36	7830	0.37	2680	1.30
5NO*MNT1P3	1039.41	18.67	37.34	42970	0.26	4560	1.24	8030	0.36	2770	1.26
5NO*MNT1P4	1067.19	18.41	36.83	42980	0.26	4810	1.19	9130	0.33	2890	1.21
5NO*MNT1P5	1050.01	18.25	36.50	41190	0.27	4960	1.15	9630	0.31	2780	1.26
5NO*MNT1P6	1072.64	19.51	39.02	43420	0.26	4290	1.30	7350	0.40	2840	1.23
5NO*MNT1P7	1050.26	19.59	39.18	42660	0.26	4220	1.32	7120	0.41	2730	1.27
4NO*MNT5P1	1097.67	24.59	49.18	10110	0.72	7240	0.87	38080	0.11	1750	1.92
4NO*MNT5P2	1162.64	26.71	53.42	9270	0.77	6750	0.93	36750	0.12	1730	1.94
4NO*MNT7Z1P1	1082.45	41.61	83.23	2790	2.16	14320	0.49	301220	0.03	2560	3.13
4NO*MNT7Z1P2	1071.71	30.72	61.44	2500	2.37	13020	0.53	304800	0.03	2300	1.51

4NO*MNT7Z2P1	1093.25	25.79	51.59	17810	0.47	4750	1.22	25850	0.15	1700	1.95
4NO*MNT7Z2P2	1086.90	28.75	57.49	16590	0.49	4050	1.42	24100	0.15	1510	2.17
3NO*MNT4Z1P1	1021.89	18.12	36.23	59600	0.21	3840	1.41	0	-1.41	3380	1.04
3NO*MNT4Z1P2	1038.90	16.89	33.77	64640	0.20	4230	1.29	0	-1.07	3740	0.95
GSC STND 1	504.83	12.89	25.78	68130	0.20	3040	1.68	3750	0.70	1770	1.90
GSC STND 2	499.34	12.98	25.96	66860	0.20	3150	1.65	3760	0.70	1730	1.99
GSC STND 3	508.50	13.08	26.17	68870	0.20	3040	1.70	3780	0.70	1800	1.91
GSC STND 4	489.13	12.61	25.22	69410	0.20	3150	1.64	3690	0.72	1750	1.97
GSC STND 5	501.58	12.98	25.96	68990	0.20	3070	1.68	3780	0.71	1780	1.94

Location of analyses within grains shown in Appendix 5

Appendix 4: BSE Images

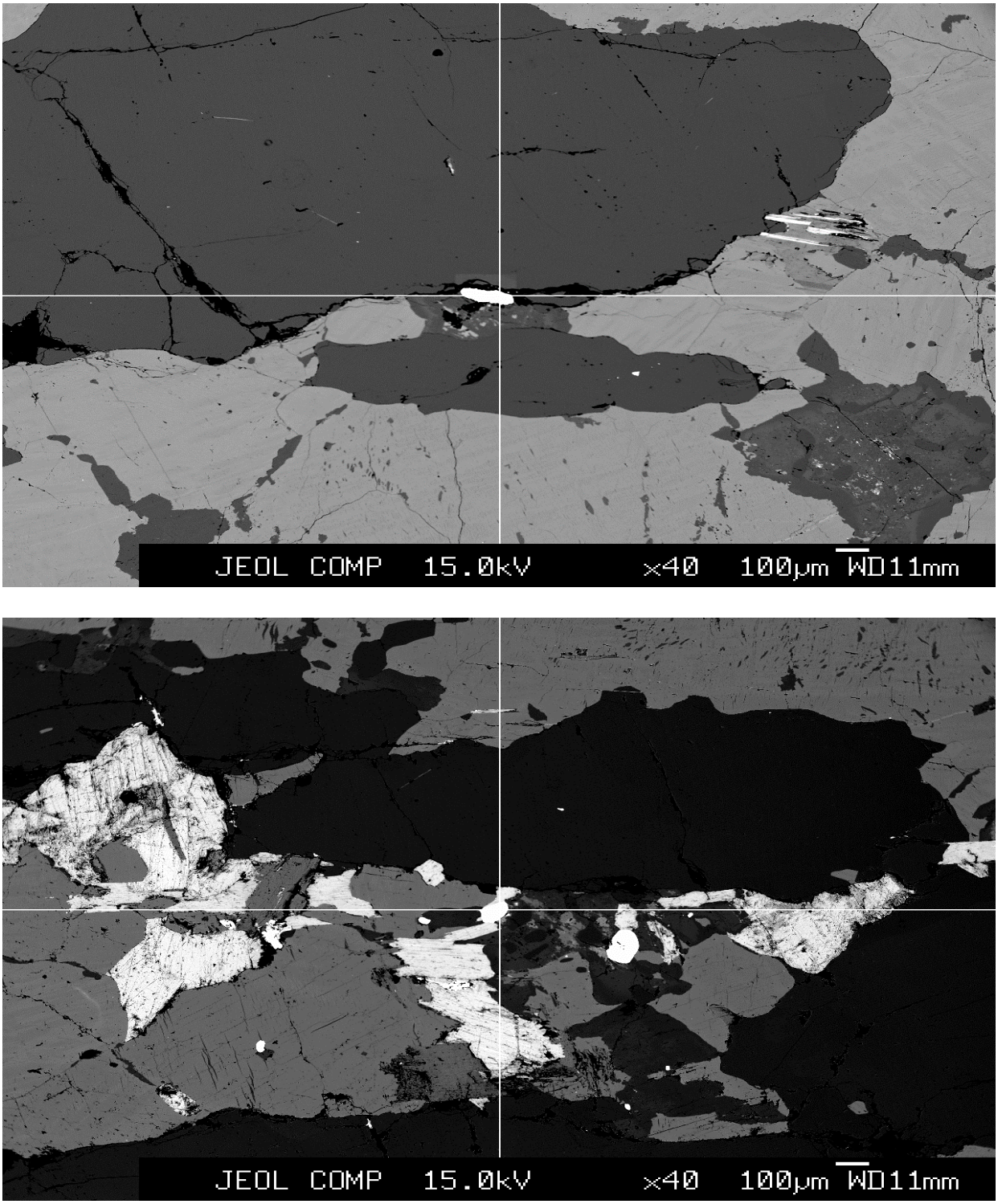

Top: 2NO MNT1

Bottom: 2NO* MNT1

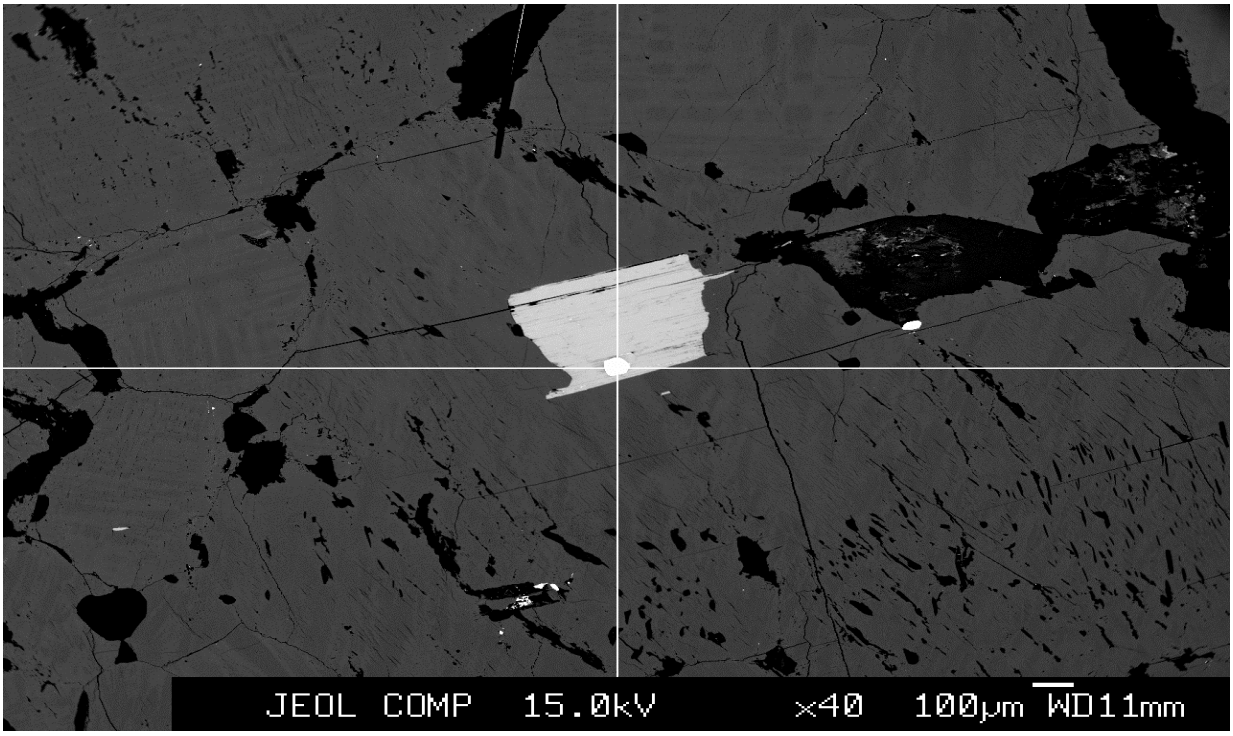

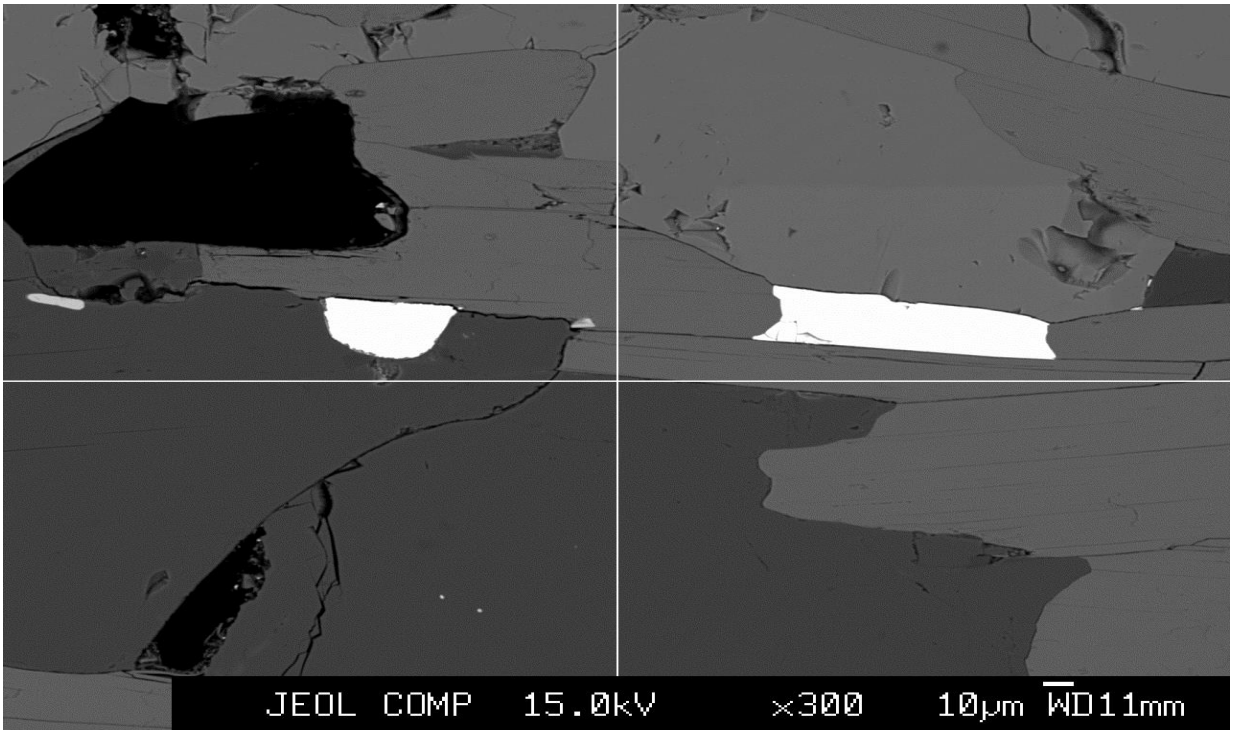

Top: 2NO* MNT2

Bottom Left: 3NO MNT4 Bottom Right: 3NO MNT2

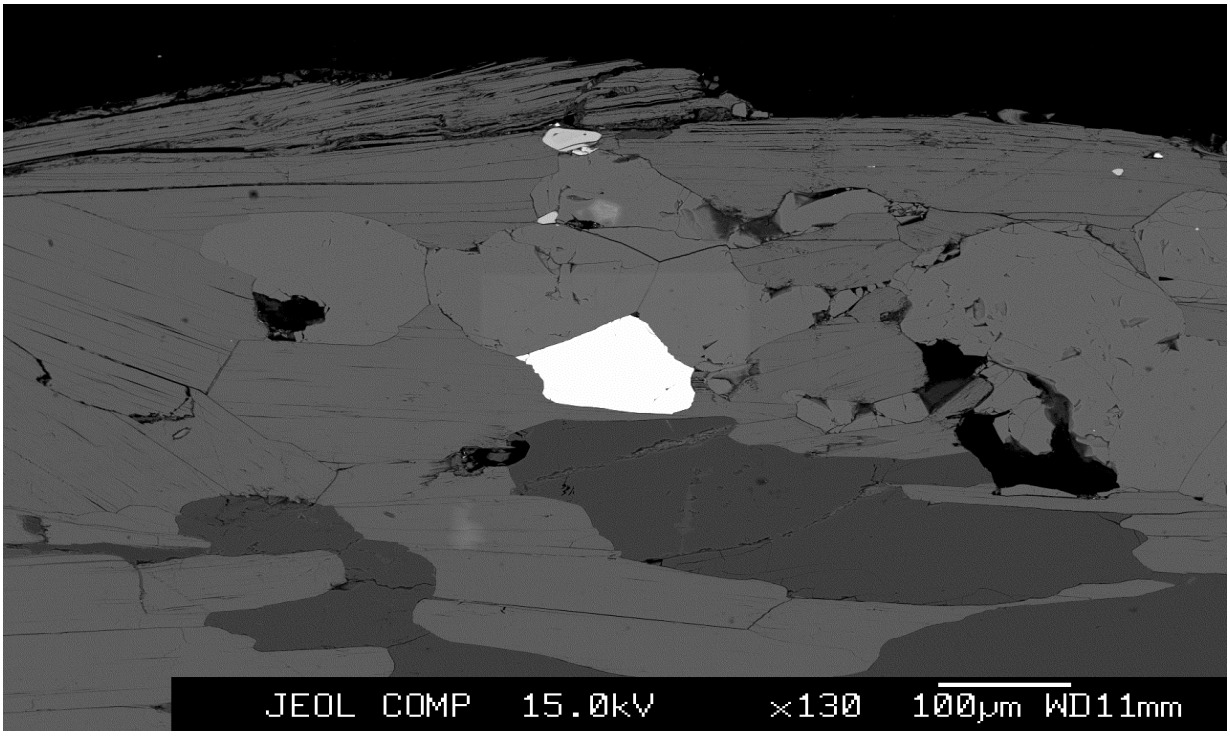

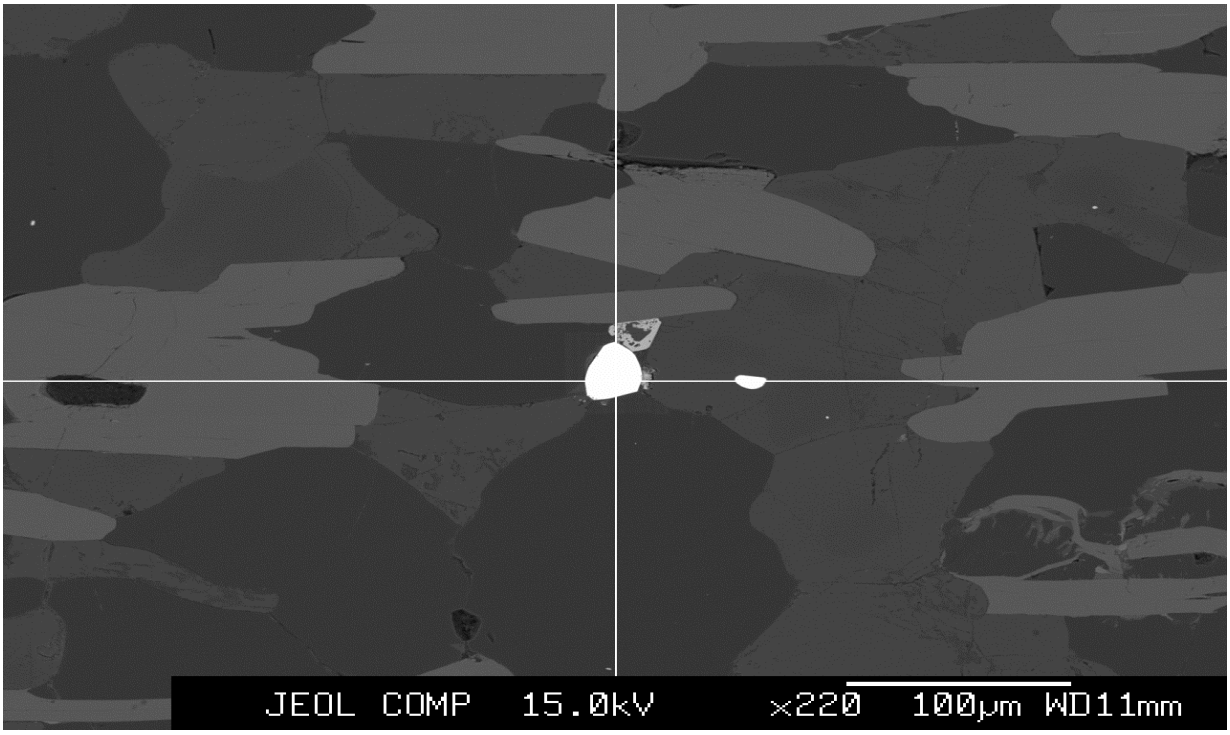

Top: 3NO MNT1

Bottom: 3NO MNT2

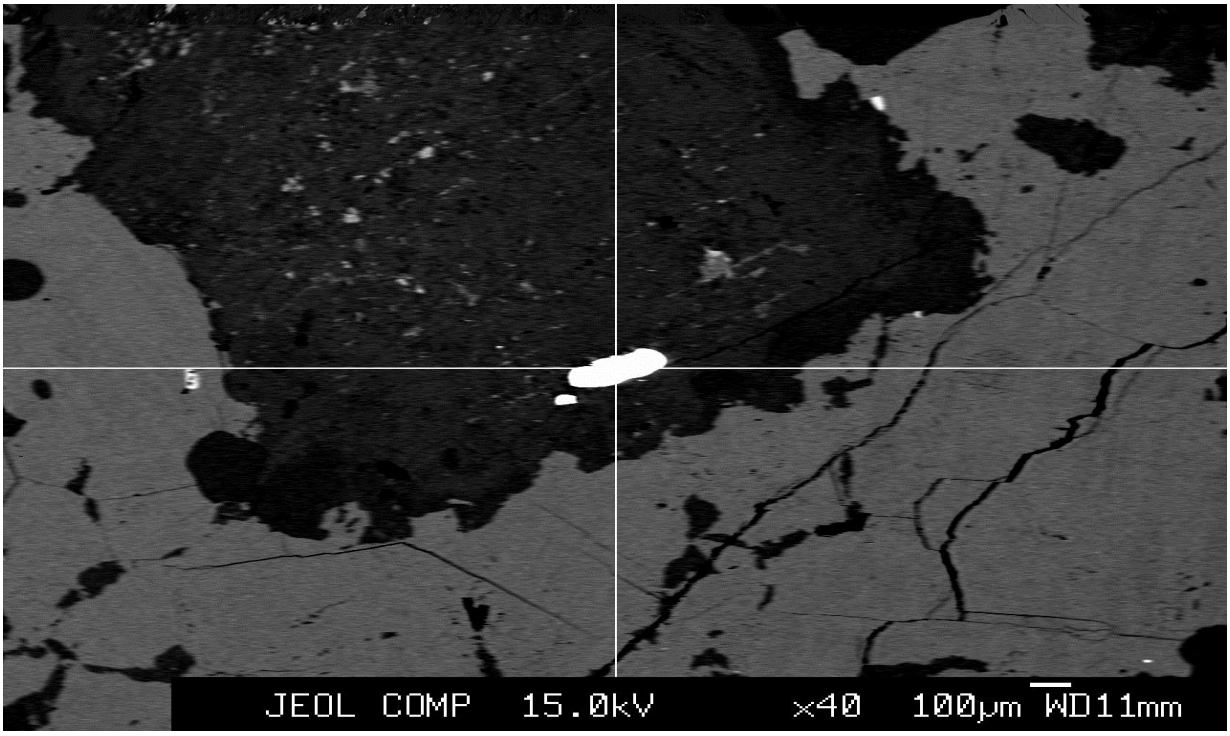

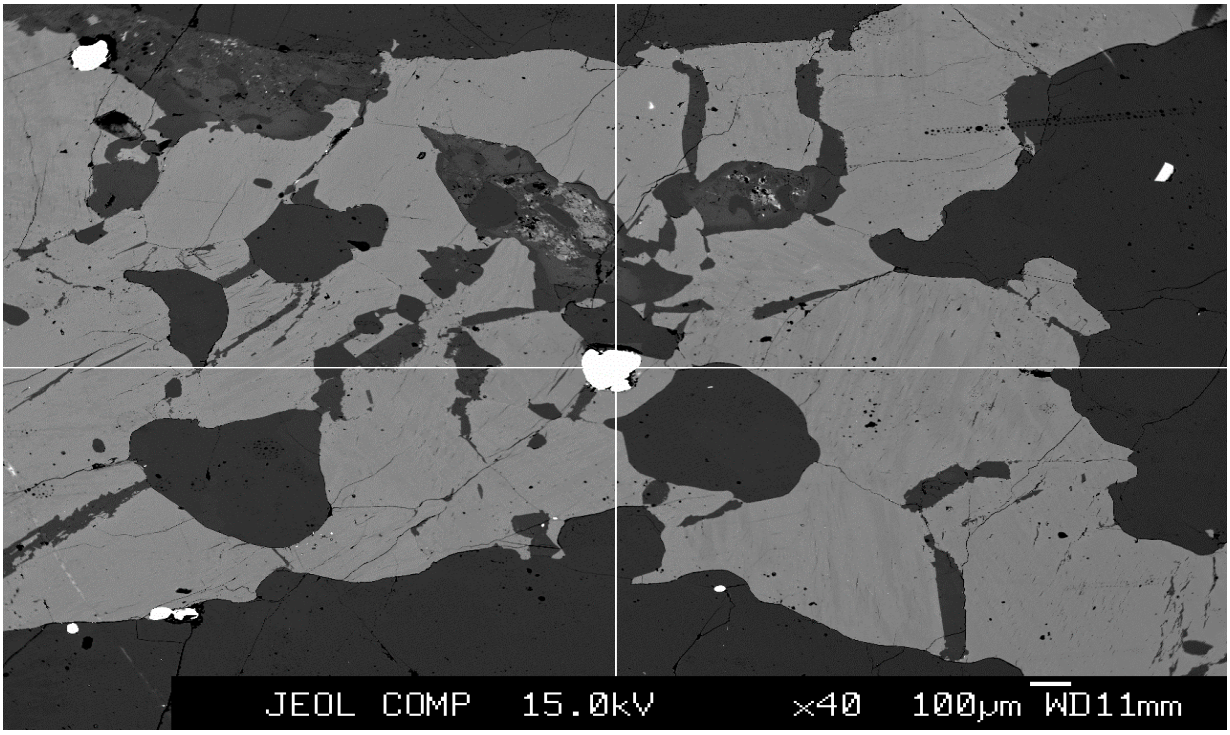

Top: 3NO* MNT4

Bottom: 3NO* MNT5

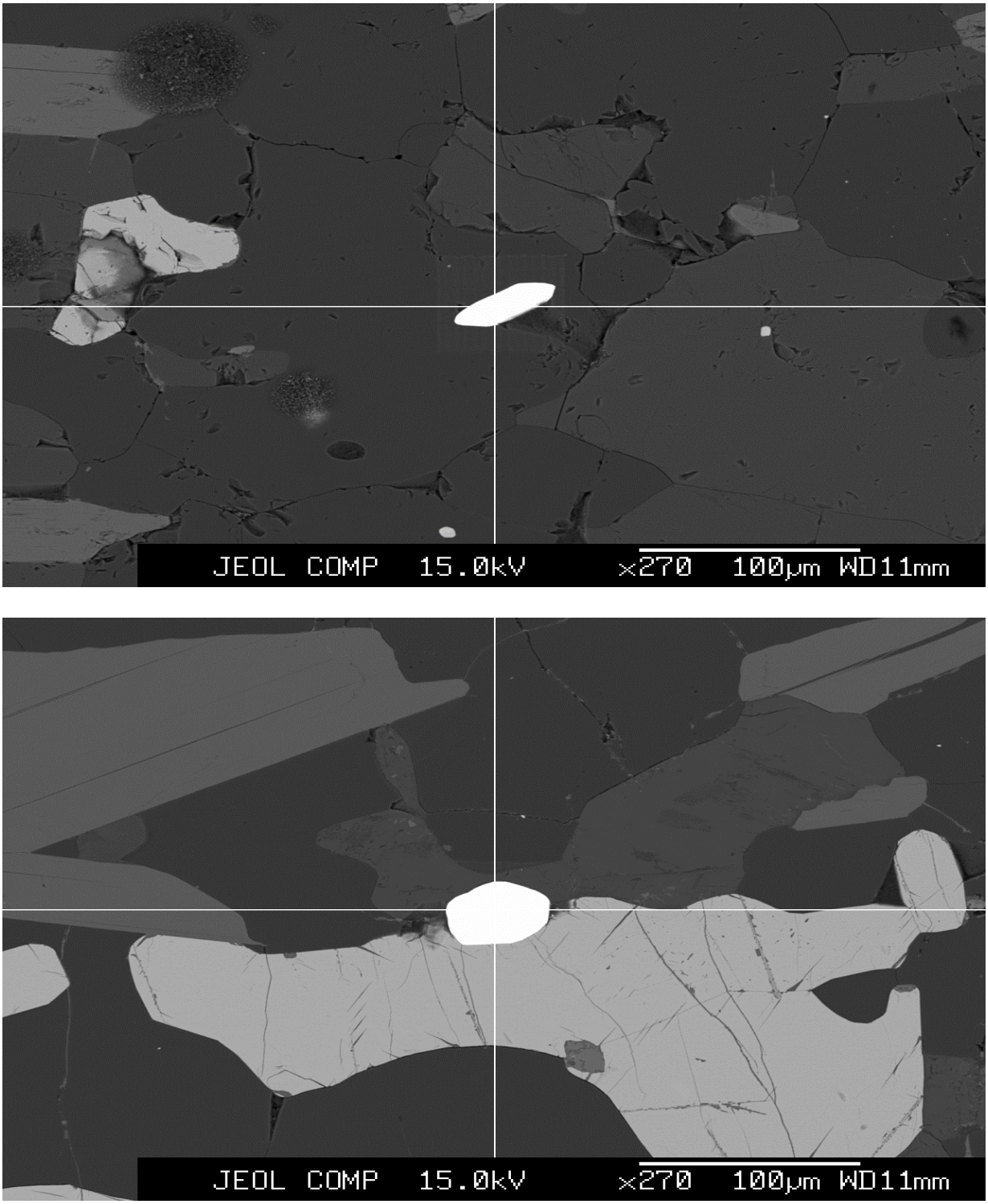

Top: 4NO* MNT1

Bottom: 4NO* MNT5

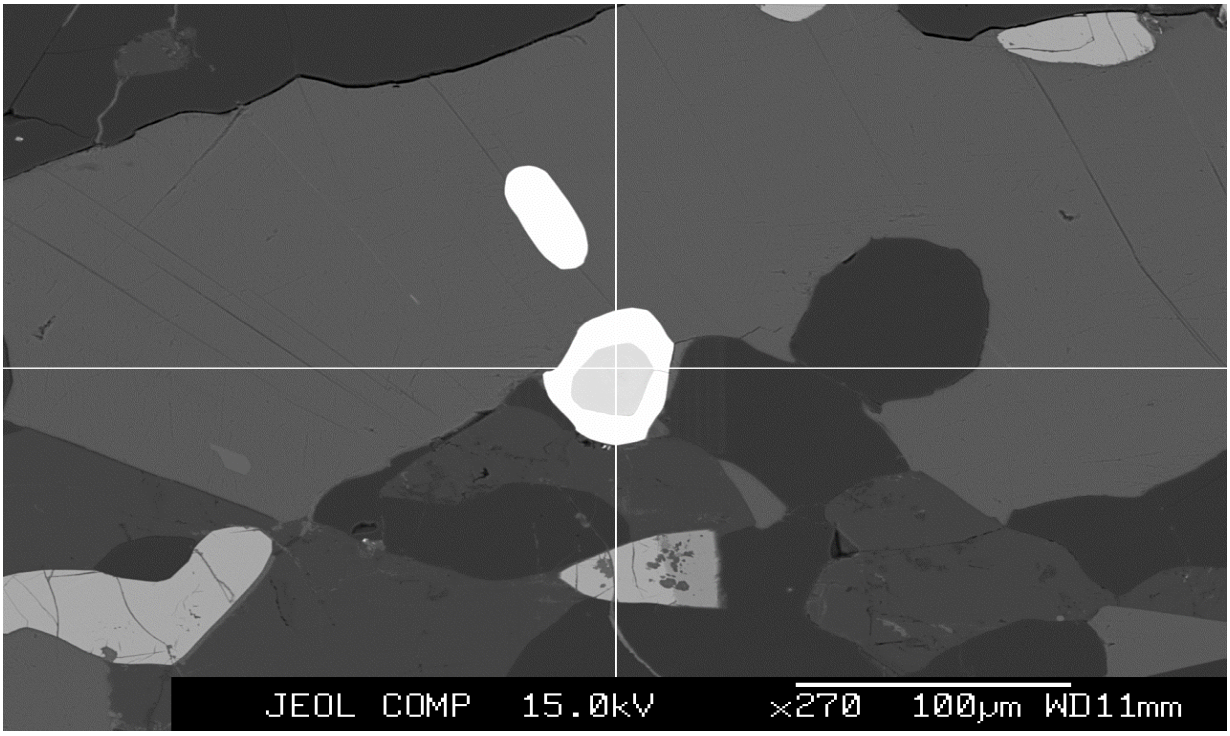

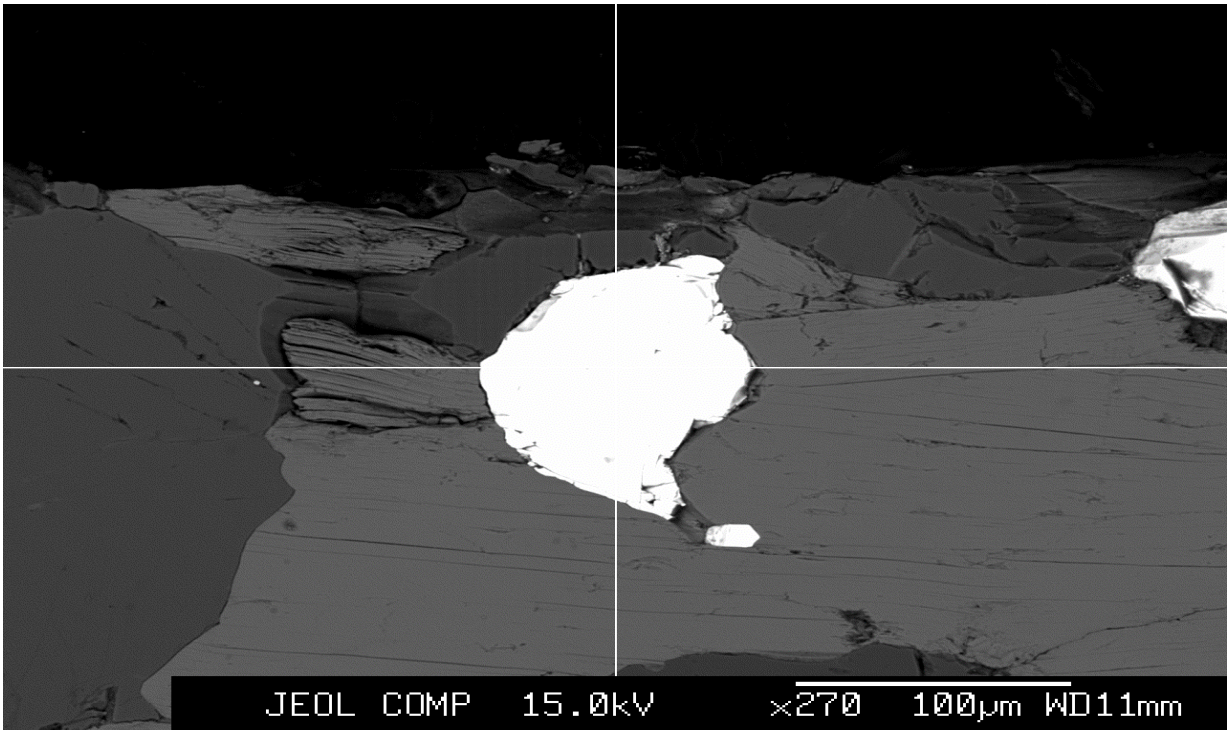

Top: 4NO* MNT7

Bottom: 5NO* MNT1

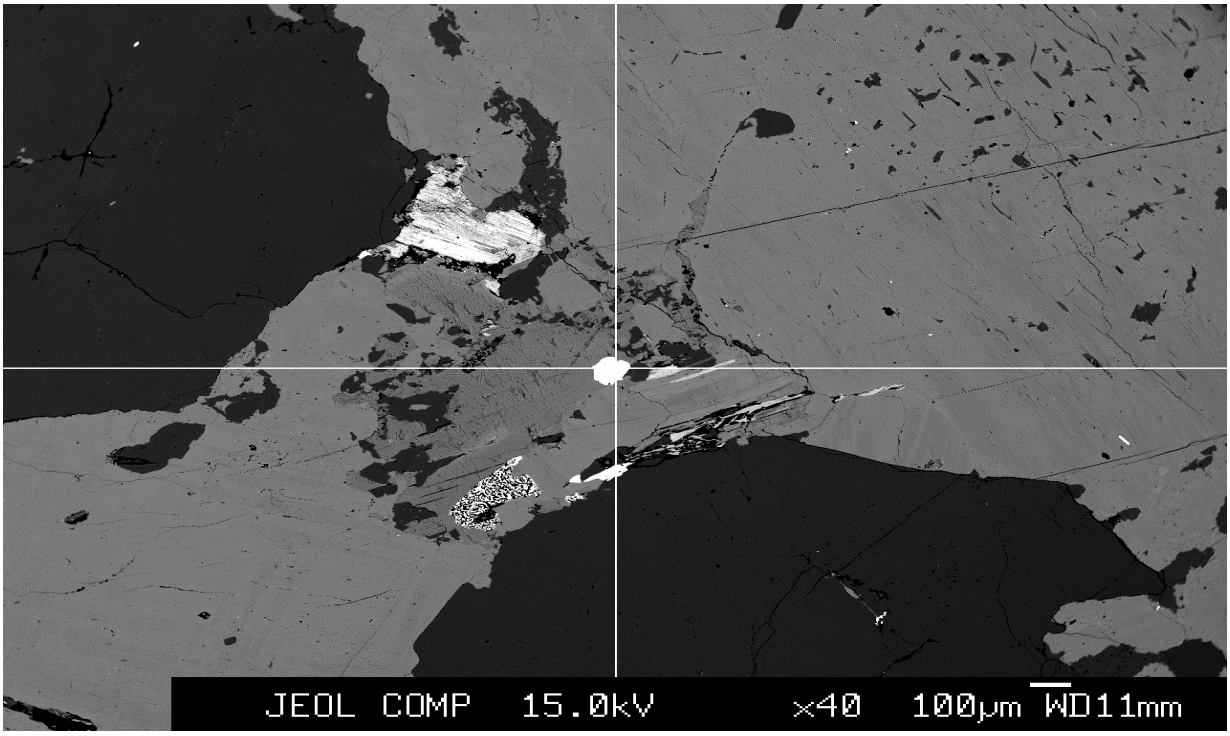

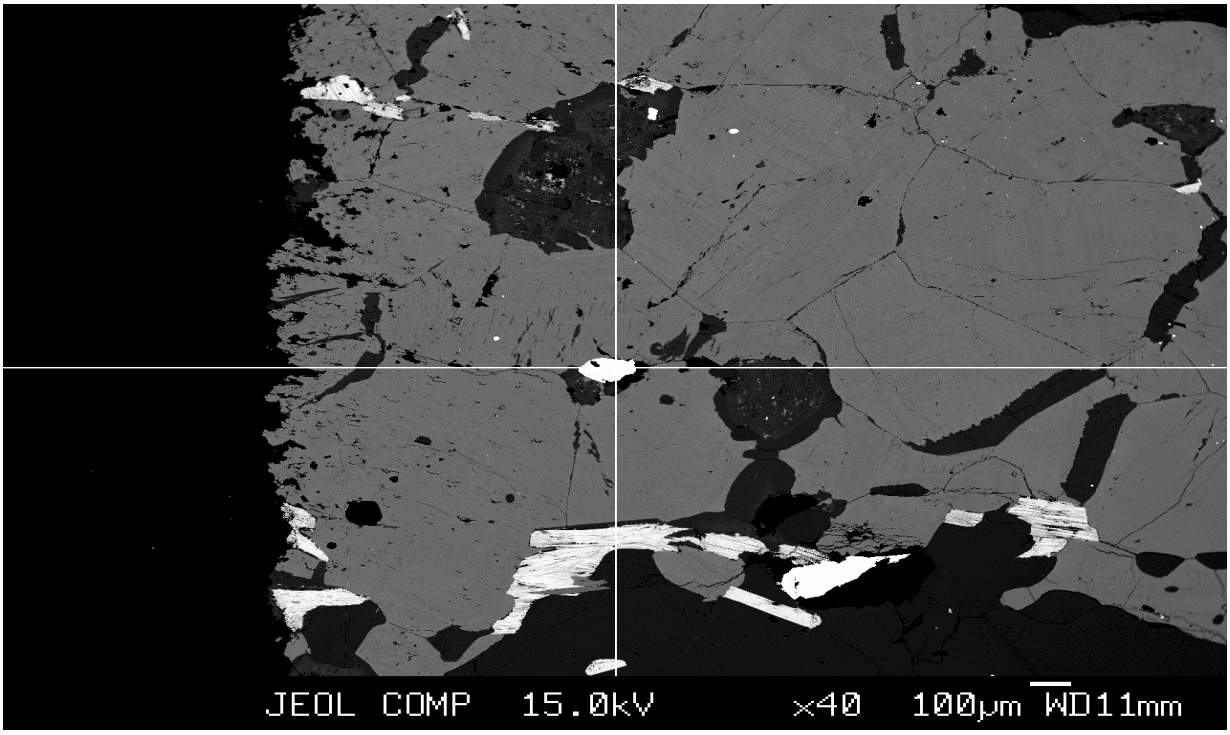

Top: 18NO* MNT1

Bottom: 18NO* MNT3

Appendix 5: Composition Maps

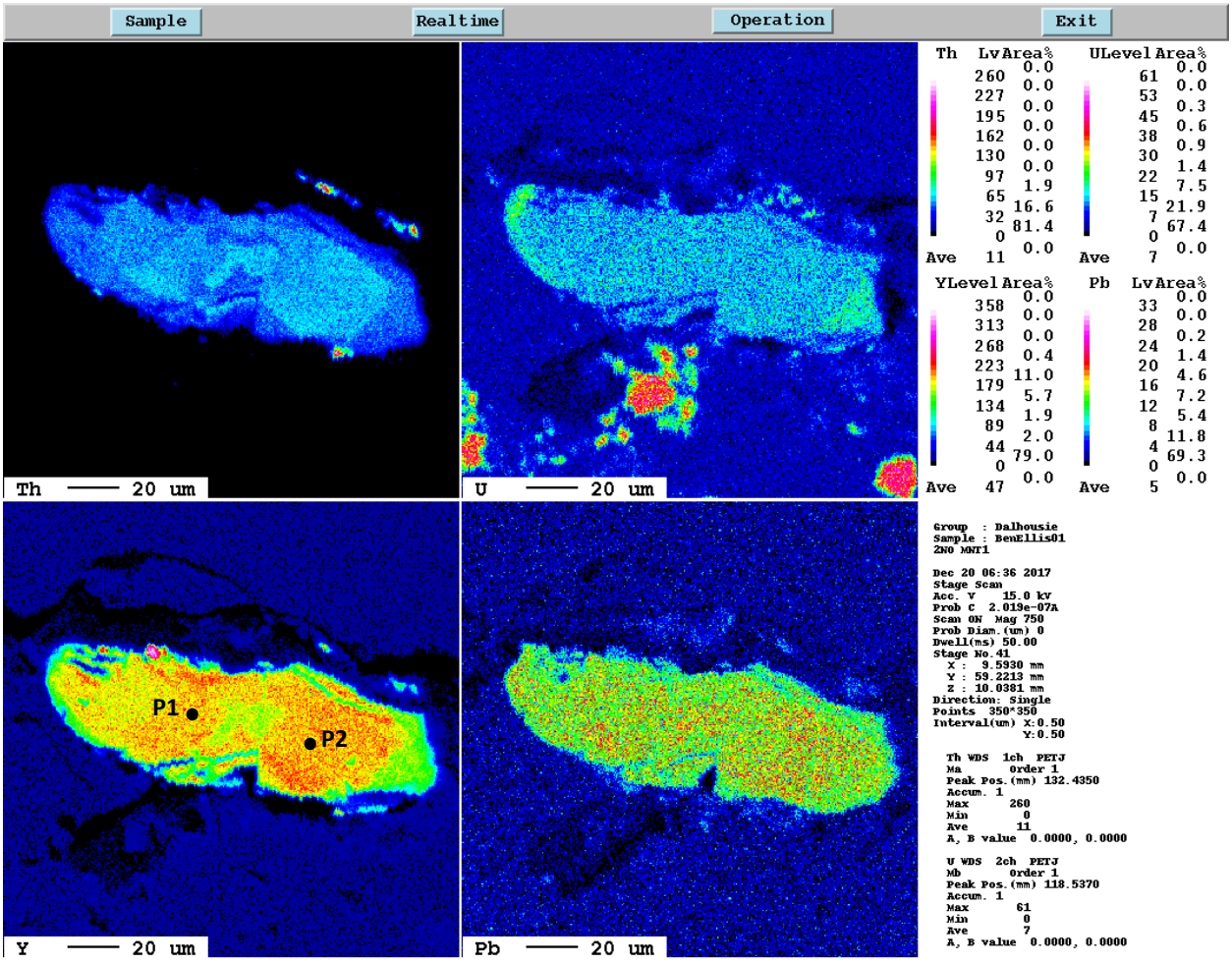

2NO MNT1

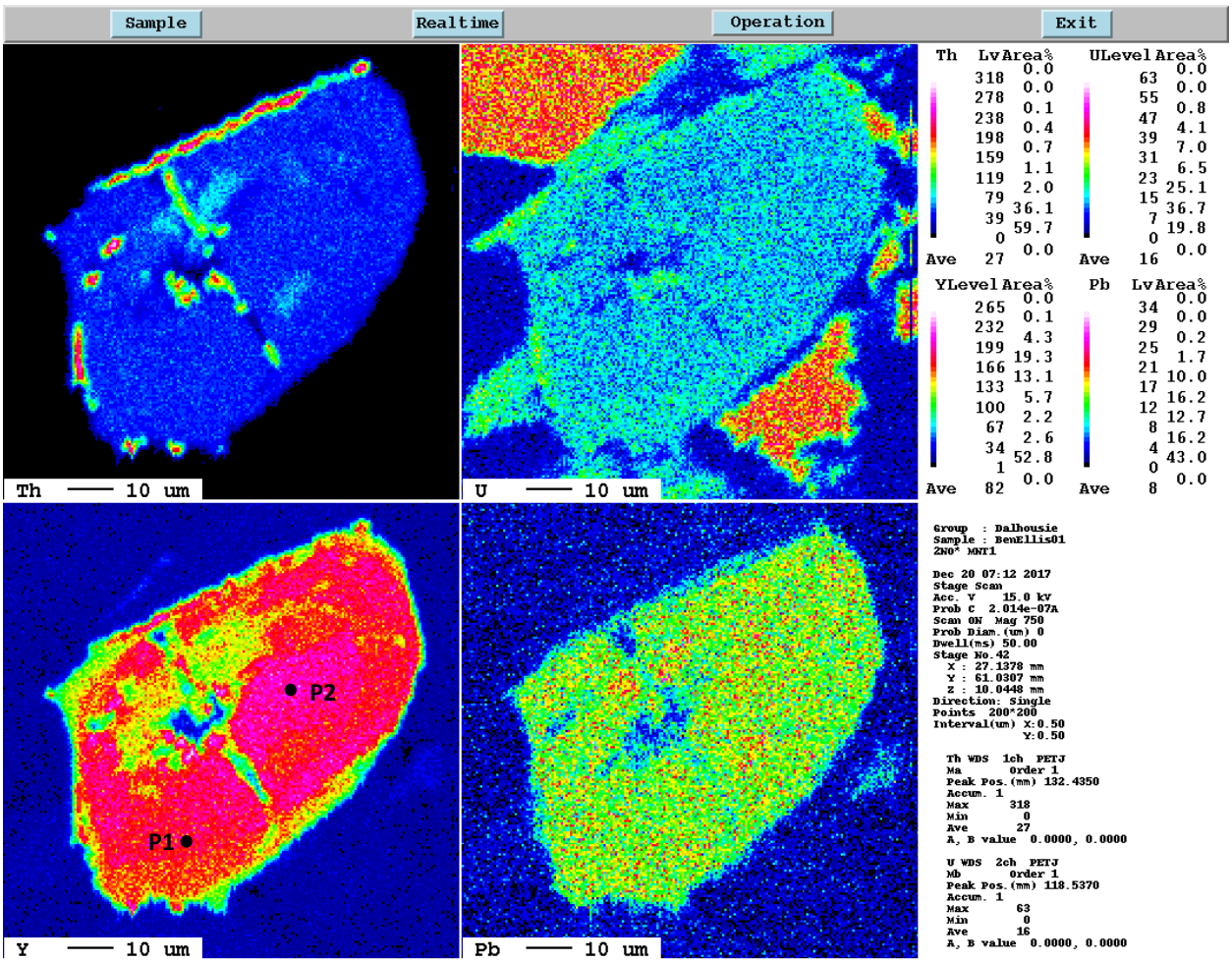
Sample
Realtime
Operation
Exit
Th — 10 um
U — 10 um
Y — 10 um
Pb — 10 um
P1
P2
Th Lv Area%
318 0.0
278 0.0
238 0.1
198 0.4
159 0.7
119 1.1
79 2.0
39 36.1
0 59.7
Ave 27 0.0
ULevel Area%
63 0.0
55 0.0
47 0.8
39 4.1
31 7.0
23 6.5
15 25.1
7 36.7
0 19.8
Ave 16 0.0
YLevel Area%
265 0.0
232 0.1
199 4.3
166 19.3
133 13.1
100 5.7
67 2.2
34 2.6
1 52.8
Ave 82 0.0
Pb Lv Area%
34 0.0
29 0.0
25 0.2
21 1.7
17 10.0
12 16.2
8 12.7
4 16.2
0 43.0
Ave 8 0.0
Group : Dalhousie
Sample : BenEllis01
2NO* MNT1
Dec 20 07:12 2017
Stage Scan
Acc. V 15.0 kV
Prob C 2.014e-07A
Scan ON Mag 750
Prob Diam.(um) 0
Dwell(ms) 50.00
Stage No.42
X : 27.1378 mm
Y : 61.0307 mm
Z : 10.0448 mm
Direction: Single
Points 200*200
Interval(um) X:0.50
Y:0.50
Th WDS 1ch PETJ
Ma Order 1
Peak Pos.(mm) 132.4350
Accum. 1
Max 318
Min 0
Ave 27
A, B value 0.0000, 0.0000
U WDS 2ch PETJ
Mb Order 1
Peak Pos.(mm) 118.5370
Accum. 1
Max 63
Min 0
Ave 16
A, B value 0.0000, 0.0000

2NO* MNT1

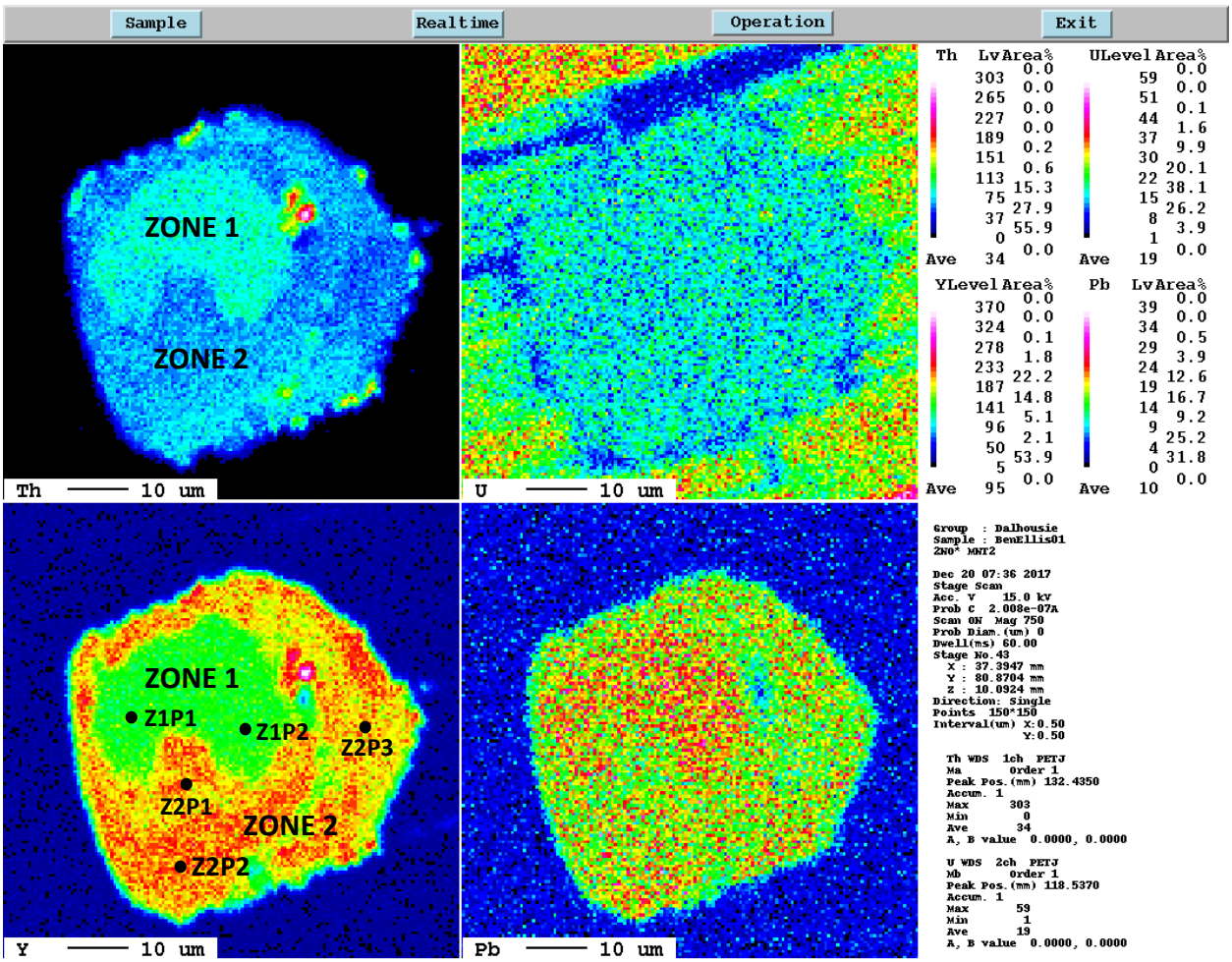
Sample
Realtime
Operation
Exit
ZONE 1
ZONE 2
Th 10 um
U 10 um
Th LvArea%
303 0.0
265 0.0
227 0.0
189 0.2
151 0.6
113 15.3
75 27.9
37 55.9
0 0.0
Ave 34
ULevel Area%
59 0.0
51 0.0
44 0.1
37 1.6
30 9.9
22 20.1
15 38.1
8 26.2
1 3.9
Ave 19 0.0
YLevel Area%
370 0.0
324 0.0
278 0.1
233 1.8
187 22.2
141 14.8
96 5.1
50 2.1
5 53.9
Ave 95 0.0
Pb LvArea%
39 0.0
34 0.0
29 0.5
24 3.9
19 12.6
14 16.7
9 9.2
4 25.2
0 31.8
Ave 10 0.0
ZONE 1
Z1P1
Z1P2
Z2P3
Z2P1
ZONE 2
Z2P2
Y 10 um
Pb 10 um
Group : Dalhousie
Sample : BenEllis01
2NO* MNT2
Dec 20 07:36 2017
Stage Scan
Acc. V 15.0 kV
Prob C 2.008e-07A
Scan ON Mag 750
Prob Diam.(um) 0
Dwell(ms) 60.00
Stage No.43
X : 37.3947 mm
Y : 80.8704 mm
Z : 10.0924 mm
Direction: Single
Points 150*150
Interval(um) X:0.50
Y:0.50
Th WDS 1ch PETJ
Ma Order 1
Peak Pos.(mm) 132.4350
Accum. 1
Max 303
Min 0
Ave 34
A, B value 0.0000, 0.0000
U WDS 2ch PETJ
Mb Order 1
Peak Pos.(mm) 118.5370
Accum. 1
Max 59
Min 1
Ave 19
A, B value 0.0000, 0.0000

2NO* MNT2

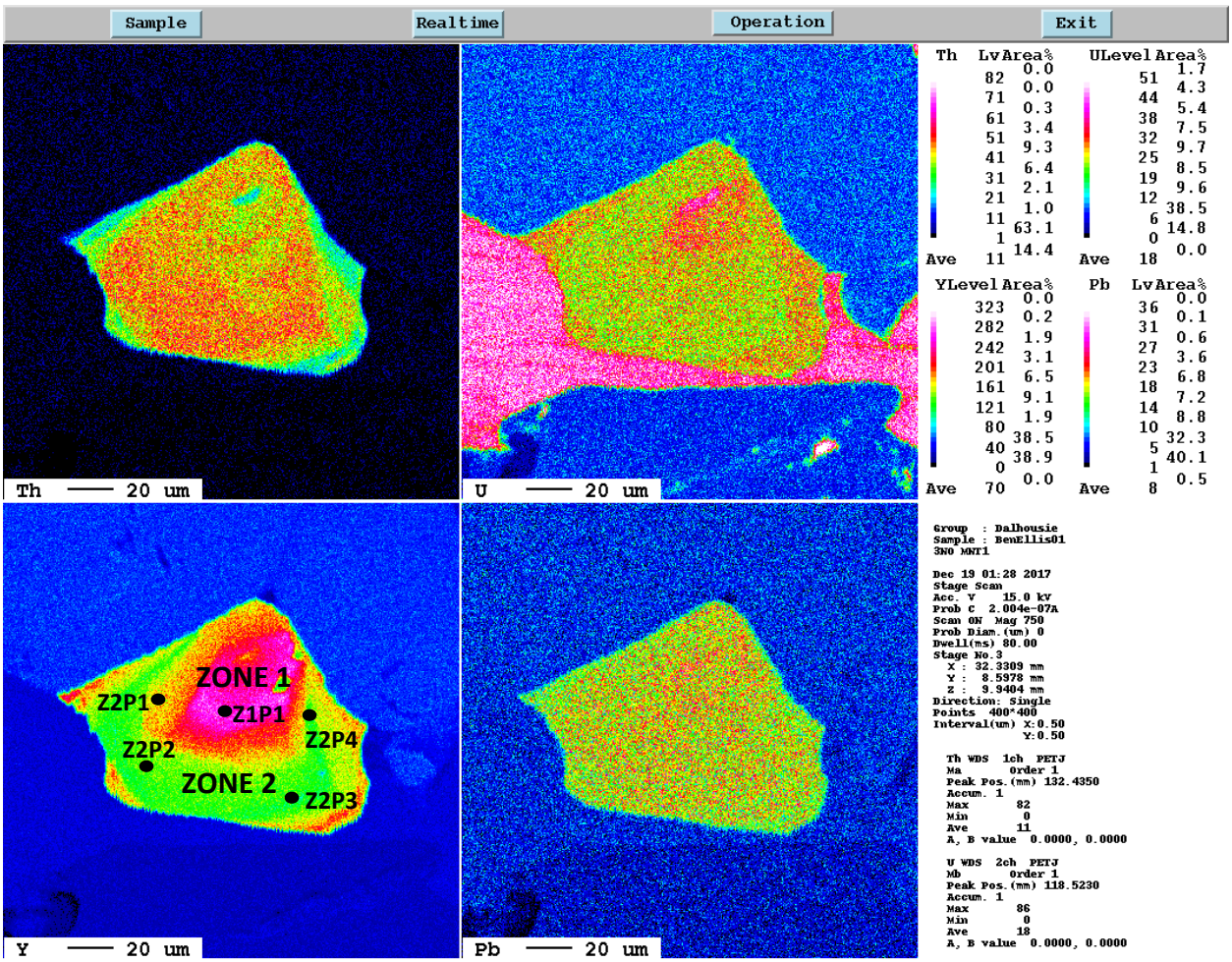
Sample
Realtime
Operation
Exit
Th
20 um
U
20 um
Y
20 um
Pb
20 um
ZONE 1
Z2P1
Z1P1
Z2P4
Z2P2
ZONE 2
Z2P3
Th Lv Area%
82 0.0
71 0.0
61 0.3
51 3.4
41 9.3
31 6.4
21 2.1
11 1.0
1 63.1
Ave 11 14.4
ULevel Area%
51 1.7
44 4.3
38 5.4
32 7.5
25 9.7
19 8.5
12 9.6
6 38.5
0 14.8
Ave 18 0.0
YLevel Area%
323 0.0
282 0.2
242 1.9
201 3.1
161 6.5
121 9.1
80 1.9
40 38.5
0 38.9
Ave 70 0.0
Pb Lv Area%
36 0.0
31 0.1
27 0.6
23 3.6
18 6.8
14 7.2
10 8.8
5 32.3
1 40.1
Ave 8 0.5
Group : Dalhousie
Sample : BenEllis01
3NO MNT1
Dec 19 01:28 2017
Stage Scan
Acc. V 15.0 kV
Prob C 2.004e-07A
Scan ON Mag 750
Prob Diam.(um) 0
Dwell(ms) 80.00
Stage No.3
X : 32.3309 mm
Y : 8.5978 mm
Z : 9.9404 mm
Direction: Single
Points 400*400
Interval(um) X:0.50
Y:0.50
Th WDS 1ch PETJ
Ma Order 1
Peak Pos.(mm) 132.4350
Accum. 1
Max 82
Min 0
Ave 11
A, B value 0.0000, 0.0000
U WDS 2ch PETJ
Mb Order 1
Peak Pos.(mm) 118.5230
Accum. 1
Max 86
Min 0
Ave 18
A, B value 0.0000, 0.0000

3NO MNT1

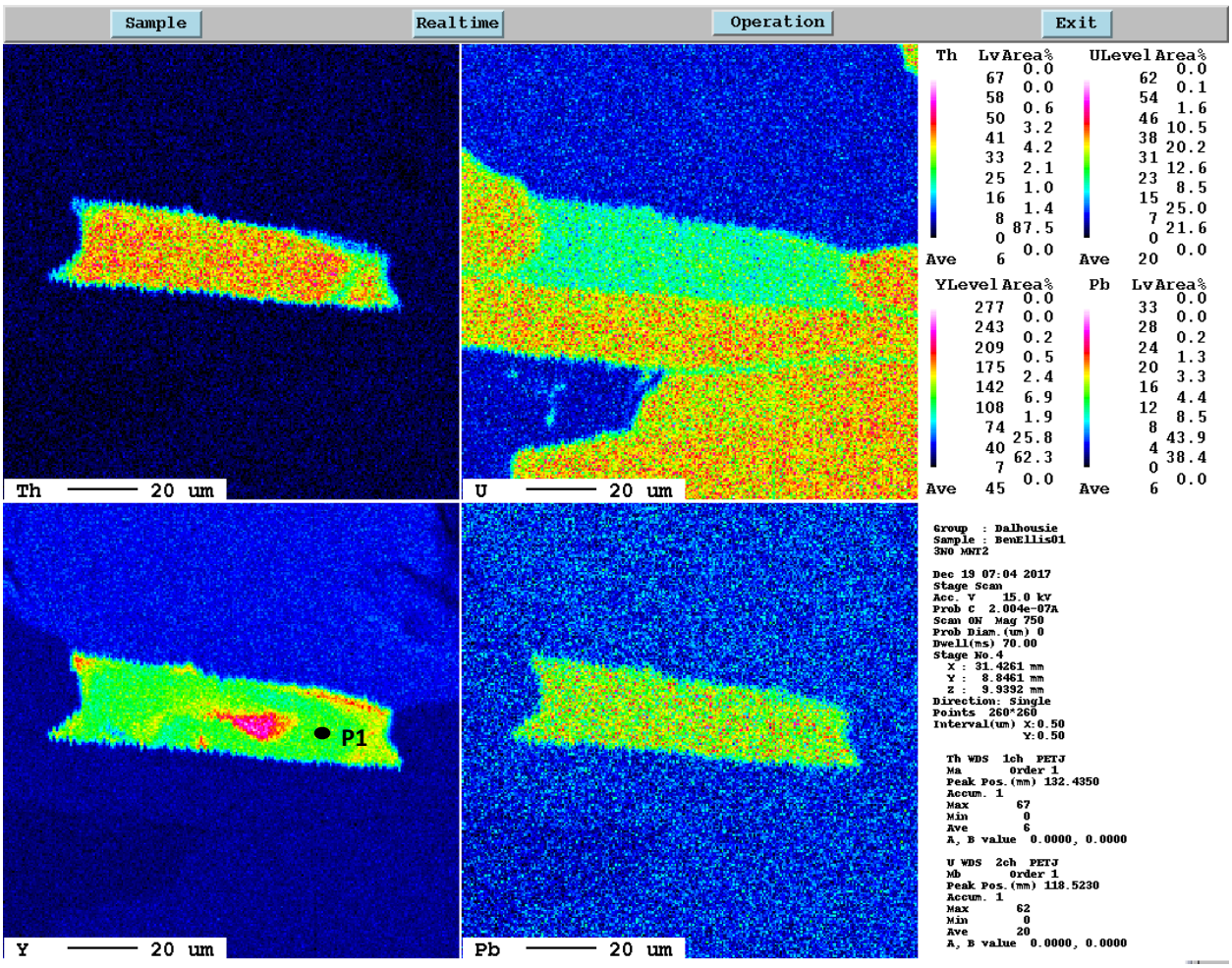
Sample
Realtime
Operation
Exit
Th
20 um
U
20 um
Y
20 um
P1
Pb
20 um
Th Lv Area%
67 0.0
58 0.0
50 0.6
41 3.2
33 4.2
25 2.1
16 1.0
8 1.4
0 87.5
Ave 6 0.0
ULevel Area%
62 0.0
54 0.1
46 1.6
38 10.5
31 20.2
23 12.6
15 8.5
7 25.0
0 21.6
Ave 20 0.0
YLevel Area%
277 0.0
243 0.0
209 0.2
175 0.5
142 2.4
108 6.9
74 1.9
40 25.8
7 62.3
Ave 45 0.0
Pb Lv Area%
33 0.0
28 0.0
24 0.2
20 1.3
16 3.3
12 4.4
8 8.5
4 43.9
0 38.4
Ave 6 0.0
Group : Dalhousie
Sample : BenEllis01
3NO MNT2
Dec 19 07:04 2017
Stage Scan
Acc. V 15.0 kV
Prob C 2.004e-07A
Scan ON Mag 750
Prob Diam.(um) 0
Dwell(ms) 70.00
Stage No.4
X : 31.4261 mm
Y : 8.8461 mm
Z : 9.9392 mm
Direction: Single
Points 260*260
Interval(um) X:0.50
Y:0.50
Th WDS 1ch PETJ
Ma Order 1
Peak Pos.(mm) 132.4350
Accum. 1
Max 67
Min 0
Ave 6
A, B value 0.0000, 0.0000
U WDS 2ch PETJ
Mb Order 1
Peak Pos.(mm) 118.5230
Accum. 1
Max 62
Min 0
Ave 20
A, B value 0.0000, 0.0000

3NO MNT2

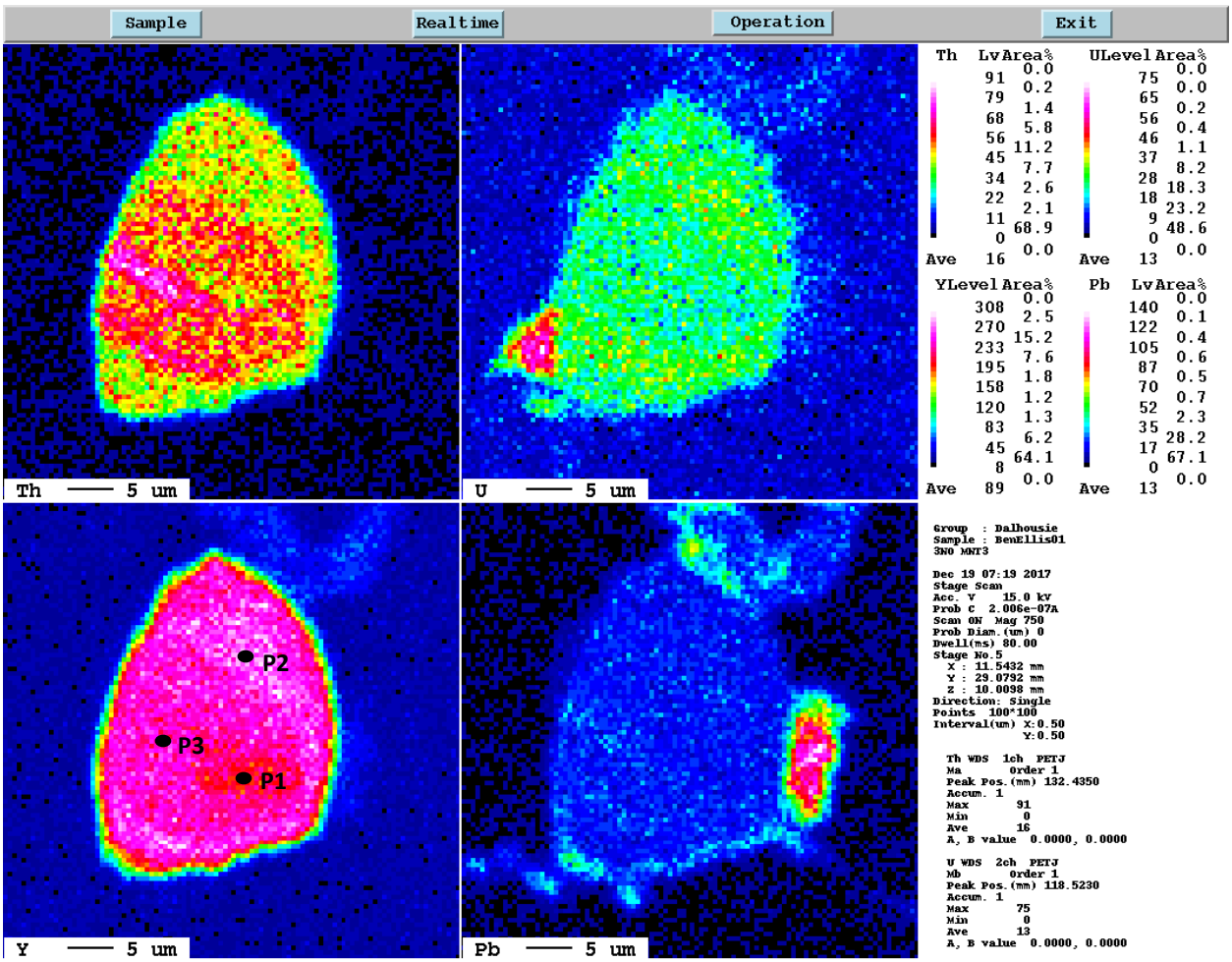
Sample
Realtime
Operation
Exit
Th
5 um
U
5 um
Th Lv Area%
91 0.2
79 1.4
68 5.8
56 11.2
45 7.7
34 2.6
22 2.1
11 68.9
0 0.0
Ave 16
ULevel Area%
75 0.0
65 0.0
56 0.2
46 0.4
37 1.1
28 8.2
18 18.3
9 23.2
0 48.6
Ave 13
YLevel Area%
308 0.0
270 2.5
233 15.2
195 7.6
158 1.8
120 1.2
83 1.3
45 6.2
8 64.1
Ave 89
Pb Lv Area%
140 0.0
122 0.1
105 0.4
87 0.6
70 0.5
52 0.7
35 2.3
17 28.2
0 67.1
Ave 13
P2
P3
P1
Y
5 um
Pb
5 um
Group : Dalhousie
Sample : BenEllis01
3NO MNT3
Dec 19 07:19 2017
Stage Scan
Acc. V 15.0 kV
Prob C 2.006e-07A
Scan ON Mag 750
Prob Diam.(um) 0
Dwell(ms) 80.00
Stage No.5
X : 11.5432 mm
Y : 29.0792 mm
Z : 10.0038 mm
Direction: Single
Points 100*100
Interval(um) X:0.50
Y:0.50
Th WDS 1ch PETJ
Ma Order 1
Peak Pos.(mm) 132.4350
Accum. 1
Max 91
Min 0
Ave 16
A, B value 0.0000, 0.0000
U WDS 2ch PETJ
Mb Order 1
Peak Pos.(mm) 118.5230
Accum. 1
Max 75
Min 0
Ave 13
A, B value 0.0000, 0.0000

3NO MNT3

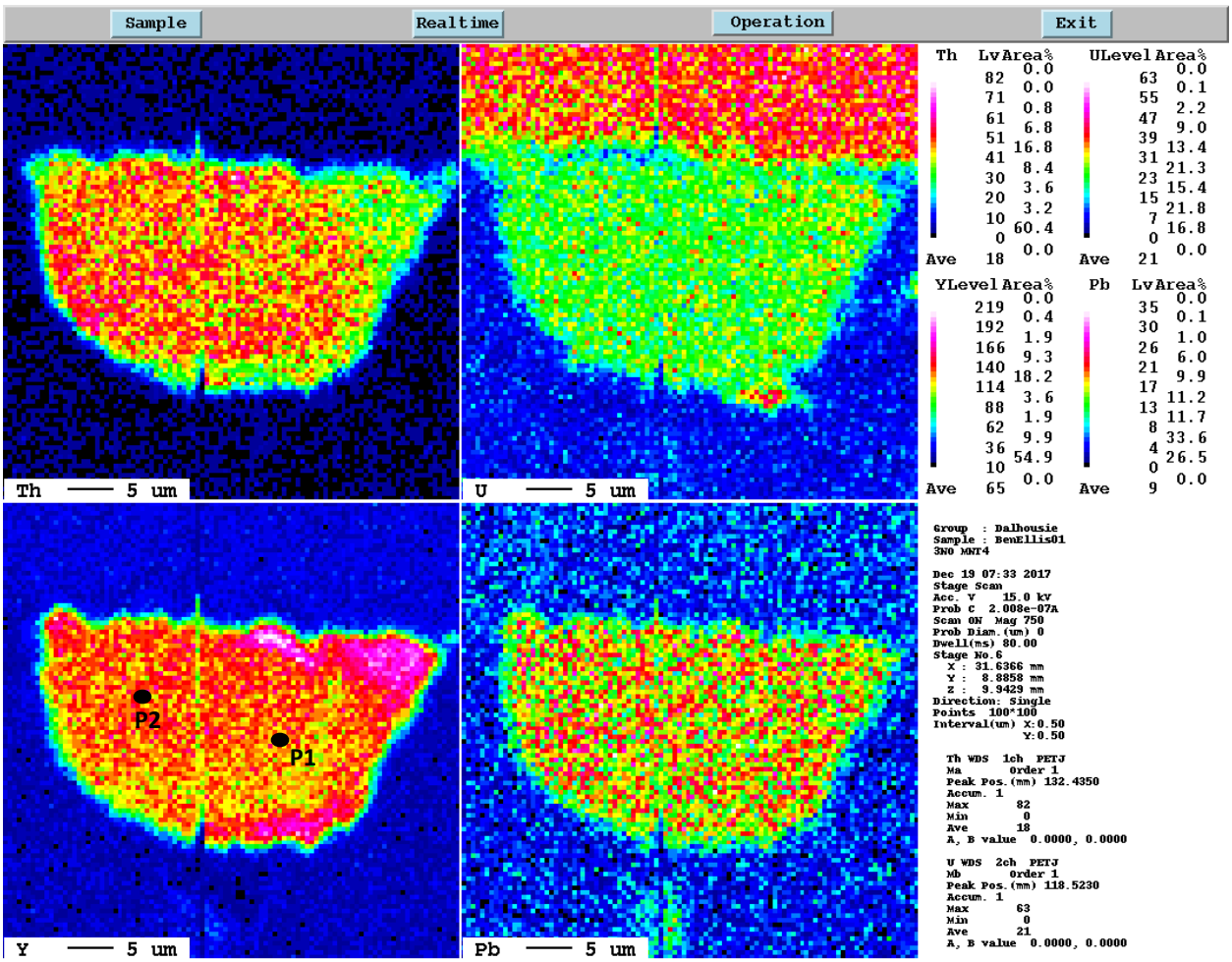
Sample
Realtime
Operation
Exit
Th
U
Y
Pb
5 um
P1
P2
Th Lv Area%
82 0.0
71 0.0
61 0.8
51 6.8
41 16.8
30 8.4
20 3.6
10 3.2
0 60.4
Ave 18 0.0
ULevel Area%
63 0.0
55 0.1
47 2.2
39 9.0
31 13.4
23 21.3
15 15.4
7 21.8
0 16.8
Ave 21 0.0
YLevel Area%
219 0.0
192 0.4
166 1.9
140 9.3
114 18.2
88 3.6
62 1.9
36 9.9
10 54.9
Ave 65 0.0
Pb Lv Area%
35 0.0
30 0.1
26 1.0
21 6.0
17 9.9
13 11.2
8 11.7
4 33.6
0 26.5
Ave 9 0.0
Group : Dalhousie
Sample : BenEllis01
3NO MNT4
Dec 19 07:33 2017
Stage Scan
Acc. V 15.0 kV
Prob C 2.008e-07A
Scan ON Mag 750
Prob Diam.(um) 0
Dwell(ms) 80.00
Stage No.6
X : 31.6366 mm
Y : 8.8858 mm
Z : 9.9429 mm
Direction: Single
Points 100*100
Interval(um) X:0.50
Y:0.50
Th WDS 1ch PETJ
Ma Order 1
Peak Pos.(mm) 132.4350
Accum. 1
Max 82
Min 0
Ave 18
A, B value 0.0000, 0.0000
U WDS 2ch PETJ
Mb Order 1
Peak Pos.(mm) 118.5230
Accum. 1
Max 63
Min 0
Ave 21
A, B value 0.0000, 0.0000

3NO MNT4

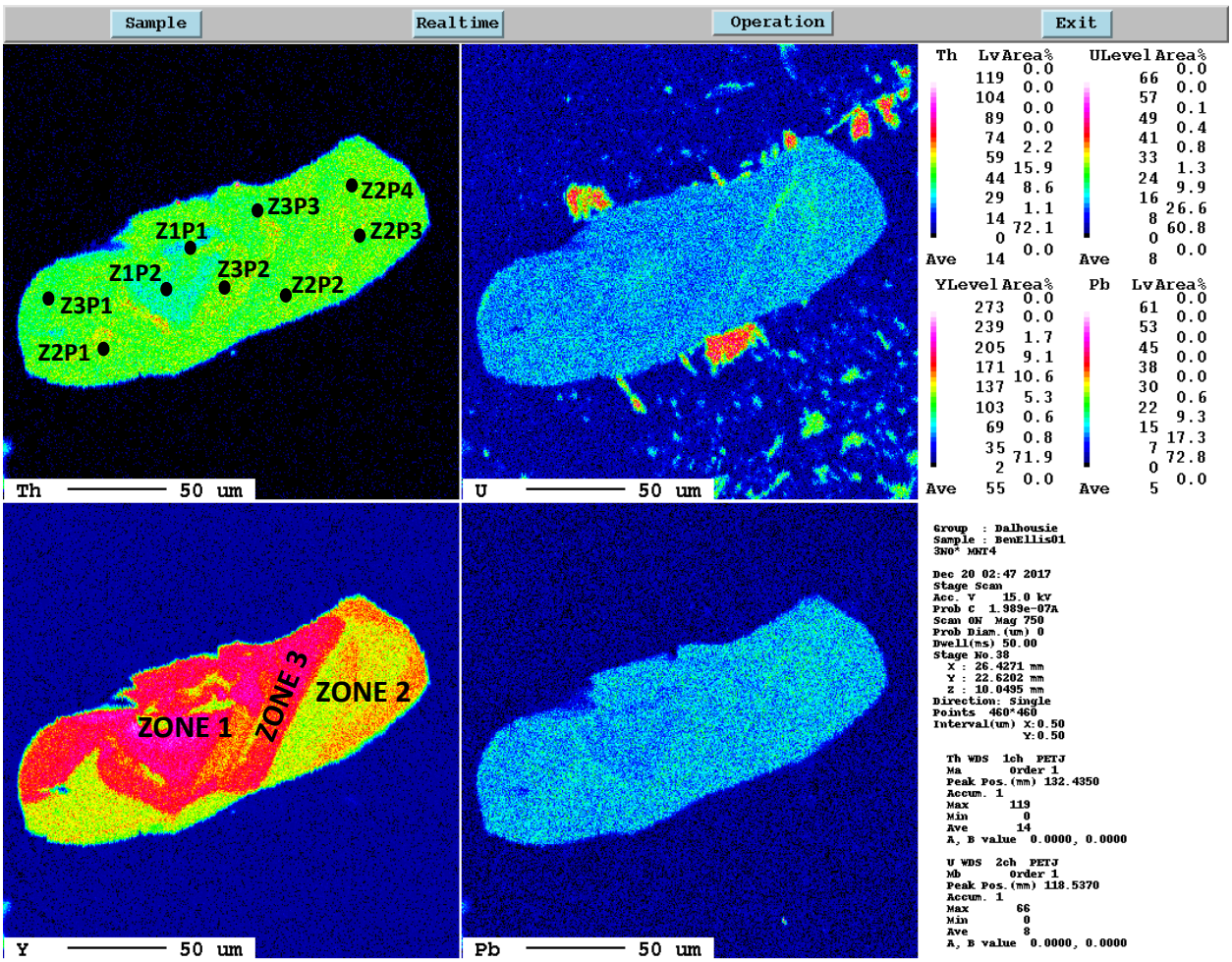
Sample
Realtime
Operation
Exit
Z1P1
Z2P4
Z3P3
Z2P3
Z1P2
Z3P2
Z2P2
Z3P1
Z2P1
Th 50 um
U 50 um
Th Lv Area%
119 0.0
104 0.0
89 0.0
74 2.2
59 15.9
44 8.6
29 1.1
14 72.1
0 0.0
Ave 14
ULevel Area%
66 0.0
57 0.0
49 0.1
41 0.4
33 0.8
24 1.3
16 9.9
8 26.6
0 60.8
Ave 8
YLevel Area%
273 0.0
239 0.0
205 1.7
171 9.1
137 10.6
103 5.3
69 0.6
35 0.8
2 71.9
Ave 55
Pb Lv Area%
61 0.0
53 0.0
45 0.0
38 0.0
30 0.0
22 0.6
15 9.3
7 17.3
0 72.8
Ave 5
ZONE 1
ZONE 3
ZONE 2
Y 50 um
Pb 50 um
Group : Dalhousie
Sample : BenEllis01
3NO* MNT4
Dec 20 02:47 2017
Stage Scan
Acc. V 15.0 kV
Prob C 1.989e-07A
Scan ON Mag 750
Prob Diam.(um) 0
Dwell(ms) 50.00
Stage No.38
X : 26.4271 mm
Y : 22.6202 mm
Z : 10.0495 mm
Direction: Single
Points 460*460
Interval(um) X:0.50
Y:0.50
Th WDS 1ch PETJ
Ma Order 1
Peak Pos.(mm) 132.4350
Accum. 1
Max 119
Min 0
Ave 14
A, B value 0.0000, 0.0000
U WDS 2ch PETJ
Mb Order 1
Peak Pos.(mm) 118.5370
Accum. 1
Max 66
Min 0
Ave 8
A, B value 0.0000, 0.0000

3NO* MNT4

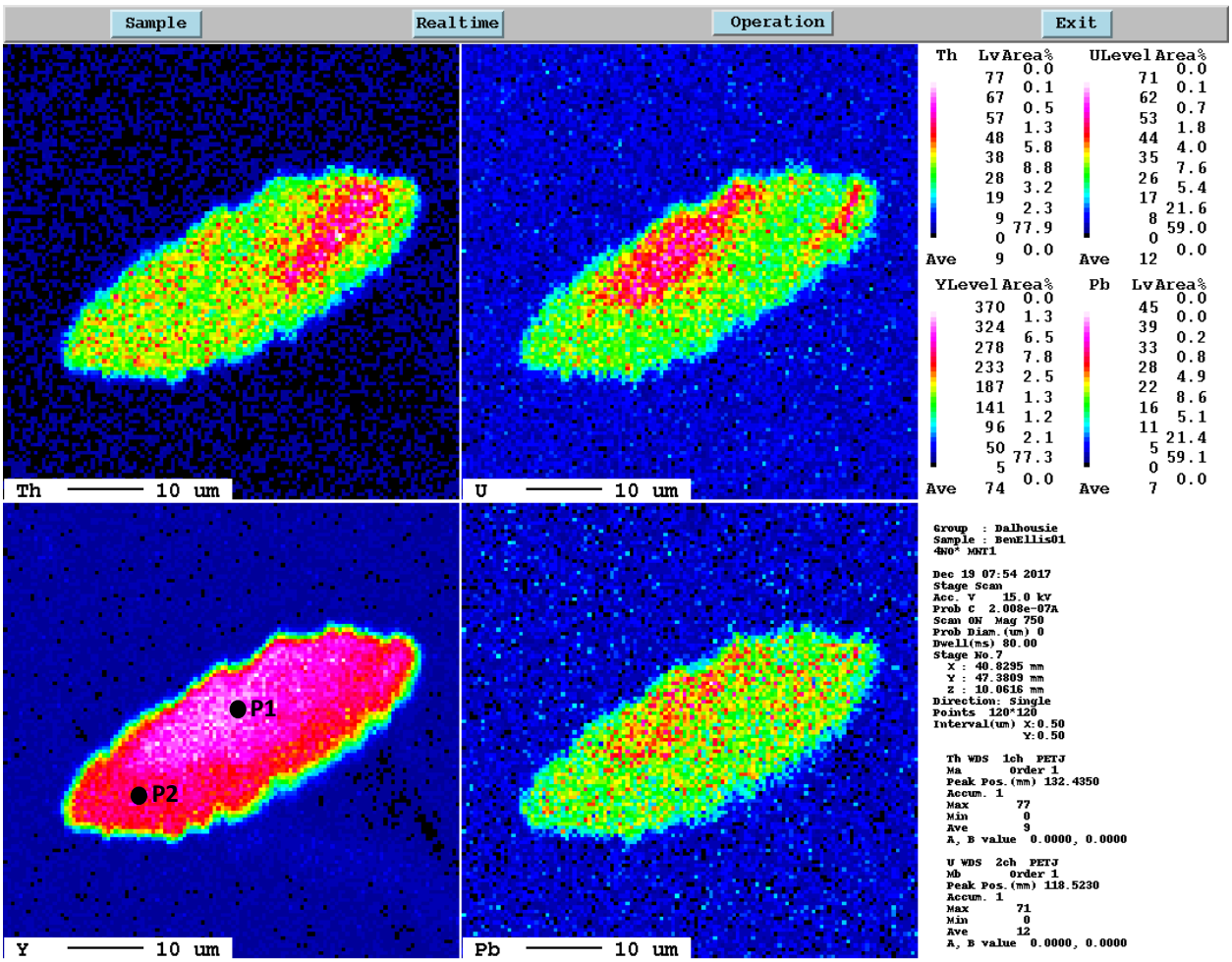
Sample
Realtime
Operation
Exit
Th
10 um
U
10 um
Y
10 um
Pb
10 um
P1
P2
Th Lv Area%
77 0.1
67 0.5
57 1.3
48 5.8
38 8.8
28 3.2
19 2.3
9 77.9
0 0.0
Ave 9
ULevel Area%
71 0.1
62 0.7
53 1.8
44 4.0
35 7.6
26 5.4
17 21.6
8 59.0
0 0.0
Ave 12
YLevel Area%
370 0.0
324 1.3
278 6.5
233 7.8
187 2.5
141 1.3
96 1.2
50 2.1
5 77.3
0.0
Ave 74
Pb Lv Area%
45 0.0
39 0.0
33 0.2
28 0.8
22 4.9
16 8.6
11 5.1
5 21.4
0 59.1
0.0
Ave 7
Group : Dalhousie
Sample : BenEllis01
4NO* MNT1
Dec 19 07:54 2017
Stage Scan
Acc. V 15.0 kV
Prob C 2.008e-07A
Scan ON Mag 750
Prob Diam.(um) 0
Dwell(ms) 80.00
Stage No.7
X : 40.8295 mm
Y : 47.3809 mm
Z : 10.0616 mm
Direction: Single
Points 120*120
Interval(um) X:0.50
Y:0.50
Th WDS 1ch PETJ
Ma Order 1
Peak Pos.(mm) 132.4350
Accum. 1
Max 77
Min 0
Ave 9
A, B value 0.0000, 0.0000
U WDS 2ch PETJ
Mb Order 1
Peak Pos.(mm) 118.5230
Accum. 1
Max 71
Min 0
Ave 12
A, B value 0.0000, 0.0000

4NO* MNT1

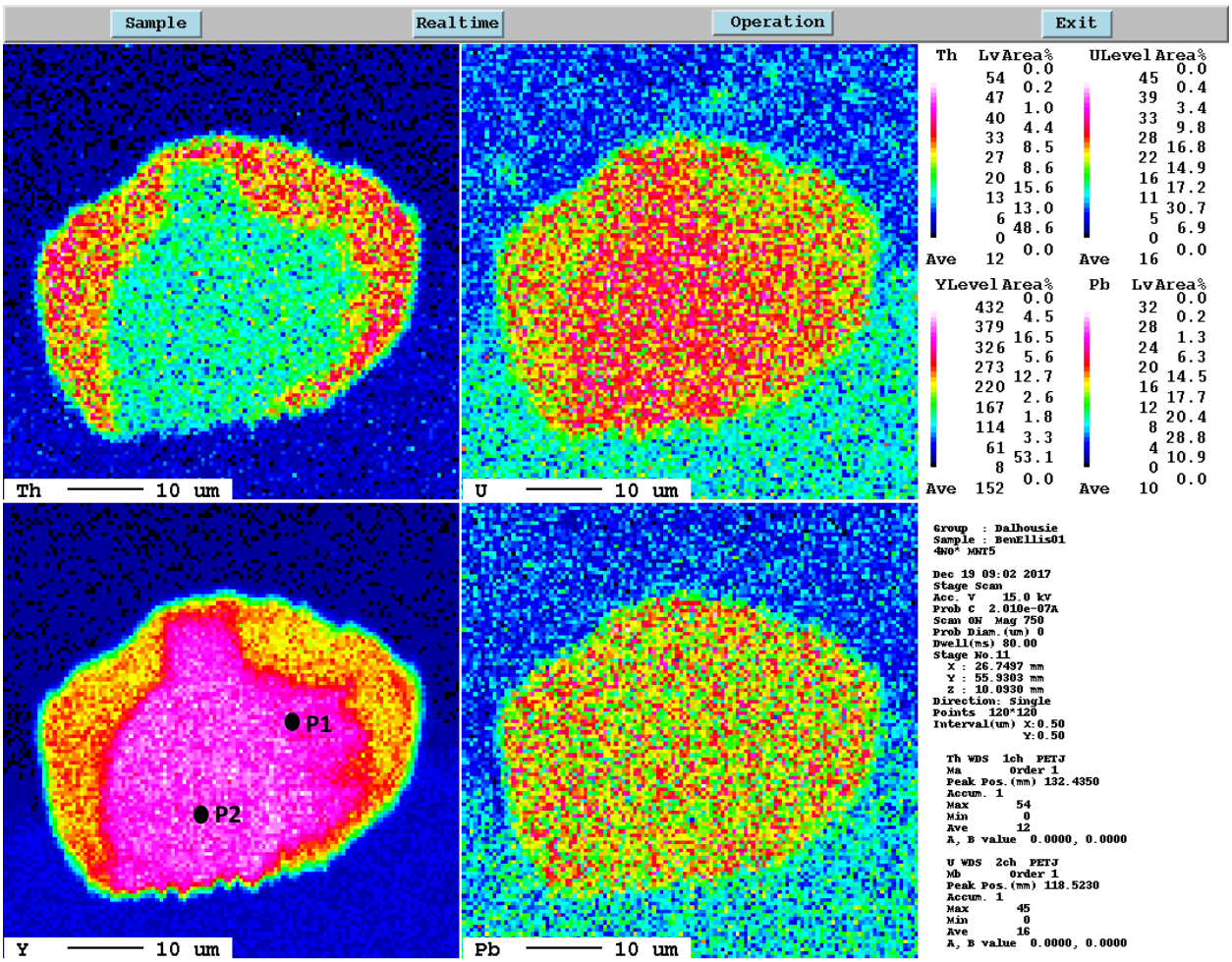
Sample
Realtime
Operation
Exit
Th
10 um
U
10 um
Th Lv Area%
54 0.2
47 1.0
40 4.4
33 8.5
27 8.6
20 15.6
13 13.0
6 48.6
0 0.0
Ave 12
ULevel Area%
45 0.4
39 3.4
33 9.8
28 16.8
22 14.9
16 17.2
11 30.7
5 6.9
0 0.0
Ave 16
YLevel Area%
432 4.5
379 16.5
326 5.6
273 12.7
220 2.6
167 1.8
114 3.3
61 53.1
8 0.0
Ave 152
Pb Lv Area%
32 0.2
28 1.3
24 6.3
20 14.5
16 17.7
12 20.4
8 28.8
4 10.9
0 0.0
Ave 10
P1
P2
Y
10 um
Pb
10 um
Group : Dalhousie
Sample : BenEllis01
4NO* MNT5
Dec 19 09:02 2017
Stage Scan
Acc. V 15.0 kV
Prob C 2.010e-07A
Scan ON Mag 750
Prob Diam.(um) 0
Dwell(ms) 80.00
Stage No.11
X : 26.7497 mm
Y : 55.9303 mm
Z : 10.0930 mm
Direction: Single
Points 120*120
Interval(um) X:0.50
Y:0.50
Th WDS 1ch PETJ
Ma Order 1
Peak Pos.(mm) 132.4350
Accum. 1
Max 54
Min 0
Ave 12
A, B value 0.0000, 0.0000
U WDS 2ch PETJ
Mb Order 1
Peak Pos.(mm) 118.5230
Accum. 1
Max 45
Min 0
Ave 16
A, B value 0.0000, 0.0000

4NO* MNT5

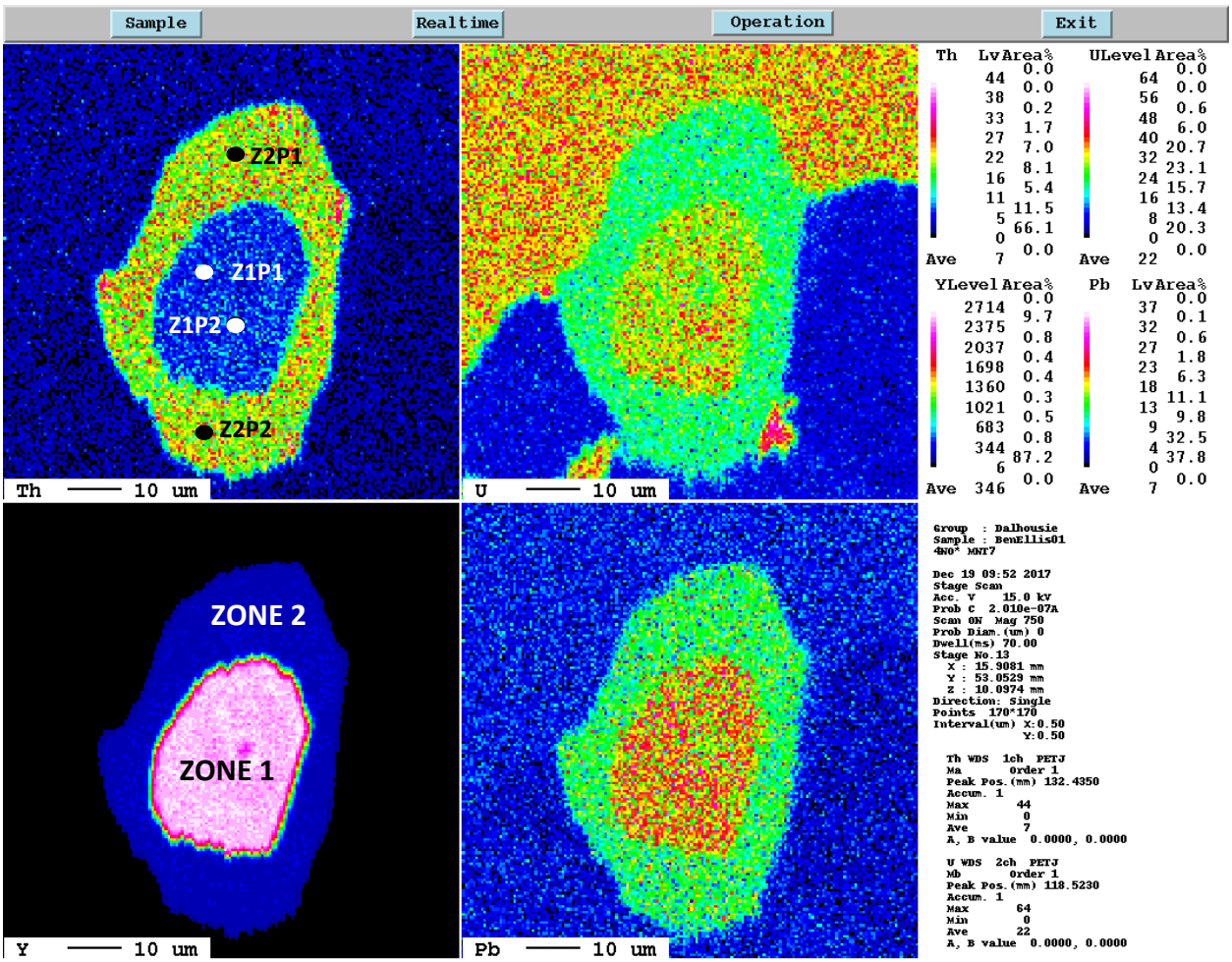
Sample
Realtime
Operation
Exit
Z2P1
Z1P1
Z1P2
Z2P2
Th 10 um
U 10 um
Th Lv Area%
44 0.0
38 0.0
33 0.2
27 7.0
22 8.1
16 5.4
11 11.5
5 66.1
0 0.0
Ave 7
ULevel Area%
64 0.0
56 0.0
48 0.6
40 6.0
32 20.7
24 23.1
16 15.7
8 13.4
0 20.3
Ave 22
YLevel Area%
2714 0.0
2375 9.7
2037 0.8
1698 0.4
1360 0.4
1021 0.3
683 0.5
344 0.8
6 87.2
Ave 346
Pb Lv Area%
37 0.0
32 0.1
27 0.6
23 1.8
18 6.3
13 11.1
9 9.8
4 32.5
0 37.8
Ave 7
ZONE 2
ZONE 1
Y 10 um
Pb 10 um
Group : Dalhousie
Sample : BenEllis01
4NO* MNT7
Dec 19 09:52 2017
Stage Scan
Acc. V 15.0 kV
Prob C 2.010e-07A
Scan ON Mag 750
Prob Diam.(um) 0
Dwell(ms) 70.00
Stage No.13
X : 15.9081 mm
Y : 53.0529 mm
Z : 10.0974 mm
Direction: Single
Points 170*170
Interval(um) X:0.50
Y:0.50
Th WDS 1ch PETJ
Ma Order 1
Peak Pos.(mm) 132.4350
Accum. 1
Max 44
Min 0
Ave 7
A, B value 0.0000, 0.0000
U WDS 2ch PETJ
Mb Order 1
Peak Pos.(mm) 118.5230
Accum. 1
Max 64
Min 0
Ave 22
A, B value 0.0000, 0.0000

4NO* MNT7

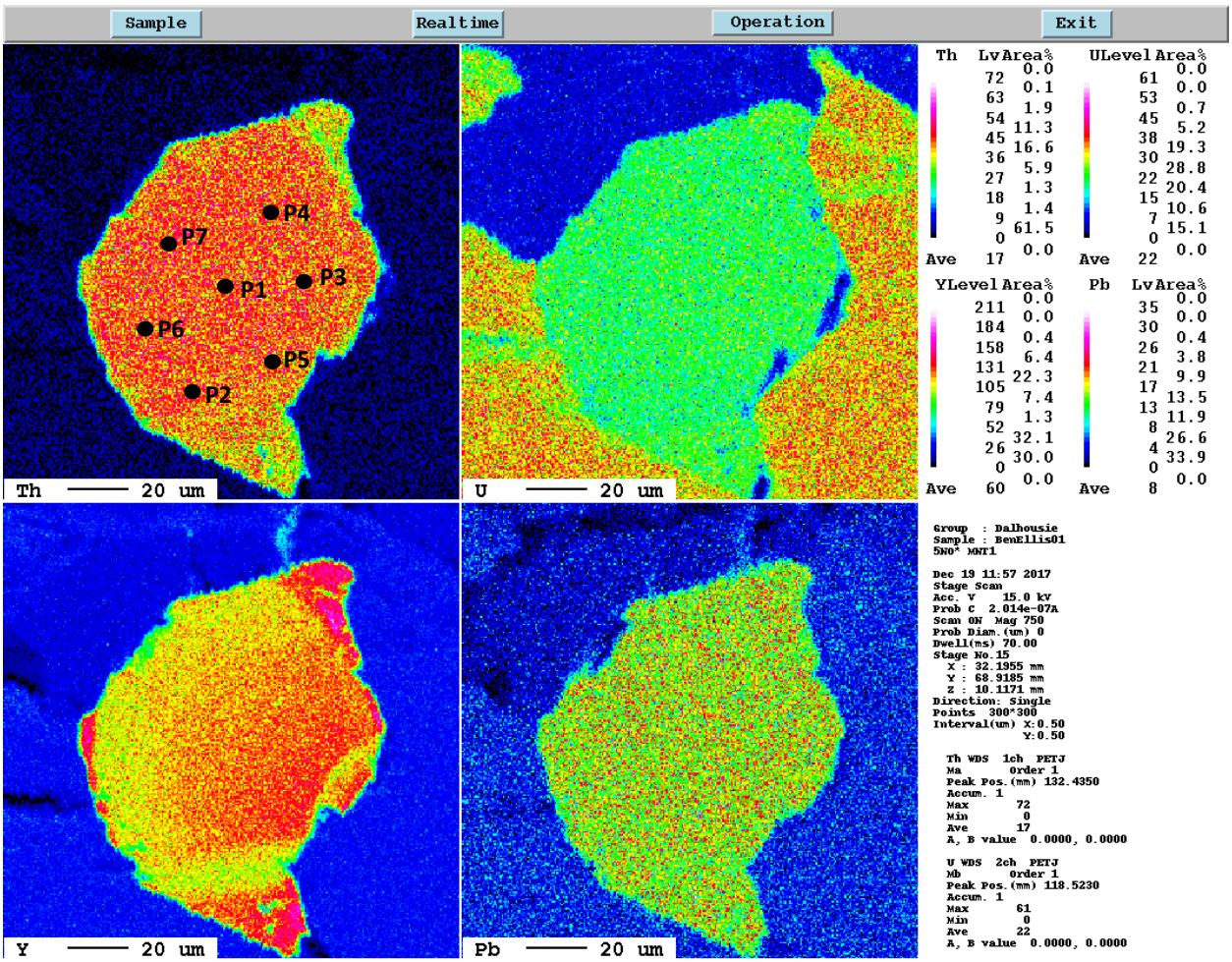
Sample
Realtime
Operation
Exit
P4
P7
P1
P3
P6
P5
P2
Th 20 um
U 20 um
Y 20 um
Pb 20 um
Th Lv Area%
72 0.1
63 1.9
54 11.3
45 16.6
36 5.9
27 1.3
18 1.4
9 61.5
0 0.0
Ave 17
ULevel Area%
61 0.0
53 0.0
45 0.7
38 5.2
30 19.3
22 28.8
15 20.4
7 10.6
0 15.1
Ave 22
YLevel Area%
211 0.0
184 0.0
158 0.4
131 6.4
105 22.3
79 7.4
52 1.3
26 32.1
0 30.0
Ave 60
Pb Lv Area%
35 0.0
30 0.0
26 0.4
21 3.8
17 9.9
13 13.5
8 11.9
4 26.6
0 33.9
Ave 8
Group : Dalhousie
Sample : BenEllis01
5NO* MNT1
Dec 19 11:57 2017
Stage Scan
Acc. V 15.0 kV
Prob C 2.014e-07A
Scan ON Mag 750
Prob Diam.(um) 0
Dwell(ms) 70.00
Stage No.15
X : 32.1955 mm
Y : 68.9185 mm
Z : 10.1171 mm
Direction: Single
Points 300*300
Interval(um) X:0.50
Y:0.50
Th WDS 1ch PETJ
Ma Order 1
Peak Pos.(mm) 132.4350
Accum. 1
Max 72
Min 0
Ave 17
A, B value 0.0000, 0.0000
U WDS 2ch PETJ
Mb Order 1
Peak Pos.(mm) 118.5230
Accum. 1
Max 61
Min 0
Ave 22
A, B value 0.0000, 0.0000

5NO* MNT1

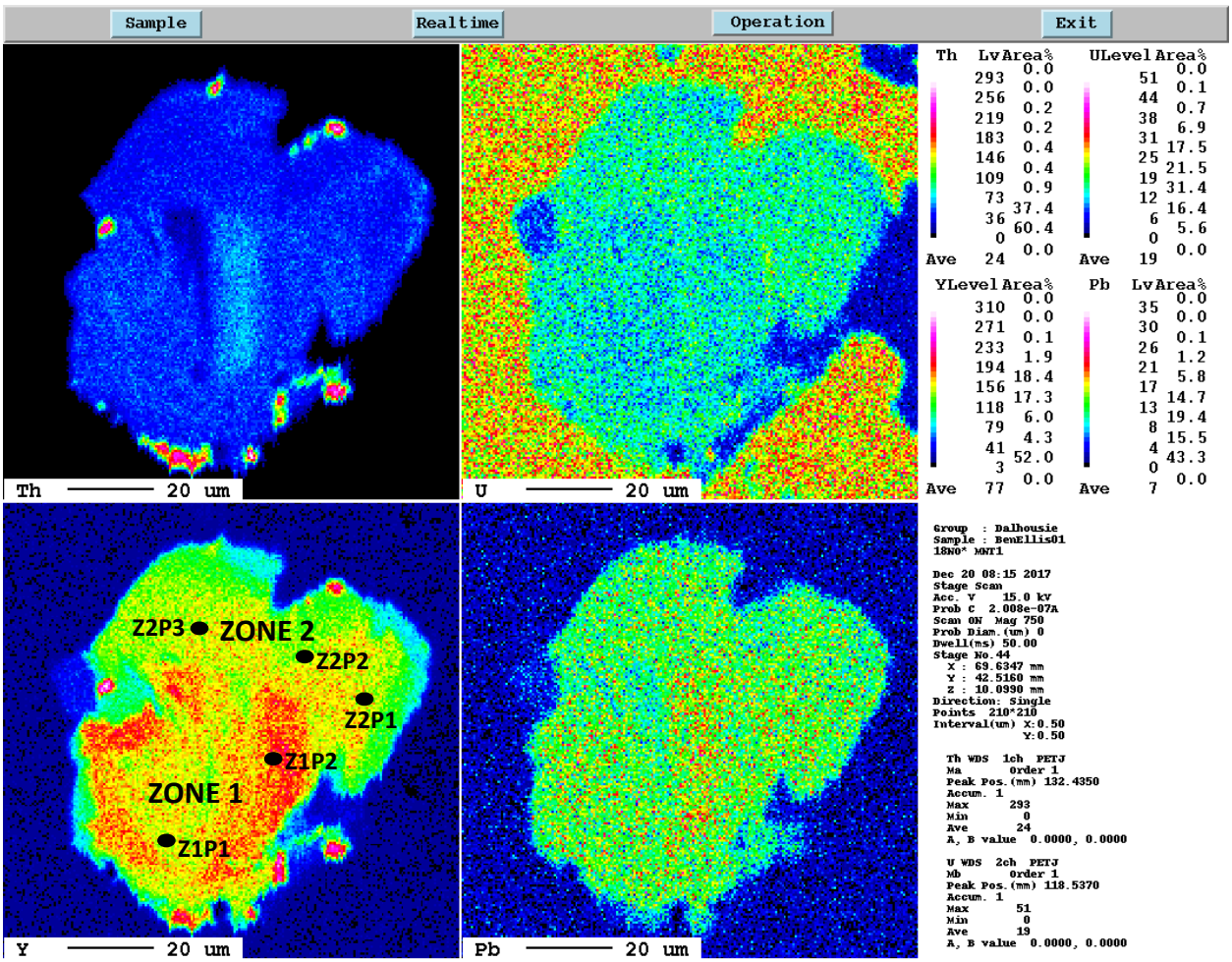
Sample
Realtime
Operation
Exit
Th
20 um
U
20 um
Th Lv Area%
293 0.0
256 0.0
219 0.2
183 0.2
146 0.4
109 0.4
73 0.9
36 37.4
0 60.4
Ave 24 0.0
ULevel Area%
51 0.0
44 0.1
38 0.7
31 6.9
25 17.5
19 21.5
12 31.4
6 16.4
0 5.6
Ave 19 0.0
YLevel Area%
310 0.0
271 0.0
233 0.1
194 1.9
156 18.4
118 17.3
79 6.0
41 4.3
3 52.0
Ave 77 0.0
Pb Lv Area%
35 0.0
30 0.0
26 0.1
21 1.2
17 5.8
13 14.7
8 19.4
4 15.5
0 43.3
Ave 7 0.0
Z2P3
ZONE 2
Z2P2
Z2P1
Z1P2
ZONE 1
Z1P1
Y
20 um
Pb
20 um
Group : Dalhousie
Sample : BenEllis01
18NO* MNT1
Dec 20 08:15 2017
Stage Scan
Acc. V 15.0 kV
Prob C 2.008e-07A
Scan ON Mag 750
Prob Diam.(um) 0
Dwell(ms) 50.00
Stage No.44
X : 69.6347 mm
Y : 42.5160 mm
Z : 10.0990 mm
Direction: Single
Points 210*210
Interval(um) X:0.50
Y:0.50
Th WDS 1ch PETJ
Ma Order 1
Peak Pos.(mm) 132.4350
Accum. 1
Max 293
Min 0
Ave 24
A, B value 0.0000, 0.0000
U WDS 2ch PETJ
Mb Order 1
Peak Pos.(mm) 118.5370
Accum. 1
Max 51
Min 0
Ave 19
A, B value 0.0000, 0.0000

18NO* MNT1

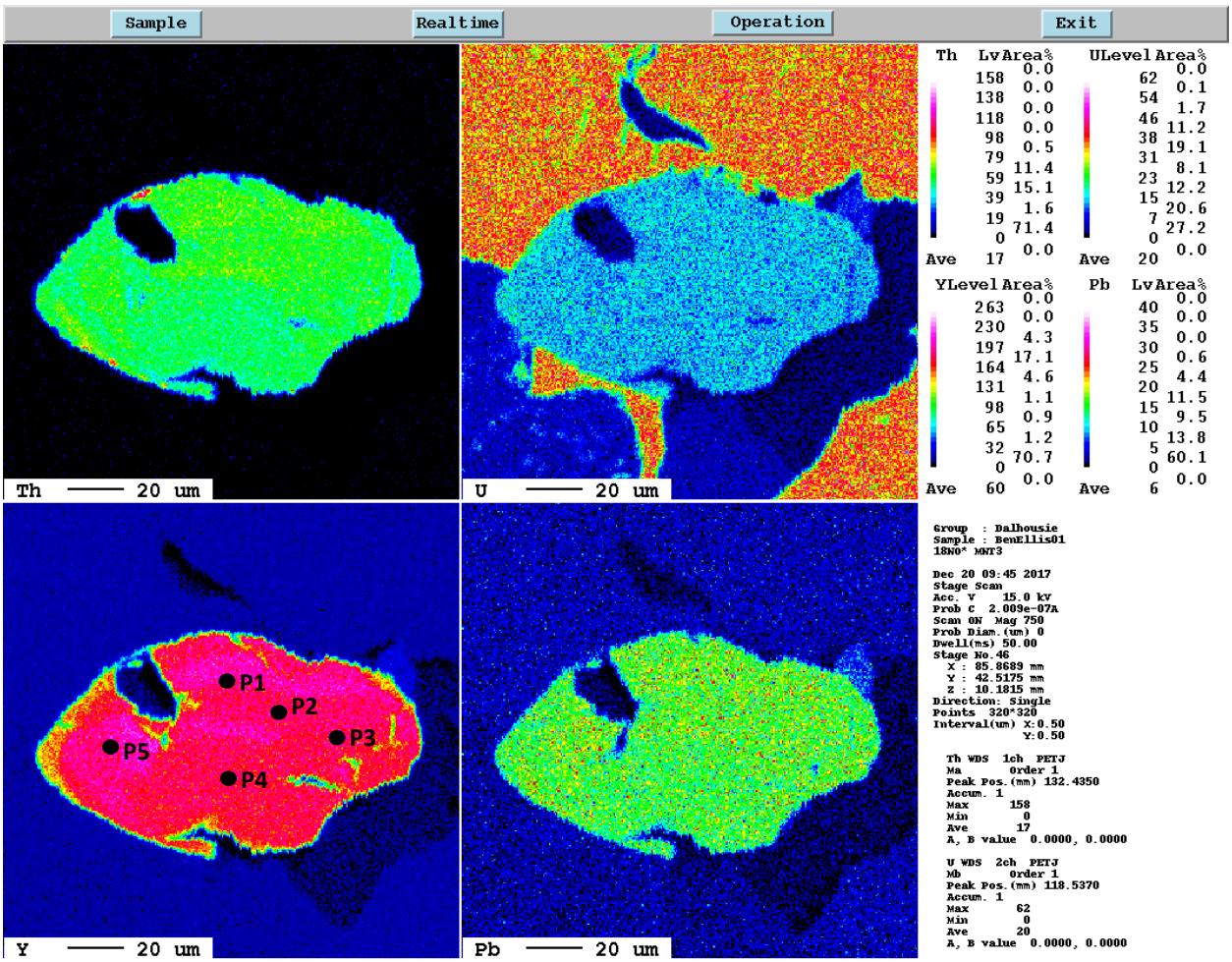
Sample
Realtime
Operation
Exit
Th
U
Y
Pb
20 um
P1
P2
P3
P4
P5
Th Lv Area%
158 0.0
138 0.0
118 0.0
98 0.5
79 11.4
59 15.1
39 1.6
19 71.4
0 0.0
Ave 17
ULevel Area%
62 0.0
54 0.1
46 1.7
38 11.2
31 19.1
23 8.1
15 12.2
7 20.6
0 27.2
Ave 20
YLevel Area%
263 0.0
230 0.0
197 4.3
164 17.1
131 4.6
98 1.1
65 0.9
32 1.2
0 70.7
Ave 60
Pb Lv Area%
40 0.0
35 0.0
30 0.0
25 0.6
20 4.4
15 11.5
10 9.5
5 13.8
0 60.1
Ave 6
Group : Dalhousie
Sample : BenEllis01
18NO* MNT3
Dec 20 09:45 2017
Stage Scan
Acc. V 15.0 kV
Prob C 2.009e-07A
Scan ON Mag 750
Prob Diam.(um) 0
Dwell(ms) 50.00
Stage No.46
X : 85.8689 mm
Y : 42.5175 mm
Z : 10.1815 mm
Direction: Single
Points 320*320
Interval(um) X:0.50
Y:0.50
Th WDS 1ch PETJ
Ma Order 1
Peak Pos.(mm) 132.4350
Accum. 1
Max 158
Min 0
Ave 17
A, B value 0.0000, 0.0000
U WDS 2ch PETJ
Mb Order 1
Peak Pos.(mm) 118.5370
Accum. 1
Max 62
Min 0
Ave 20
A, B value 0.0000, 0.0000

18NO* MNT3

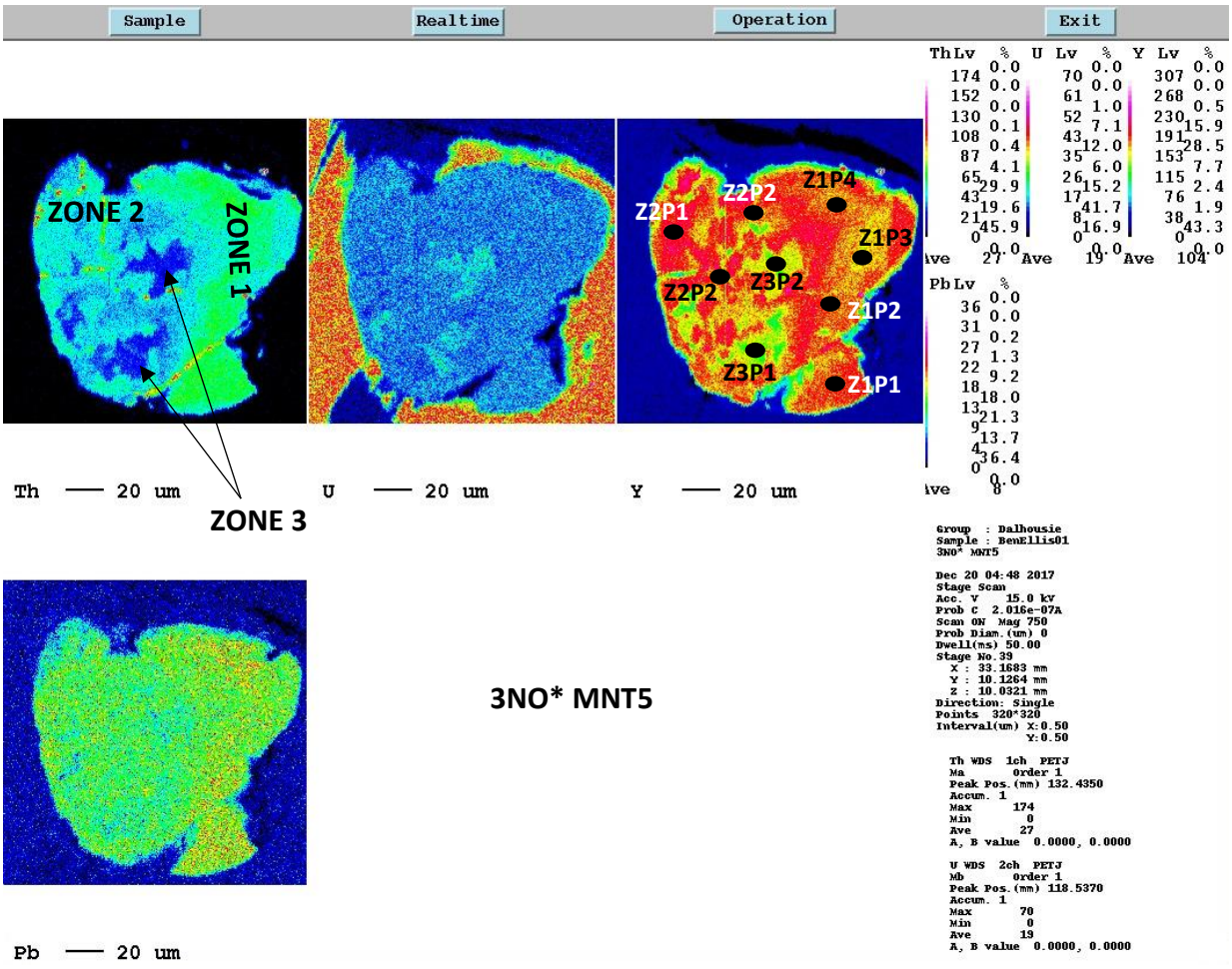
Sample
Realtime
Operation
Exit
ZONE 2
ZONE 1
ZONE 3
Z1P4
Z2P2
Z2P1
Z1P3
Z2P2
Z3P2
Z1P2
Z3P1
Z1P1
Th Lv % U Lv % Y Lv %
174 0.0 70 0.0 307 0.0
152 0.0 61 0.0 268 0.0
130 0.0 52 1.0 230 0.5
108 0.1 43 7.1 191 15.9
87 0.4 35 12.0 153 28.5
65 4.1 26 6.0 115 7.7
43 29.9 17 15.2 76 2.4
21 19.6 8 41.7 38 1.9
0 45.9 0 16.9 0 43.3
0.0 0.0 0.0
ave 27 Ave 19 Ave 104
Pb Lv %
36 0.0
31 0.0
27 0.2
22 1.3
18 9.2
13 18.0
9 21.3
4 13.7
0 36.4
0.0
ave
Th — 20 um
U — 20 um
Y — 20 um
Pb — 20 um
3NO* MNT5
Group : Dalhousie
Sample : BenEllis01
3NO* MNT5
Dec 20 04:48 2017
Stage Scan
Acc. V 15.0 kv
Prob C 2.016e-07A
Scan ON Mag 750
Prob Diam.(um) 0
Dwell(ms) 50.00
Stage No.39
X : 33.1683 mm
Y : 10.1264 mm
Z : 10.0321 mm
Direction: Single
Points 320*320
Interval(um) X:0.50
Y:0.50
Th WDS 1ch PETJ
Ma Order 1
Peak Pos.(mm) 132.4350
Accum. 1
Max 174
Min 0
Ave 27
A, B value 0.0000, 0.0000
U WDS 2ch PETJ
Mb Order 1
Peak Pos.(mm) 118.5370
Accum. 1
Max 70
Min 0
Ave 19
A, B value 0.0000, 0.0000